論文 / 著書情報
Article / Book Information

題目(和文)	福島第一原発事故により影響された森林流域における降雨流出，土壌侵食及び放射性セシウムの移行モデリングに関する研究
Title(English)	Modeling rainfall-runoff, soil erosion and radiocesium transport in a forested catchment affected by the Fukushima Daiichi Nuclear Power Plant accident
著者(和文)	WEI Lezhang
Author(English)	WEI Lezhang
出典(和文)	学位:博士（工学）, 学位授与機関:東京工業大学, 報告番号:甲第10200号, 授与年月日:2016年3月26日, 学位の種別:課程博士, 審査員:木内 豪,石川 忠晴,中村 恭志,豊田 栄,吉村 千洋
Citation(English)	Degree:, Conferring organization: Tokyo Institute of Technology, Report number:甲第10200号, Conferred date:2016/3/26, Degree Type:Course doctor, Examiner:,,,,
学位種別(和文)	博士論文
Type(English)	Doctoral Thesis

Modeling rainfall-runoff, soil erosion and radiocesium transport in a forested catchment affected by the Fukushima Daiichi Nuclear Power Plant accident

WEI Lezhang

Supervised by

Prof. Tsuyoshi KINOUCHI

Department of Environmental Science and Technology

Interdisciplinary Graduate School of Science and Engineering

Tokyo Institute of Technology

January 2016

Modeling rainfall-runoff, soil erosion and radiocesium transport in a forested catchment affected by the Fukushima Daiichi Nuclear Power Plant accident

WEI Lezhang

Department of Environmental Science and Technology

Interdisciplinary Graduate School of Science and Engineering

Tokyo Institute of Technology

January 2016

Abstract

The Fukushima nuclear accident in 2011 resulted in ^{137}Cs contamination in large areas of northeast Japan. ^{137}Cs transport associated with hydrological processes across landscapes is of primary concern for contamination management and environmental risk assessment. Aiming to understand transport and fate of the Fukushima-derived ^{137}Cs, rainfall-runoff, soil erosion and watershed ^{137}Cs migration processes in a forested catchment (i.e. the Kuchibuto River catchment) were studied based on a distributed model, which was developed by improving the two-dimensional runoff erosion and export (TREX) framework in this study.

Firstly, for our continuous hydrological simulation in a typical Japanese forested catchment, the TREX framework was improved by newly including additional hydrologic processes such as evapotranspiration, subsurface and groundwater flows. Infiltration and interception parts were also modified according to the characteristic of our study catchment. Soil erosion and transport processes were simulated by considering multiple solid classes at fine spatial-temporal scales. Then, a watershed ^{137}Cs transport model was developed based on the improved TREX framework. Multiple solid particle classes, the effect of vegetation canopy/litter layer, ^{137}Cs downward movement in soil and radiocesium phases in water, which are important controlling facts for ^{137}Cs migration but were ignored in prior modeling studies in Fukushima, were considered in our study. The sources and sinks of ^{137}Cs transport coupling with critical soil erosion areas were identified in the studied catchment. The results of our study indicate:

(1) The model calculated acceptable flow discharges, suspended solid (SS) and ^{137}Cs concentrations at the observation sites in the Kuchibuto River catchment during the simulation period (Jan. 1, 2011 – Dec. 31, 2014). This case study shows the model is a good tool for study of ^{137}Cs transport along with hydrological processes at the watershed scale in Fukushima, Japan.

(2) For the case of the Kuchibuto River catchment, about 5500 t of clay, 52000 t of silt, 22000 t of sand along with 4.1×10^8 m^3 water were transported to the Abukuma River

from Mar. 12, 2011, when the accident began, and Dec. 31, 2014. The area-specific sediment yield was about 155 t/y/km^2 according to our simulated sediment budget. By the end of 2014, the total ^{137}Cs reduction was 3.39 TBq (including natural radioactive decay), which means about 90% ^{137}Cs remained in the catchment. This estimation confirms the necessity of artificial decontamination in the following years. An estimated 4.85 TBq of ^{137}Cs remained in the canopy/litter layer. Hence, as a stock, this layer still stored a considerable amount of radiocesium. During the 3.5-year study, 0.57 TBq of ^{137}Cs was transported from the catchment. It mainly carried by eroded suspended sediment. During this period, the average ^{137}Cs reduction rate and reduction ratio by rainfall-runoff wash-off were 1.24 GBq/km^2/y and 1.6%, respectively.

(3) The ^{137}Cs reduction rate and reduction ratio by rainfall-runoff wash-off show spatial distributions related to the spatial variation of the ^{137}Cs contamination level and soil erosion. The ^{137}Cs reduction rate was higher in the upper stream areas, which corresponds to the initial ^{137}Cs distribution. In contrast, the ^{137}Cs reduction ratio and sediment supply ratio of the subwaterhseds in the middle portion of the catchment were higher, which indicates that decontamination for critical erosion areas in the middle portion of catchment is also of the great priority. The sinks of ^{137}Cs, which accumulated a considerable amount of ^{137}Cs owing to sediment deposition, can be targeted areas for decontamination. The results of this study are useful for understanding transport behavior and fate of radiocesium and ultimately for assessing environmental risks at the watershed scale.

Contents

Chapter 1

Introduction

1.1 Background

The Fukushima Daiichi Nuclear Power Plant (FDNPP) exploded on Mar.12 and 14, 2011 as the result of a magnitude 9.0 (Mw) earthquake and following tsunami in northeastern Japan. Consequently, huge amounts of radionuclides, including ^{131}I, ^{137}Cs, ^{134}Cs, ^{132}Te, and etc., were emitted from FDNPP into the surrounding environment (Endo *et al*., 2012). Among all kinds of those radionuclides, ^{137}Cs persists in the environment for the longest time because of its long half-life (30.2 years). It is estimated that the total amount of ^{137}Cs released into the atmosphere was on the order of $1–2×10^{16}$ Bq (IAEA, 2011). Airborne surveys by the Ministry of Education, Culture, Sports, Science, and Technology (MEXT) revealed that the contaminants were spread widely; in particular, the area northwest of FDNPP was heavily contaminated (MEXT, 2013). Because of winds, rainfall and etc., radionucesium deposited onto land surface such as forest, agricultural land, and residential areas. Forest is the most contaminated land use type. 4% of the forests in Fukushima prefecture were heavily contaminated (>=$^{134,\ 137}Cs$ 1000 KBq/m^2) (Hashimoto *et al.*, 2012). Shaw (2007) summarized three main phases after deposition of nuclear released contamination in forests based on the Chernobyl nuclear accident. 1-3 months after the accident was the “early phase”. In this phase, radioactive substances were transported from canopy to the underlying litter and soil rapidly. The following 2 or 3 years was the ‘medium term phase’, which included the “biological decontamination” of the canopy and the root uptake of radionuclides. The last was “long term phase” for a long term period, during which the steady state will continue. Although differences exist between the two accidents, radiocesium in the Fukushima accident also follows the three phases. For example, field studies in Japanese forests show, most of the deposited radiocesium was initially intercepted by the tree canopy, some of which gradually fell onto litter or soil layer by throughfall, stemflow, and litterfall (Kato, *et al.*, 2012; Teramage, *et al.*, 2014). Because it was early spring in Japan when the accident occurred, most of the agricultural land was not planted or vegetated, which enhanced direct fallout deposition onto the soil surface. Radioactive substances in some residential areas which were considered as sensitive areas have been cleaned up manually or washed up by rain soon after the accident. As a consequence of direct radiation exposure risk to local residents (Taira *et al.*, 2012), and the potential transfer from the environment to plants and to animals through food chains (Kanasashi *et al.*, 2015; Ayabe *et al.*, 2014; Sato *et al*., 2014; Harada *et al*., 2013), the transport and fate of ^{137}Cs have become a worldwide concern for the public and researchers as well as environmental managers.

1.2 Watershed models

Hydrological processes are key factors for ^{137}Cs transport in the environment. For example, released radiocesium can be absorbed by raindrops that fall onto land. A portion of deposited ^{137}Cs was intercepted by vegetation. The trapped radiocesium can be washed out, and then move downward into the soil gradually along with water infiltration; laterally, once ^{137}Cs reaches the ground surface, it is easily absorbed by finer soil particles. During flood storms, ^{137}Cs associated with water flow and eroded sediments can be transported across landscapes, then discharged into river systems. The processes accelerate on-site ^{137}Cs reduction, however, this horizontal migration results in the spreading of ^{137}Cs to downstream areas with greater population that previously had low contamination. Therefore, ^{137}Cs transport associated with hydrological processes across watersheds is of primary concern for contamination management and environmental risk assessment. Numerical watershed models are good tools to trace ^{137}Cs transport at the watershed scale. Many models have been developed to simulate hydrological and substance transport processes.

^{137}Cs transport from contaminated upland to river systems is a kind of non-point source contamination diffusion. Many nonpoint source pollutant models have been developed, e.g. AnnAGNPS model, HSPF model (Johanson *et al.*, 1980), SWAT (Arnold *et al.*, 1998), TREX (Velleux *et al.*, 2008).

Annualized Agricultural Non-Point Source Pollution model (AnnAGNPS) is a upgraded version of the Agricultural Non-Point Source model (AGNPS, Young *et al.*, 1989). It is a continuous simulation, daily time step, pollutant-loading model. The model divides watershed into several small areas ("cells"), which are often grouped into hydrological similar areas. AnnAGNPS considers five particle size classes and employs the Revised Universal Soil Loss Equation (RUSLE) for the calculation of sediment delivered by runoff to a field edge. The total sediment yield leaving each field to the stream reach is estimated basing on the Hydro–geomorphic Universal Soil Loss Equation (HUSLE). Einstein deposition equation with Bagnold transport capacity is used to calculate sediment transport. For chemical transport simulation, AnnAGNPS has the capability to simulate transport and fate of dissolved and attached nitrogen, phosphorous, organic carbon, and pesticides.

Hydrological Simulation Program—FORTRAN model (HSPF), was developed by USGS and USEPA. It is a lumped parameter watershed model, composed by three application modules: PERLAND, IMPLAND and RCHRES. Any time step from 1 minute to 1 day can be used for long−term continuous simulation, typically in mixed agricultural and urban watersheds (Borah and Bera, 2004). The model uses sub-basin approach for segmentation to simulate hydrological processes such as soil water content, evapotranspiration, surface runoff, interflow, base flow, ground-water recharge, snowfall/snowmelt, and etc.. HSPF simulates three sediment types (i.e. sand, silt, and clay). Re-suspension and settling of silt and clay are defined in terms of shear stress at the sediment-water interface. For sand, the capacity to transport sand by water flow is calculated and re-suspension or settling is defined by the transport capacity. HSPF has been widely applied to evaluate nutrients and agricultural chemicals contribution to water body, develop Total Maximum Daily Load (TMDL) standards, and evaluate alternative land-use and select Best Management Practices (BMPs) scenarios in US and other countries.

The Soil and Water Assessment Tool (SWAT) is a watershed-scale, deterministic model for long−term continuous simulations on water, sediment, nutrient and pesticide yields. The model divides a watershed into sub-watersheds that are further sub-divided into hydrological response units (HRUs) which comprises unique combinations of land use, soil type and slope. The model calculates mass balances of water, sediment, chemical based on daily time step. Surface runoff is estimated using a modification of the Soil Conservation Service (SCS) Curve Number (CN) method. A simple kinematic storage routing method is used to predict lateral flow, and a simple lumped model is used to calculate flow from a shallow aquifer. SWAT calculates sediment yield using the Modified Universal Soil Loss Equation (MUSLE). The transport of sediment in the river channel is controlled by the simultaneous operation of two processes, deposition and degradation, which are determined by the comparison between maximum concentration of sediment and the concentration of sediment. Previous applications show SWAT model is a good tool for agricultural non-point source pollutant simulation (Gassman *et al.*, 2007).

Two-dimensional Runoff, Erosion and eXport model (TREX) is a fully distributed model which can simulate rainfall-runoff, sediment transport, and chemical transport and fate at the watershed scale on the basis of event. Hydrological module in the model is original from CASC2D model (Julien and Saghafian, 1991). The model can simulate soil erosion on the upland and sediment transport in the river channel with unlimited particle classes. Sediment transport capacity is used to determine soil/sediment transport. The model has been tested and applied for metals (Cu, Cd, and Zn) transport simulation in the California Gulch watershed mine-waste site in Colorado, US (Velleux *et al.*, 2006; 2008).

Additionally, after the Chernobyl accident, some specialized models were developed to simulate radioactive substances migration, e.g. a MOdel based computerized system for management support to Identify optimal remedial strategies for Restoring radionuclide contaminated Aquatic ecosystems and drainage areas (MOIRA model) (Monte, 2001). Those kinds of models are not designed to simulate detailed, single event flood routing. They usually consider whole catchment as a target, and use simple water balance method to predict monthly hydrological variables (e.g. water flow).

Recently, to understand ^{137}Cs transport after Fukushima nuclear accident, some models, such as SACT model (Yamaguchi *et al*., 2013); WEP model (Jia *et al.*, 2001, Kinouchi *et al.*, 2015), were developed (or improved) and applied in the Abukuma River watershed and other small catchments near the FDNPP.

A simple, novel and fast Soil and Cesium Transport model (SACT) model considers three solid types: sand (2mm-62mm), silt (4-62mm) and clay (<4mm). Sediment is modeled independently on the land surface, in rivers, and in lakes (dam reservoirs) respectively. Annual sediment discharge are estimated based on the USLE and simple sediment discharge formulas. The model was employed to predict long-term ^{137}Cs distribution in Fukushima without considering ^{137}Cs downward movement in soil profile (Kitamura *et al.*, 2014; Yamaguchi *et al.*, 2014).

Water and Energy transfer Process model (WEP) was extended by newly included soil erosion and ^{137}Cs transport modules (Kinouchi *et al.*, 2015). The model does not consider multiple particle classes and assumes that the suspended sediments follow the behavior defined by the mean particle size of sediments. Sediment transport is modeled basing on the formulas used in KINEROS (Woolhiser *et al.*, 1990), which accounts for splash erosion induced by raindrop energy and hydraulic erosion by flowing water, as well as the advective transport of sediments. The particulate radiocesium concentration in the surface flow is calculated using an advective transport model of contaminated sediments flowing on the upland and in the river channel.

Moreover, Tanaka *et al.* (2013) developed a distributed rainfall and sediment transport model to reproduce rainfall-runoff and estimate suspended load and associated radoicesium movement. In the model, radiocesium attached to suspended sediment is modeled by considering solid particle size distribution. However, that model neglects some key processes such as sediment resuspension and deposition in river channels.

1.3 Model selection

Different types of model, from lumped conceptual models to more sophisticated distributed models, have been developed to simulate hydrological and associated processes; however, models available for the purpose of our environmental study are very limited. We want to know not only the total amount of contaminants flowing into rivers, but also where the contaminants originate from and how they are redistributed. Thus, a distributed model is fitter than a lumped model. Several factors limit the performance of the models for sediment-cesium transport study (Table 1-1). Firstly, size distribution of soil particles is important factor because experimental studies demonstrate that the sorption properties of soil particles is size-dependent and that radionuclide sorption to soils preferentially occurs with finer particles because they have higher specific surface areas (He and Walling, 1996). Field studies in Fukushima also confirmed that finer particles have high radionuclide enrichment ratios and that most radiocesium transported in the basin's fluvial system was carried in a particle-associated form (Tanaka *et al*., 2014; Yamashiki *et al.*, 2014). Thus, for modeling ^{137}Cs transport along with soil/sediment particles transport, it is necessary to consider multiple soil particle classes. However, most of the models mentioned above simulate soil erosion with one single particle class. Second, extreme flood events have led to punctuated horizontal remobilization of significant quantities of radionuclides at watershed scale. Studies have reported that during the Typhoon Roke on Sept. 21–22 2011, an estimated 61% of the total radiocesium load recorded during August 10 2011, and May 11, 2012 was exported from the Abukuma River watershed (Yamashiki *et al*., 2014). This export flux of radiocesium accounted for about 30–50% of the annual flux in 2011 from Natsui River and the Same River (Nagao *et al.*, 2013). Therefore. Models with finer time step than a year or day are more helpful for tracing water-sediment-radiocesium dynamics for each flood event. However, the time step of the model, such as SWAT model, MOIRA model, SCAT model, is daily, or monthly or yearly. Moreover, the dominant landscape of the contaminated area in Fukushima is forest with the characteristic of steep slope, it is quite different from the agriculture landscape where the SWAT model and AGNPS model were usually applied. Considering all of those factors, a distributed watershed model with consideration of multiple solid particle classes to model the rainfall-runoff, soil erosion and transport, and radiocesim migration at finer spatial and temporal scales is needed. Although HSPF is well-proven tool to simulate chemical transport and considers multiple solid classes, it is not an adequate framework for our study. The model is not expected to be fully compatible with raster GIS without loss of spatial detail because raster cells need to be aggregated into the sub-basin units that the model supports. This sub-basin approach used for segmentation in HSPF may prevent the model from being used with fully distributed parameters (Velleux, 2005). The TREX is a promising model for our study because it can meet all the requirements mentioned above. The current TREX model combines surface hydrology and sediment transport with chemical transport features from the WASP/IPX series of water quality models. Usually, 1D model assumes the steepest slope direction is flow direction. While, water flow can be 4 directions in TREX model, so, the pathway of water flow and substance transport is more flexible. Comparing with other models used in Japan, those are advantages to use this model for the study of radiocesium watershed-scale migration.

1.4 Objective and structure of this study

Although, the TREX model is better than other models for our study, it is not a prefect model. The model is an event-based model, which just simulate Hortonian overland flow. In Japanese forested catchments, due to high infiltration rate of the top soil, Hortonian overland flow rarely generates. Therefore, it is difficult for the model to simulate hydrologic processes in our catchment. Although the model was employed for heavy metal transport simulation, ^{137}Cs deposition and migration processes after the Fukushima accident is different with common heavy metal. Therefore, the TREX model needs to be modified firstly for our study. Then, a distributed watershed radiocesium transport model was developed based on the improved TREX framework, and applied in our study catchment. Specifically, the objective of our study is twofold:

(1) to improve the TREX framework and develop watershed ^{137}Cs transport model based on the improved TREX framework.

(2) to analyze the characteristics of radiocesium migration in a forest catchment in Fukushima by modeling study.

The structure of this study is described briefly as follows:

Chapter 1. Introduction

Chapter 2. Study area and data collection

This study focused on a small forested headwater catchment, which was heavily contaminated by radiocesium after the Fukushima nuclear accident. The model input data includes landuse, soil type, precipitation and meteorological data and etc.. Measured data were used for the model calibration and validation.

Chapter 3. Improvement of the TREX model for continuous rainfall-runoff simulation for forested catchments

The original TREX model is an event-based model which can only simulate Hortonian overland flow. To apply this model in Japanese forested catchments for continuous simulations, the model needs to be improved. In this chapter, the model was improved by newly including subsurface flow in topsoil, groundwater flow, and evapotranspiration, methods to simulate canopy storage and infiltration rate were modified as well. The enhancement improved applicability of this model in forested catchments.

Chapter 4. Simulation of soil erosion and transport with consideration of multiple solid classes

Contaminated soil particles, especially finer soil particles, are transport media for ^{137}Cs migration during flood events. Soil erosion and transport processes in the Kuchibuto River catchment were simulated with considering multiple solid classes. According to spatial variation of soil erosion, critical erosion areas were identified. Comparisons between simulated and measured suspended solid concentration, flux and load for 2011 ~ 2014 demonstrate that simulated results are acceptable. Simulation results also indicate that between Mar. 12, 2011, when the accident began, and Dec. 31, 2014, about 5500 t of clay, 52000 t of silt, 22000 t of sand were eroded and transported to the Abukuma River. Soil erosion mainly occurred in the middle portion of the catchment, where slopes are steep and the primary land use is agricultural.

Chapter 5. Modeling ^{137}Cs migration based on a hydrological and sediment erosion model in a forested catchment

In this chapter, a watershed ^{137}Cs transport model was developed based on the improved TREX framework. Taking the Kuchituto River catchment as an example, the model was applied for watershed-scale ^{137}Cs migration simulation. The controlling factors such as the effect of vegetation canopy/litter layer, multiple solid particle classes, ^{137}Cs downward movement in soil and dissolved and particulate radiocesium in water, which are important for ^{137}Cs migration but were ignored in prior modeling studies in Fukushima, were considered in our study. Comparisons with measurement in the river show the simulated ^{137}Cs concentrations are acceptable. The result that about 90% ^{137}Cs remained in the catchment indicates artificial decontamination are necessary in the following years. For simulation period, 0.57 TBq of ^{137}Cs was transported from the catchment, thus, the average ^{137}Cs reduction rate and reduction ratio by rainfall-runoff washoff were 1.24 $GBq/km^2/y$ and 1.60%, respectively. The ^{137}Cs reduction rate and reduction ratio by runoff show spatial distributions related to the spatial variation of the ^{137}Cs contamination level and soil erosion. This finding helped to better understand watershed-scale ^{137}Cs transport and fate, and supported useful information for developing various decontamination strategies in Fukushima.

Chapter 6. Summary and conclusions

Table 1-1. Some characteristics of models for comparison

models	solid particle size	temporal scale	applications
AnnAGNPS	five classes	daily time step; continuous simulation	mainly applied in agricultural watersheds
HSPF	three classes	1min -1day; continuous simulation	typically in mixed agricultural and urban watersheds
SWAT	single class	daily time step; continuous simulation	mainly applied in agricultural watersheds
TREX	multiple classes	seconds; event simulation	the California Gulch watershed, US
MOIRA	single class	monthly; continuous simulation	European fresh water systems
SACT	three classes	yearly; continuous simulation	several watersheds in Fukushima
WEP	single class	hourly; continuous simulation	the Kuchibuto River watershed in Fukushima
Tanaka's model	single class	hourly; continuous simulation	the Kuchibuto River watershed in Fukushima

Reference

Arnold, J. G., Srinivasan, R., Muttiah, R. S., and Williams, J. R. (1998) Large area hydrologic modeling and assessment: Part I. Model development. *J. American Water Resour. Assoc.* 34(1): 73-89.

Ayabe, Y., Kanasashi, T., Hijii, N., and Takenaka, C. (2014) Radiocesium contamination of the web spider Nephila clavata (Nephilidae: Arachnida) 1.5 years after the Fukushima Dai-ichi nuclear power plant accident. *Journal of Environmental Radioactivity*, 127:105-110.

Borah, D.K., and Bera M. (2004) Watershed-scale hydrologic and nonpoint-source pollution models: Review of applications. *Trans. ASAE,* 47(3): 789-803.

Endo, S., Kimura, S., Takatsuji, T., Nanasawa, K., Imanaka, T., Shizuma, K. (2012) Measurement of soil contamination by radionuclides due to the Fukushima Dai-ichi Nuclear Power Plant accident and associated estimated cumulative external dose estimation. *Journal of Environmental Radioactivity*, 111:18–27.

Gassman, P. W., Reyes, M., Green, C. H., and Arnold, J. G. (2007) The Soil and Water Assessment Tool: Historical development, applications, and future directions. *Trans. ASABE,* 50(4): 1211-1250.

Harada, K., Fujii, Y., Adachi, A., Tsukidate, A., Asai, F., Koizumi, A. (2013) Dietary intake of radioactive cesium in adult residents in Fukushima Prefecture and neighboring regions after the Fukushima Nuclear Power Plant Accident: 24 hr -Food Duplicate Survey in December 2011. *Environ. Sci. Technol.*, 47 (6): 2520–2526.

Hashimoto, S., Ugawa, S., Nanko, K. & Shichi, K. (2012) The total amounts of radioactively contaminated materials in forests in Fukushima, Japan. *Sci. Rep.* 2, 416; DOI: 10.1038/srep00416.

He, Q., Walling, D. E. (1996) Interpreting particle size effects in the adsorption of ^{137}Cs and unsupported ^{210}Pb by mineral soils and sediments. *Journal of Environmental Radioactivity*, 30: 117-137.

IAEA. (2011) Additional report of Japanese Government to IAEA—accident at TEPCO's Fukushima nuclear power stations transmitted by nuclear emergency response headquarters, Government of Japan, 15 September 2011. International Atomic Energy Agency (IAEA); [Accessed online (July 1, 2012) http://www.iaea.org/newscenter/focus/fukushima/japan-report2/].

Jia, Y., Ni, G., Kawahara, Y. and Suetsugi, T. (2001) Development of WEP model and its application to an urban watershed, *Hydrological Processes,* 15(11): 2175-2194.

Johanson, R. C., Imhoff, J. C., and Davis, H. H. (1980) "User's Manual for the Hydrologic Simulation Program -FORTRAN (HSPF)." EPA-600/9-80-105, U.S. EPA Environmental Research Laboratory, Athens, GA.

Julien, P.Y., Saghafian, B. (1991) CASC2D User's Manual – A Two Dimensional Watershed Rainfall-runoff Model. Civil Eng. Report CER90-91PYJ-BS-12, Colorado State University, Fort Collins, CO.

Kanasashi, T., Sugiura, Y., Takenaka, C., Hijii, N., Umemura, M. (2015) Radiocesium distribution in sugi (Cryptomeria japonica) in Eastern Japan: translocation from needles to pollen. *Journal of Environmental Radioactivity*. 139: 398-406

Kitamura, A., Yamaguchi, M., Kurikami, H., Yui, M. and Onishi, Y. (2014) Predicting sediment and cesium-137 discharge from catchments in eastern Fukushima. *Anthropocene*, 5: 22–31.

Kato, H., Onda, Y., Gomi, T., (2012) Interception of the Fukushima reactor accident derived 137Cs, 134Cs and 131I by coniferous forest canopies. *Geophys. Res. Lett.* 39, L20403. http://dx.doi.org/10.1029/2012GL052928.

Kinouchi, T., Yoshimura, K., Omata, T. (2015) Modeling radiocesium transport from a river catchment based on a physically-based distributed hydrological and sediment erosion model. *Journal of Environmental Radioactivity,* 139: 407–415.

MEXT. (2013) Extension site of distribution map of radiation dose, etc.. http://ramap.jmc.or.jp/map/eng/.

Monte, L. (2001) A generic model for assessing the effects of countermeasures to reduce the radionuclide contamination levels in abiotic components of fresh water systems and complex catchments. *Environmental Modelling & Software*. 16: 669–690.

Nagao, S., Kanamori, M., Ochiai, S., Tomihara, S., Fukushi, K., Yamamoto M. (2013) Export of ^{134}Cs and ^{137}Cs in the Fukushima river systems at heavy rains by Typhoon Roke in September 2011. *Biogeosciences Discuss*. 10: 2767–2790.

Sakaguchi, A., Tanaka, K., Iwatani, H., Chiga, H., Fan, Q., Onda, Y., Takahashi, Y., (2014) Size distribution studies of ^{137}Cs in river water in the Abukuma riverine system following the Fukushima Dai-ichi Nuclear Power Plant accident. *J. Environ. Radioact*. 139: 379-389.

Sato, I., Okada, K., Sasaki, J., Chida, H., Satoh, H., Miura, K., Kikuchi, K., Otani, K. and Sato, S. (2014) Distribution of radioactive cesium and stable cesium in cattle kept on a highly contaminated area of Fukushima nuclear accident. *Animal Science Journal.* DOI: 10.1111/asj.12345

Shaw, G. (2007) Radionuclides in forest ecosystems S. George (Ed.), Radioact Environ [Internet], Elsevier, pp. 127–155.

Taira, Y., Hayashida, N., Yamaguchi, H., Yamashita, S., Endo, Y., Takamura, N. (2012) Evaluation of Environmental Contamination and Estimated Radiation Doses for the Return to Residents' Homes in Kawauchi Village, Fukushima Prefecture. *PLoS ONE* 7(9): e45816. doi:10.1371/journal.pone.0045816

Tanaka, K., Iwatani, H., Sakaguchi, A., Takahashi, Y., Onda, Y. (2014) Relationship between particle size and radiocesium in river suspended sediment related to the Fukushima Daiichi Nuclear Power Plant accident. *J Radioanal. Nucl. Chem.*, 301(2): 607-613.

Tanaka, T., Tachikawa, Y., Shiiba, M., Yorozu, K., Kim, S. (2013) Numerical modeling and estimation of radioactive cesium movement at the Kuchibuto river basin, Fukushima. *Journal of Japan Society of Civil Engineers, Ser. B1 (Hydraulic Engineering)* 69: 1_487-1_492.

Teramage, M. T., Onda, Y., Kato, H., Gomi, T. (2014) The role of litterfall in transferring Fukushima-derived radiocesium to a coniferous forest floor. *Science of the Total Environment*, 490: 435–439.

Ueda, S., Hasegawa, H., Kakiuchi, H., Akata, N., Ohtsuka, Y., Hisamatsu, S., (2013) Fluvial discharges of radiocaesium from watersheds contaminated by the Fukushima Dai-ichi Nuclear Power Plant accident, Japan. J. Environ. Radioact. 118: 96-104.

Velleux, M. (2005) Spatially distributed model to assess watershed contaminant transport and fate. Ph.D. dissertation, Department of Civil Engineering, Colorado State University, Fort Collins, Colorado.

Velleux, M., Julien, P.Y., Rojas-Sanchez R., Clements, W.H., England. J.F. (2006) Simulation of metals transport and toxicity at a mine impacted watershed: California Gulch, Colorado. *Environ. Sci. Technol.,* 40(22): 6996–7004.

Velleux, M., England, J., Julien, P. (2008) TREX: Spatially Distributed Model to Assess Watershed Contaminant Transport and Fate. *Science of the Total Environment*, 404(1): 113-128.

Woolhiser, D. A., Smith, R. E., Goodrich, D. C. (1990) KINEROS, A Kinematic Runoff and Erosion Model: Documentation and User Manual. U S. Department of Agriculture, Agricultural Research Service, ARS-77, 130 p

Yamaguchi, M., Maekawa, K., Takeuchi, S., Kitamura, A., Onishi, Y. (2013) Development of a model to predict a radionuclide distribution based on soil migration after Fukushima Dai-ichi Nuclear Power Plant accident. *J. Nucl. Fuel. Cycle Environ.,* 20: 53-69.

Yamaguchi, M., Kitamura, A., Oda, Y., Onishi, Y. (2014). Predicting the long-term 137Cs distribution in Fukushima after the Fukushima Dai-ichi nuclear power plant accident: a parameter sensitivity analysis. *Journal of Environmental Radioactivity*, 135: 135-146.

Yamashiki, Y., Onda, Y., Smith, H. G., Blake, W. H., Wakahara, T., Igarashi, Y., Matsuura, Y., Yoshimura, K. (2014) Initial flux of sediment-associated radiocesium to the ocean from the largest river impacted by Fukushima Daiichi Nuclear Power Plant. *Scientific Reports* 4, 3714. doi:10.1038/srep03714.

Young, R. A., Onstad, C. A., Bosch, D. D. and Anderson, W. P. (1989) AGNPS user's guide, version 3.5. USDA-ARS North Central Soil Conservation Research Laboratory, Morris, MN.

Chapter 2

Study area and data collection

2.1 Study area

The study area is the Kuchibuto River catchment (37.51~37.63 N, 140.52~140.73 E), which is a headwater catchment within the Abukuma River watershed (Figure 2-1).

The Kuchibuto River catchment area is about 137 km^2. The elevation ranges from 200 m to 1000 m and average slope is about 9.19°(data source: 90m-SRTM DEM). The catchment belongs to subtropical humid climate zone and experiences high levels of annual precipitation. Weathering granite covers top soil resulting in high permeability, especially in forest which covers more than 60% of the catchment. Thus, this targeted catchment is a typical Japanese forested catchment.

This catchment is located about 33-49 km northwest of the Fukushima Diichi Nuclear Power Plant (FDNPP). High ^{137}Cs levels have been monitored in the catchment (Figure 2-1 and Figure 2-5). Some upstream areas of the catchment are within the evacuation/off-limits zone. Because of water flow and soil erosion, radioactive substances have being delivered to the more populated downstream regions that lead to the Pacific Ocean. Therefore, it is necessary to study the transport and fate of ^{137}Cs in this catchment.

2.2 Data collection

The collected data for the model simulation includes spatial data (Table 2-1) and on-site observation data.

Topography determines water flow in a catchment. A SRTM-based 90-meter Digital Elevation Model (DEM) was downloaded (http://glcf.umd.edu/data/srtm/) and used for generating slope, flow direction, flow accumulation, river links and sub catchments (Figure 2-1). Channel geometry of river channel (width, bank height, etc.) was defined as measured by a field survey.

Land use and soil data were obtained from the Japan Ministry of Land, Infrastructure, Transport, and Tourism (MLIT) (http://nlftp.mlit.go.jp/ksj/). There are mainly 3 land use classes (i.e. forest, cropland and paddy field) and the dominant type is forest (Figure 2-2). Four natural soil types, evolved mainly from granitic parent materials, cover the catchment: kuroboku soil, granitic forest soil, lowland soil, and gley soil. (Figure 2-3). Land use and soil properties have been measured and used by previous study (Kinouchi and Musiake, 2008). The native resolution of landuse and soil type data are about 100 m and 1000 m respectively. Landuse and soil type data were resampled into 90-m spatial solution using the majority resampling method within ArcGIS software. Radar precipitation data from the Japan Meteorological Agency (JMA) was used to specify rainfall inputs in the model (Figure 2-4). The distribution of ^{137}Cs was obtained from the airborne monitoring survey (MEXT, 2013) (Figure 2-5).

On-site measurement data which includes flow discharge, suspended sediment concentration (SSC) and solid particle size distribution. Totally, there are 19 water sampling sites in the river channel within the catchment, in which, St. D and St. M are also observation stations at the down main stream site and middle main stream site respectively for long term water levels and turbidity observation (Figure 2-1). Water levels and turbidity have been monitored at the two stations at 10-minute intervals since June 2011. These measurements are surrogates for flow rate and SSC. Water levels were monitored using a pressure-transducer gauge and were converted to flow rates using a rating curve. Turbidity was monitored by an optical sensor (MacVan Analite turbidity meter, 3000-NTU). Turbidity meter output (in mV) was converted to SSC (in g/l) based on a relationship between turbidity and laboratory analyses of SSC in stream water samples (Kinouchi et al., 2015; Yoshimura et al., 2015). Some data used were originally collected by researchers at the University of Tsukuba. Additional data to define the relationship between turbidity and SSC was obtained based on turbidity monitoring performed as part of this study (JFE-Advantec Infinity turbidity meter). During March and October 2013, suspended solid particle-size distributions were monitored at the downstream site using a Sequoia Scientific LISST-Streamside meter to measure the volume of 24 classes of solid particle ranging in size from 1.89μm to 386.38μm. The mass fraction of each suspended sediment size class of interest can be determined from measured volume fraction by assuming same particle density of different solids (2.65 kg/l). Thus, the SSC of each solid type can be determined from total SSC by multiplying it by mass fraction of each size class. Furthermore, SSC and flow rate were used to estimate the flux of each solid type.

As Kinouchi *et al.* (2015) introduced, the collected sediment samples from the downstream, middle stream and/or the upper stream sites (time-integrated or instantaneous samples) were dried in an oven at 105 ^{0}C for 24 h and disaggregated using a pestle and mortar. And then, radiocesium concentrations in sediment samples were measured by gamma-ray spectroscopy. Gamma-ray emissions at energies of 662 keV was measured using a high-purity n-type germanium coaxial gamma-ray detector (EGC25-195-R, Canberra-Eurisys) coupled to an amplifier (PSC822, Canberra-Eurisys) and a multichannel analyzer (DSA1000, Canberra). The measured results were radioactive decay-corrected to the time of sampling. Besides the measured samples in Kinouchi *et al.*'s study, additional samples were collected and measured, and used in this study.

Table 2-1. Collected spatial data for the study

items	description	data source
topography	90m×90m DEM	SRTM
land use	about 100m×100m, 6 classes	MLIT
soil properties	about 1km×1km, 4 natural soil types	MLIT
precipitation data	radar precipitation data resolution is about 1km×1km	JMA
meteorological data	air temperature, relative humidity, wind velocity and sunshine duration	MLIT
river link	generated from DEM	SRTM

* SRTM: Shuttle Radar Topography Mission digital elevation data;
MLIT: the Japan Ministry of Land, Infrastructure, Transport, and Tourism;
JMA: the Japan Meteorological Agency

Table 2-2. Landuse properties in the Kuchibuto River catchment

land use type	areal fraction	*kv*												*LAI*											
		Jan.	Feb.	Mar.	Apr.	May	Jun.	Jul.	Aug.	Sept.	Oct.	Nov.	Dec.	Jan.	Feb.	Mar.	Apr.	May	Jun.	Jul.	Aug.	Sept.	Oct.	Nov.	Dec.
paddy field	8.73%	0.01	0.01	0.1	0.1	0.3	0.5	0.7	0.8	0.5	0.5	0.01	0.01	0.01	0.01	0.1	0.5	1.0	2.0	3.0	3.0	1.5	1.0	0.01	0.01
cropland land	25.9%	0.1	0.1	0.2	0.3	0.5	0.7	0.8	0.8	0.5	0.5	0.2	0.1	0.2	0.2	0.6	1.0	1.5	1.8	2.0	2.0	1.6	1.0	0.5	0.2
forest	62.6%	0.2	0.2	0.3	0.4	0.6	0.7	0.8	0.8	0.7	0.5	0.3	0.2	1.0	1.0	1.3	1.8	2.5	2.8	3.0	3.0	2.8	2.3	1.8	1.0

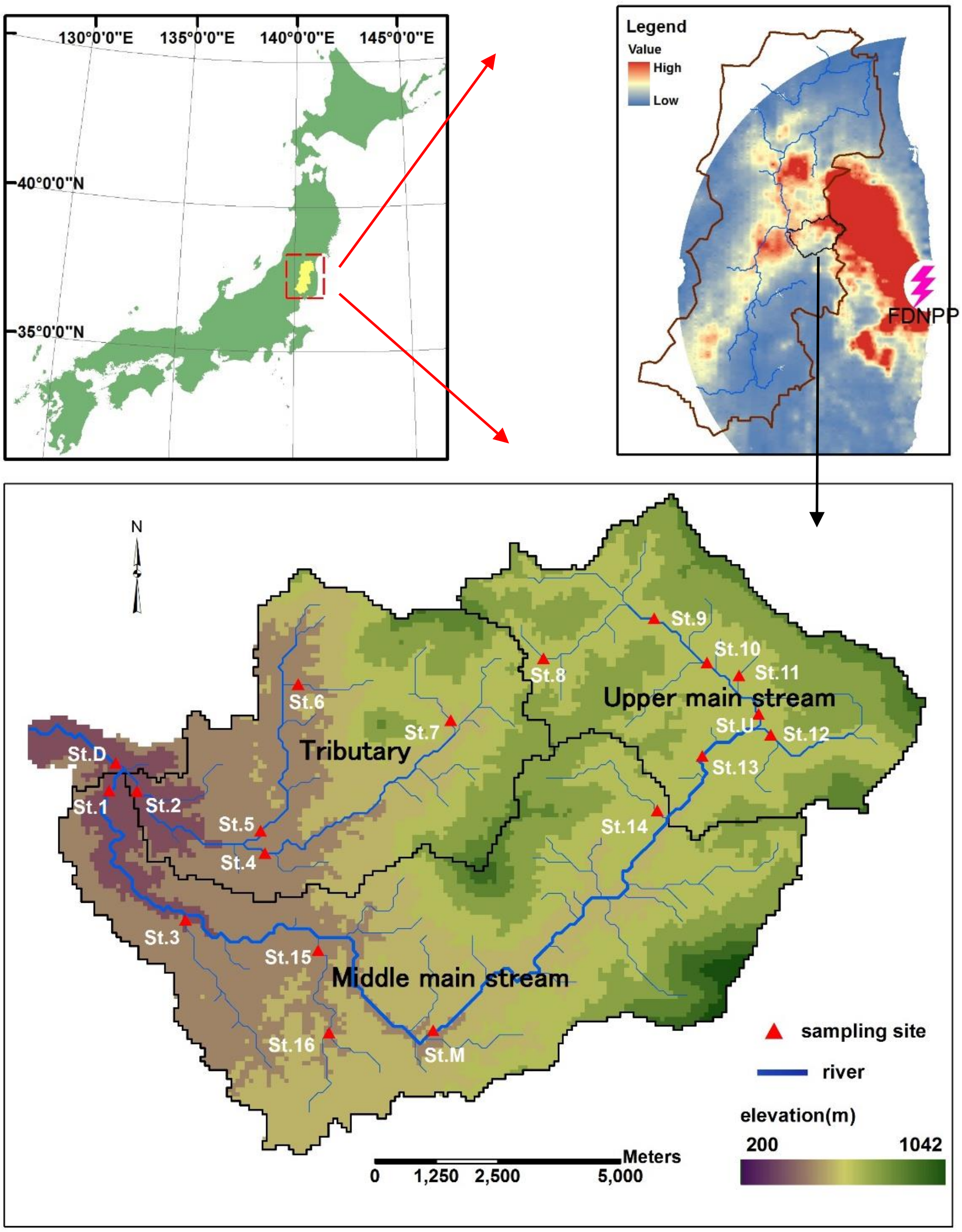

The outlet of the catchment is located about 2 kilometers below the confluence of the biggest tributary (referred to hereafter as the "Tributary") and the main Kuchibuto River. Above the confluence, the main Kuchibuto River is divided into the "Middle main stream" and "Upper main stream" in this study.

Figure 2-1. Location, topography and river systems of the Kuchibuto River catchment

.

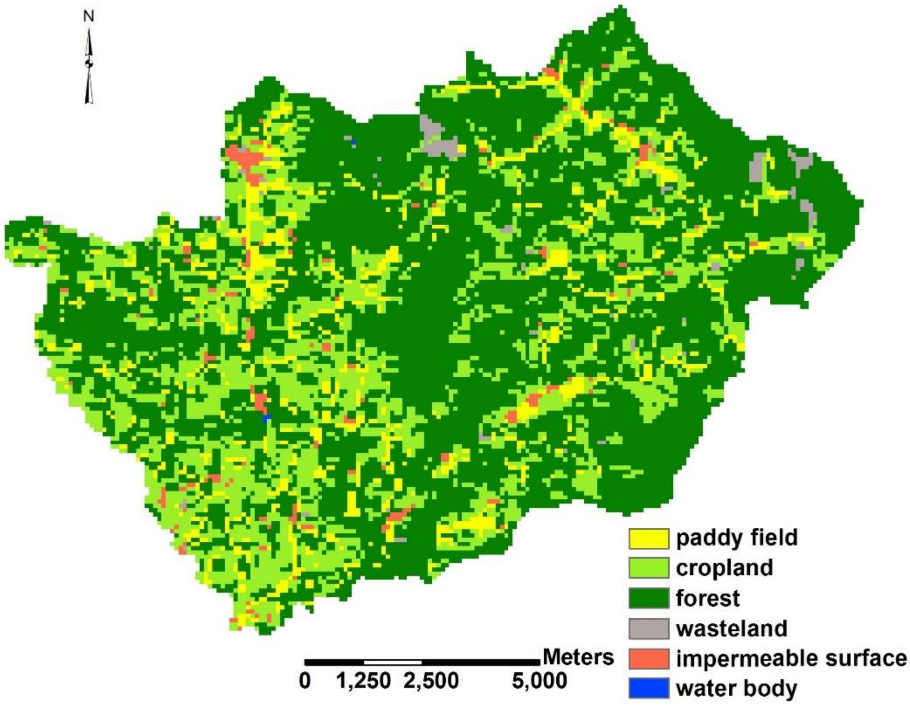

Figure 2-2. Land use in the Kuchibuto River catchment

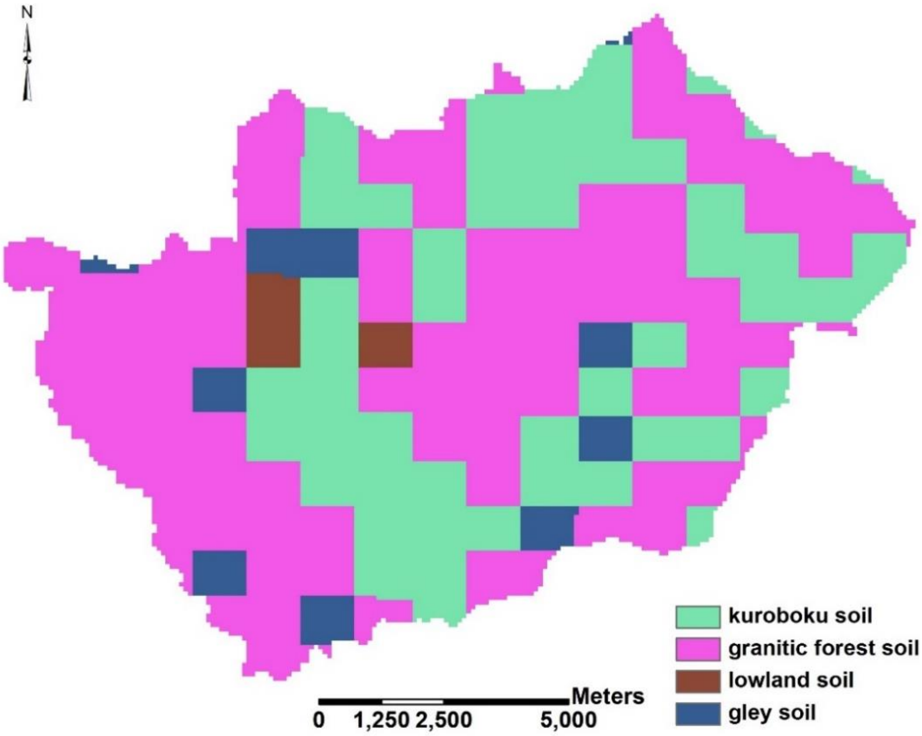

Figure 2-3. Natural soil types in the Kuchibuto River catchment

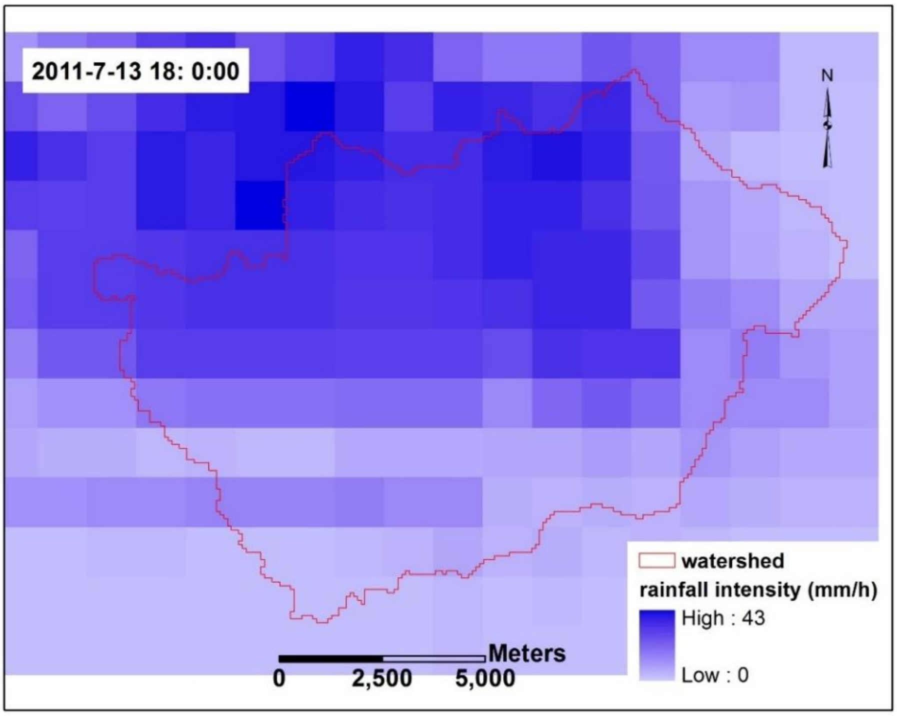

Figure 2-4. An example of input radar precipitation data (rainfall intensity at 18:00:00 on Jul. 13th, 2011)

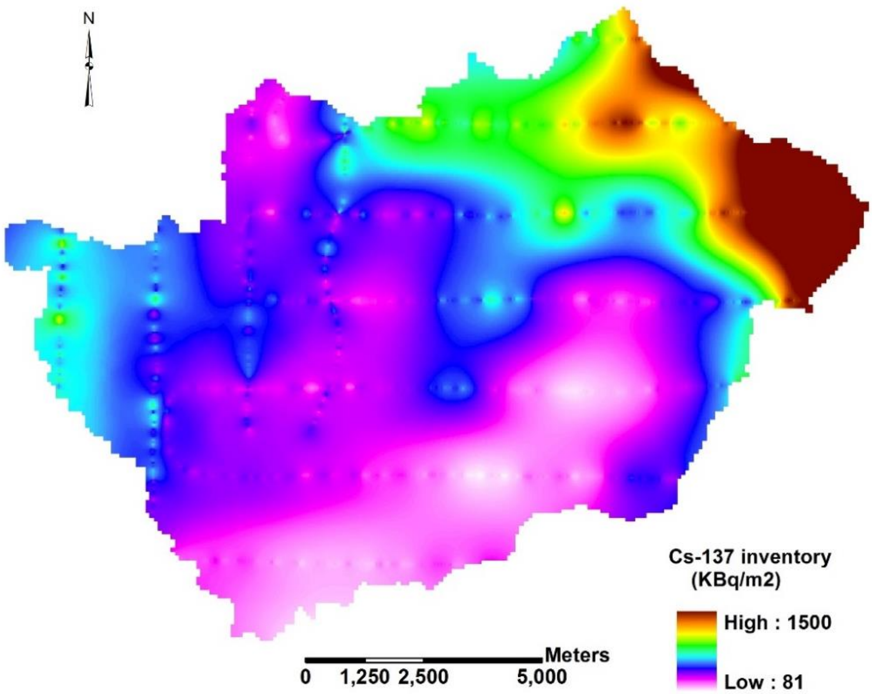

Figure 2-5. The inventory of ^{137}Cs distribution in the Kuchibuto River catchment on Jul. 2nd, 2011 (the 3rd airborne monitoring survey by MEXT (2013)).

Reference

Kinouchi, T., Yoshimura, K., Omata, T. (2015) Modeling radiocesium transport from a river catchment based on a physically-based distributed hydrological and sediment erosion model. *Journal of Environmental Radioactivity,* 139: 407–415.

Kinouchi, T., and Musiake, K. (2008) Simulating hydrological impact of environmental change in the Abukuma Watershed, Japan. 4th APHW Conference.

MEXT. (2013) Extension site of distribution map of radiation dose, etc.. http://ramap.jmc.or.jp/map/eng/.

Yoshimura, K., Onda, Y., Sakaguchi, A., Yamamoto, M., Matsuura, Y. (2015) An extensive study of the concentrations of particulate/dissolved radiocaesium derived from the Fukushima Dai-ichi Nuclear Power Plant accident in various river systems and their relationship with catchment inventory. *Journal of Environmental Radioactivity*. 139: 370-378.

Chapter 3

Improvement of the TREX model for continuous rainfall-runoff simulation for forested catchments

3.1 Introduction

Water system is a vital driving force for radioactive substances migrating from one place to another. Among various processes involved in the water cycle in catchments, rainfall-runoff is the most influential process for substance transport on land surface. Therefore, rainfall-runoff simulation is the fundamental work of our radiocesium migration study.

As mentioned in chapter 1, The TREX model was selected for our study because the model satisfies our requirements for modeling hydrological transport of radioactive substances. The TREX model is a rainfall-runoff-sediment and chemical transport model with features such as spatially distributed modeling approach, two-dimensional flow routing, well compatibility with GIS data, and capability to simulate sediment erosion and transport. The model was widely used in flood forecasting (Julien *et al.*, 1995; England *et al.*, 2007), soil erosion (Julien and Rojas, 2002), and analysis of contaminant transport and fate (Velleux *et al.*, 2006; 2008).

The hydrological module of the TREX model is original from CASC2D model (Julien *et al.,* 1995), which is an event-based rainfall-runoff model. The model can only simulate infiltration-excess Hortonian overland flow. In humid forested catchments, due to high infiltration rate of the top soil, Hortonian overland flow rarely generates. Contrarily, subsurface flow, which is formed in surface soil layer, is very important for runoff generation. This subsurface flow phenomenon is prevailing in Japanese catchments (Ishihara and Takasao, 1962). Surface soil layer with a depth of several tens-or-hundreds centimeters commonly exists in Japanese forested catchment. Beneath this layer, there is a relatively impermeable layer, which consists of fine soil deposits. Water infiltrated from the surface will be temporally stored in this topsoil layer, and then, the lateral subsurface flow along its bottom occurs when soil water volume is bigger than field capacity. Therefore, it is challenge to apply TREX model for simulation in Japanese forested catchments (e.g. the Kuchibuto River catchment). Thus, to overcome the shortcomings of the model for hydrological simulation, the main objective of this chapter is to improve hydrological module of the model to enable us to simulate rainfall-runoff processes in forested catchments while taking a full advantage of features of TREX model to study the migration of radioactive substances in Fukushima.

3.2 Model description

The hydrological module of the TREX model includes precipitation, interception, infiltration, storage, two-dimensional overland and one dimensional channel flows as shown in Figure 3-1(Julien *et al.,* 1995; Velleux, 2005, Velleux *et al.*, 2008). As Figure 3-2 shows, we improved this model by considering subsurface flow in a top soil layer, and change of soil moisture due to the water movement in the ground and from the surface soil. Infiltration and interception parts were also modified. The modified model will be described in following sections.

3.2.1 Precipitation

In the model, the rainfall intensity can be assumed to be variable or uniform depending on data source (e.g. station data or radar precipitation data). When more than one rain station data are used in estimation of the precipitation, an interpolation scheme (e.g. the inverse distance weighted mothed) can be used to calculate rainfall intensity for each computational cell. For our study, we modified the model to read radar precipitation data every half an hour continuously, and consider rainfall intensity is uniform within 1 km × 1 km grid (spatial resolution of radar data is 1km).

The total gross precipitation (i_g) includes both rainfall and snowfall. Snowfall can be represented as an equivalent precipitation. Snow melt rate can be simply estimated by temperature degree-day method:

$$i_{sn} = \frac{1}{86400000} \alpha_{sn} \ (T - T_0) \tag{3.1}$$

where, i_{sn} is snow melt rate (m/s); α_{sn} is the degree-day coefficient (mm/degree-day C); T is temperature (°C); T_0 is base temperature for snowmelt (°C).

3.2.2 Canopy interception

As precipitation falls to the surface, a portion of the gross precipitation at the surface may contact vegetative canopy and may be held on foliage by surface tension (Eagleson, 1970). Much of the precipitation falling during the early period of an event may be stored on vegetative surfaces (Linsley *et al.*, 1982), and the intercepted water can be evaporated and return to the atmosphere. In hydrological model, the intercepted water is usually subtracted from the rainfall/snowfall before infiltration is calculated. The original model gives an interception depth depending on land use type. Canopy interception depends strongly on vegetation type and stage of development, which can be characterized by the leaf area index (*LAI*) (Kozak *et al.*, 2007). We use the method developed by Von Hoyningen-Huene (1981) to calculate the maximum canopy storage capacity (S_{max}^{c}), which is considered as interception depth.

$$S_{\max}{}^{c} = 0.935 + 0.498LAI - 0.00575(LAI)^2 \tag{3.2}$$

Net rainfall intensity (i_n) is calculated as:

$$i_n = i_g - \frac{S_{\max}{}^{c} - S_c}{\Delta t} \tag{3.3}$$

where, i_n is net rainfall intensity (m/s); S_c is water stored in canopy (m); Δt ls time interval (s).

3.2.3 Evapotranspiration

Evapotranspiration is calculated to update top soil moisture timely, which is an initial condition of infiltration. In this study, evapotranspiration is estimated by FAO Penman-Monteith method, which takes grass as a reference, and uses the formula of the reference evapotranspiration (ET_0) (Allen *et al.*, 1998; 2006):

$$ET_0 = \frac{0.408\Delta(R_n - G) + \gamma \dfrac{C_n}{T + 273} U_2 (e_s - e_a)}{3600[\Delta + \gamma(1 + C_d U_2)]} \tag{3.4}$$

where, ET_0 is a reference evapotranspiration (m/s); R_n is the net radiation (MJ/m^2/hour); G is the soil heat flux (MJ/m^2/hour); ($e_s - e_a$) represents the vapor pressure deficit of the air (kPa); Δ is the slope of the saturation vapor pressure temperature relationship (kPa/°C); γ is the psychrometric constant (kPa/°C); U_2 is daily or hourly wind speed at 2-m height (m/s); C_n and C_d are constants. For hourly time step simulation, C_n=37, and C_d=0.24 and 0.96 during daytime and nighttime, respectively.

We assumes that evapotranspiration occurs from vegetated and non-vegetated surface (bare land, or water surface), following the formulation described below.

a) Evapotranspiration from vegetated surface

Potential evapotranspiration rate from vegetated surface (*etp*1) is given by:

$$etp1 = kv \cdot kc \cdot kl \cdot ET_0 \tag{3.5}$$

where, *etp*1 is potential evapotranspiration rate from vegetation (m/s); *kv* is fraction of vegetation in each cell (-); *kl* is relative leaf area index, which is a ratio of *LAI* and maximum *LAI* in one year (-); *kc* is crop coefficient (-), which is related to vegetation types, growing season, agricultural practices, and etc.

FAO provides tabulated *kc* values of different vegetation types in different seasons. In this study, for simplicity, we divided the period of vegetation growth into two stages — growing season (from April to October) and non-growing season, and three dominant vegetation types — tree, grass and paddy are considered. For tree, grass/plant and paddy, *kc* are set to 1.2, 1.0, 1.1 in growing season, and 0.9, 0.3, 0.3 in non-growing season, respectively.

Evapotranspiration from soil in vegetated surface, *etr*1 (m/s), is given by:

$$etr1 = kr(etp1 - ET_c) \tag{3.6}$$

where, ET_c is evapotranspiration from vegetation canopy (m/s), and given by:

$$ET_c = etp1 \qquad if\ (Sc > etp1\Delta t) \tag{3.7a}$$

$$ET_c = \frac{Sc}{\Delta t} \qquad if\ (Sc \le etp1\Delta t) \tag{3.7b}$$

kr is coefficient related to soil characteristic:

$$kr = 1 \qquad if\ (\theta > \theta_f) \tag{3.8a}$$

$$kr = \frac{\theta - \theta_w}{\theta_f - \theta_w} \qquad if\ (\theta_f \geq \theta \geq \theta_w) \tag{3.8b}$$

$$kr = 0 \qquad if\ (\theta < \theta_w) \tag{3.8c}$$

where, θ is soil water content (m^3/m^3); θ_f is field capacity (m^3/m^3); θ_w is wilting point (m^3/m^3).

b) Evaporation from non-vegetated surface

Potential evaporation from non-vegetated surface, *etp*2 (m/s), is given by:

$$etp2 = (1 - kv)ET_0 \tag{3.9}$$

Evaporation from soil in non-vegetation area is given by:

$$etr2 = kr(etp2 - ET_s) \tag{3.10}$$

where, *etr*2 is evaporation from non-vegetated soil (m/s).

ET_s is the evaporation from non-vegetated land surface (m/s), and given by:

$$ET_s = etp2 \qquad if\ (S_l > etp2\Delta t) \tag{3.11a}$$

$$ET_s = \frac{S_l}{\Delta t} \qquad if\ (S_l \leq etp2\Delta t) \tag{3.11b}$$

where, S_l is water stored in land surface (m).

Total amount of evapotranspiration *ET* is the sum of evapotranspiration from canopy and overland surface stored water (ET_c and ET_s) and evaporation from soil (*etr*1 and *etr*2). Soil water content is reduced by the sum of *etr*1 and *etr*2.

3.2.4 Infiltration

Infiltration is simulated by a single-layer Green-Ampt infiltration model, which assumes that soil profile is vertical homogeneous.

$$f = K_s(1 + \frac{\varphi\Delta\theta}{F}) \quad (3.12)$$

where, f is infiltration rate (m/s); K_s is saturated hydraulic conductivity (m/s); φ is suction head (m); $\Delta\theta$ is soil moisture deficit (m^3/m^3); F is infiltration depth (m).

In the model, one constraint condition of infiltration is that if ponding water is not available for potential infiltration, actual infiltration rate will be equal to water depth divided by time:

$$f = \min(f, \frac{h}{\Delta t}) \quad (3.13)$$

where, h is surface water depth (m).

Because our study area is hilly catchment with steep slopes, and well developed drainage system (many small streams, brooks, and even ditches), there is almost no ponding water. Therefore, we modify constraint condition as:

$$f = \min(f, i_n) \quad (3.14)$$

3.2.5 Storage

The model can consider storage capacity both on the land surface and river channel. Water on the land surface may be stored in depressions because of micro topography and/or land use (e.g. paddy field). Water in channels may also be stored as dead storage.

3.2.6 Overland flow and channel flow

In this study, we still use the proposed methods to calculate overland and channel flows (Julien *et al*., 1995; Velleux, 2005).

Overland flow is routed in two-dimensional and simulated using the diffusive wave approximation. Flow occurs when the water depth exceeds the storage depth and the friction slope is bigger than zero. Overland flow is governed by conservation of mass and conservation of momentum. The two-dimensional continuity equation for gradually-varied flow over a plane is:

$$\frac{\partial h}{\partial t}+\frac{\partial q_x}{\partial x}+\frac{\partial q_y}{\partial y}=i_n+i_w \tag{3.15}$$

where, q_x, q_y are unit discharge x- or y- directions respectively (m^2/s); i_w is unit discharge from/to a point source/sink (m/s).

Momentum equations for the x- and y-directions may be derived by relating the net forces per unit mass to flow acceleration. By neglecting small terms (terms for local and convective acceleration), the full Saint-Venant equations may be simplified in the diffusive wave approximation for the x- and y-directions:

$$S_{f\,x}=S_{f\,ox}-\frac{\partial h}{\partial x} \tag{3.16}$$

$$S_{f\,y}=S_{f\,oy}-\frac{\partial h}{\partial y} \tag{3.17}$$

where, S_{fx}, S_{fy} are friction slope in x- or y- directions respectively (-); S_{ox}, S_{oy} are ground surface slope in the x- or y-direction (-).

Manning formulation is used to solve the overland flow equations. The depth-discharge relationships are:

$$q_x=\frac{\sqrt{S_{f\,x}}}{n}h^{\frac{5}{3}} \tag{3.18}$$

$$q_y=\frac{\sqrt{S_{f\,y}}}{n}h^{\frac{5}{3}} \tag{3.19}$$

where, n is manning roughness coefficient (-);

Channel flow is one-dimensional (along the channel in the down-gradient direction) and also simulated using the diffusive wave approximation. The one-dimensional continuity equation for gradually-varied flow along a channel is:

$$\frac{\partial A_c}{\partial t}+\frac{\partial Q}{\partial x}=q_l \tag{3.20}$$

where, A_c is channel flow cross-sectional Area (m^2); Q is total channel discharge (m^3/s); q_l is lateral unit flow (into or out of the channel) (m^2/s);

Based on the momentum equation for the down-gradient direction and neglecting small terms, the diffusive wave approximation may be used for the friction slope. Similarly, the Manning relationship was used to solve the channel flow equations:

$$Q = \frac{1}{n} A_c R^{\frac{3}{2}} S_f^{\frac{1}{2}} \tag{3.21}$$

where, R is hydraulic radius of flow (m); S_f is channel friction slope in the down-gradient direction (-);

3.2.7 Subsurface flow in top soil

In our modification, we calculate lateral subsurface flow and vertical flow in the top soil. Lateral subsurface flow is calculated by a simple kinematic storage model (Sloan *et al.*, 1983). The water balance in soil layer is expressed as:

$$\frac{dSW}{dt} = fL - dq_l - dq_p - (etr1 + etr2)L \tag{3.22}$$

where, SW is volume of stored water per unit width (m^3/m); L is slope length (m); dq_l and dq_p are lateral flow and vertical percolation rate per unit overland width (m^2/s), respectively.

According to Darcy's law, the lateral flow rate is determined as:

$$dq_l = cl \frac{2SW_e}{(\theta_s - \theta_f)L} K_e \sin\alpha_{slp} \tag{3.23}$$

$$SW_e = SW - D\theta_f L \tag{3.24}$$

where, cl is adjustable coefficient of lateral flow rate (-); SW_e is drainable volume of water in the soil layer (m^3/m); θ_s is saturated water content (m^3/m^3); θ_f is field capacity (m^3/m^3); K_e is efficient lateral hydraulic conductivity (m/s); α_{slp} is slope angle (°); D is soil depth (m).

Because of soil porosity and characteristic of drainage systems in hillslope, efficient lateral hydraulic conductivity (K_e) is usually bigger than measured saturated hydraulic conductivity (K_s) from the small-scale soil matrix (Borah, 2007; Brooks *at al.*, 2004). Furthermore, because of micro-relief in hillslope, real slope angle sometimes is bigger than the grid-based computed slope angle α_{slp}. In this study, we set K_e as equal to K_s, and α_{slp} was calculated from grid-averaged elevation data. *cl* was calibrated with K_s and α_{slp} kept unchanged.

Two kinds of return flow were considered in our modification. As Figure.3-3 shows, the first one: when the water depth in the top soil exceeds the thickness of the top soil the interflow in the top soil will return to the ground surface and become overland flow. The second is if there is river channel in the computational cell, the subsurface lateral flow will also return and become surface flow. In our hilly catchment, drainage ways are not limited in rivers, but also very small streams, ditches, and even roads, so, the second type of return flow is very common. In light of this phenomenon, in the model the lateral water flow returns to the overland, and joins the overland flow.

Vertical water percolation from topsoil to underlying soil and aquifer layers is calculated using a storage routing method, which is used in SWAT model (Arnold, 1998).

$$dq_p = SW_e\left[1 - e^{\left(\frac{\Delta t}{K_s}(\theta_s - \theta_f)\right)}\right] \tag{3.25}$$

3.2.8 Groundwater flow

A linear reservoir method is employed to calculate groundwater flow (zhao, 1997):

$$dq_{g,t_2} = \omega dq_{g,t_1} + (1-\omega)dq_p \tag{3.26}$$

where, dq_p is water percolated from top soil (m^3/s); dq_g is groundwater flow (m^3/s). Subscripts *t1* and *t2* refer to the beginning and end of the time period, respectively. ω is recession coefficient (-).

The whole catchment is divided into many small sub-watersheds. The groundwater flow joins the channel flow at the outlet of each sub-watershed.

3.3 Model evaluation

In this study, three metrics were used to evaluate simulation results.

Nash-Sutcliffe Efficiency (*NSE*):

$$NSE = 1 - \frac{\sum_{i}^{n} (Q_i^{obs} - Q_i^{sim})}{\sum_{i}^{n} (Q_i^{obs} - Q_{mean}^{obs})} \quad (3.27)$$

RMSE-observation standard deviation ratio (*RSR*):

$$RSR = \frac{\sqrt{\frac{1}{n}\sum_{i}^{n} (Q_i^{obs} - Q_i^{sim})}}{\sqrt{\frac{1}{n}\sum_{i}^{n} (Q_i^{obs} - Q_{mean}^{obs})}} \quad (3.28)$$

Percent bias (*PBIAS*):

$$PBIAS = \frac{\sum_{i}^{n} (Q_i^{obs} - Q_i^{sim})}{\sum_{i}^{n} Q_i^{obs}} * 100\% \quad (3.29)$$

where, $Q^{obs}{}_i$ and $Q^{sim}{}_i$ are the observed and simulated value, respectively, $Q^{obs}{}_{mean}$ is the average observed value.

Moriasi *et al.* (2007) proposed that simulations can be judged as "satisfactory" when $NSE > 0.50$, $RSR < 0.70$, and $|PBIAS| < 25\%$ for streamflow and when $|PBIAS|$ is $< 55\%$ for sediment over a monthly performance evaluation period. As the model evaluation time period increases, more stringent acceptability criteria may be warranted. However, the performance metrics and criteria suggested by Moriasi *et al.* (2007) served as an established point of reference and were used to evaluate the acceptability of model results for this study.

3.4 Model application and results

The enhanced model was applied in the Kuchibuto River catchment, which was introduced in chapter 2. As a result of industrial and agricultural activities, the properties of natural soil have been altered. Thus, besides the four natural soil types, other three soil types were introduced in our classification of the top soil considering the actual land use, i.e., sealed soil, where the land use types mainly are residual, road, etc., paddy soil, and cropland soil. As plough layer exists, the vertical variation of soil properties of paddy and cropland soil is significant. Therefore, the thickness of topsoil for paddy and cropland soil was assumed to be less than that of other soil types. Soil properties that used in this study are listed in Table 3-1. Leaf area index (*LAI)* and vegetation fraction *(kv)* were determined by land use and season (Table 2-2).

Four flood events in 2011 (event 20110704, event 20110819, event 20110919, event 20111005) were selected to calibrate the model. From our preliminary simulations, we found that *cl* was sensitive and need to be well calibrated. We used "basin-wide multipliers" to adjust these parameters (Vertessy, 2000). 10, 15, 20, 25, 30, 40, 45, 50 for multipliers of *cl*. Performances of each parameter setting were compared by *PBIAS, NSE* and *RSR* averaged for four events (Figure 3-4). The Figure shows that best result (*PBIAS* is closed to 0, and *NSE* is biggest and *RSR* is smallest) was obtained when *cl* = 30, which means lateral saturated hydraulic conductivity (K_s) and slope angle (α_{slp}) need to be multiplied by 30. The combination gave reasonable results of hydrographs for four events (Figure 3-5, 3-6, 3-7, and 3-8). Hereafter, we used this combination in further simulations.

Table 3-2 shows the compared evaluation criteria of simulated flow rates by the original model and improved model. From Figure 3-5 to Figure 3-8, the results that were simulated using original TREX model with the same parameters were also plotted. The evaluation criteria and hydrograph indicate that improved model is superior to the original model, mainly because of the inclusion of subsurface and groundwater flow processes, and modification of infiltration constraint condition. We take the event 19 September 2011 as an example to analyze the contribution of them. Figure 3-9 compared the simulated result for different cases. The observed total flow volume in this event (Sep. 19 19:00 ~ 24 0:00) is 8.7×10^6 m^3. Simulated total flow volume by the original model (case

1) was 2.7×10^6 m^3. If infiltration constraint condition was modified only, simulated total flow volume (case 2) was 5.1×10^6 m^3. For case 3, which included subsurface and groundwater flow processes and modification of infiltration constraint condition, simulated total flow volume was 9.0×10^6 m^3.

Comparisons between measured and simulated flows for 2011 ~ 2014 at the downstream site and the middle stream site are shown in Figure 3-10 and Figure 3-11 respectively (data collection of flow rates started on Jun. 21, 2011 13:00 and ended on Oct. 7, 2013 16:00 at the middle stream site and ended on Dec. 31, 2014 24:00 at the downstream site.). Table 3-3 shows the three evaluation criteria for flow in 2011 ~ 2014. Because $NSE \geq 0.61$, $RSR \leq 0.62$, and $|PBIAS| \leq 18\%$ at the middle and downstream sites in the three years, the simulated flow rates are acceptable. During the simulation period (i.e. Jan. 1, 2011- Dec. 31, 2014), it is estimated 4.1×10^8 m^3 water flowed out of the catchment to the Abukuma River.

3.5 Summary and conclusions

In this chapter, hydrological module of the TREX model was improved by taking subsurface flow, groundwater flow, and evapotranspiration into account. Lateral and vertical subsurface flows were calculated by a simple kinematic storage model and a storage routing method, respectively. A linear reservoir method was employed to calculate groundwater flow. Evapotranspiration was estimated by FAO Penman-Monteith method. Infiltration and interception parts also were modified.

The improved TREX model was applied to the Kuchibuto River catchment, Fukushima Prefecture, Japan. Four events in 2011 and events in 2012-2014 were selected to calibrate and validate the model, respectively. The comparisons show the improved TREX model gave better results than the original TREX with same parameters. The simulated flow rates for 2011-2014 are acceptable. It is estimated 4.1×10^8 m^3 water flowed out of the catchment to the Abukuma River during the three years. This improved TREX model will be further used to study the transport of eroded sediments and radiocesium in this catchment.

Table 3-1. Soil properties used in the model.

Soil name	D	K_s	φ	θ_s	θ_f
kuroboku soil	1.00	7.00×10^{-6}	0.15	0.60	0.35
forest soil	1.00	1.00×10^{-5}	0.15	0.60	0.35
lowland soil	1.00	5.50×10^{-7}	0.20	0.60	0.35
gley soil	1.00	5.00×10^{-7}	0.20	0.60	0.35
sealed soil	1.00	1.00×10^{-9}	0.15	0.60	0.35
paddy soil	0.50	1.00×10^{-8}	0.25	0.55	0.40
cropland soil	0.50	2.00×10^{-6}	0.20	0.60	0.35

* D: thickness of top soil (m), φ: suction head (m), K_s: saturated hydraulic conductivity (m/s), θ_s: saturated water content (m^3/m^3), θ_f: field capacity (m^3/m^3).

Table 3-2. Evaluation criteria of simulated flow rates

		event 20110704		event 20110819		event 20110919		event 20111005	
		modification	original	modification	original	modification	original	modification	original
the downstream site	*NSE*	0.92	0.09	0.79	-0.25	0.96	0.29	0.73	-0.35
	RSR	0.29	0.95	0.46	1.12	0.21	0.84	0.51	1.2
	PBIAS (%)	7	57	-8	27	-3	12	-17	47
the middle stream site	*NSE*	0.95	0.70	0.46	0.01	0.98	0.13	0.67	-1.0
	RSR	0.23	0.54	0.73	0.99	0.14	0.93	0.57	1.43
	PBIAS (%)	-16	39	-17	21	2	16	9	54

Table 3-3. Evaluation criteria of simulated flow rates

location	coefficient	2011	2012	2013	2014
the downstream site	*NSE*	0.93	0.69	0.91	0.80
	RSR	0.26	0.56	0.30	0.45
	PBIAS (%)	-9%	-18%	-17%	11%
the middle stream site	*NSE*	0.96	0.62	0.80	-
	RSR	0.20	0.62	0.45	-
	PBIAS (%)	5%	-10%	14%	-

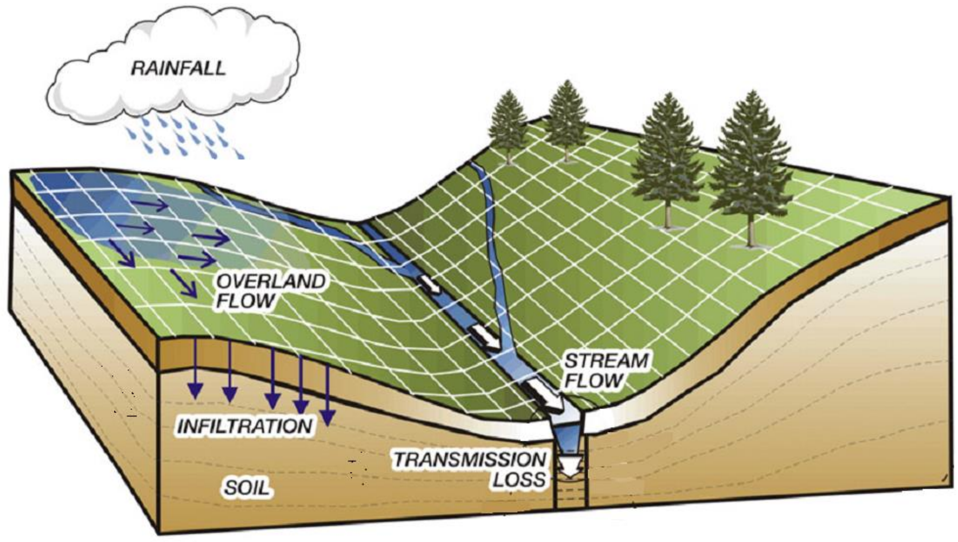

Figure 3-1. Hydrological components of the original TREX model (Velleux *et al.*, 2008)

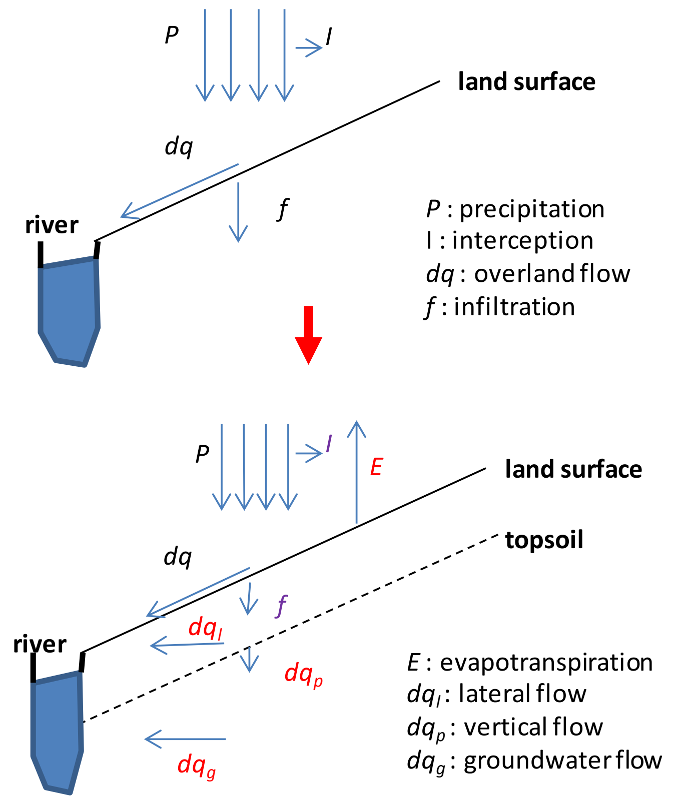

Figure 3-2. Hydrological module of the original TREX model and modification in this study (*E*, dq_l, dq_p, dq_g are newly included, *I and f* are modified)

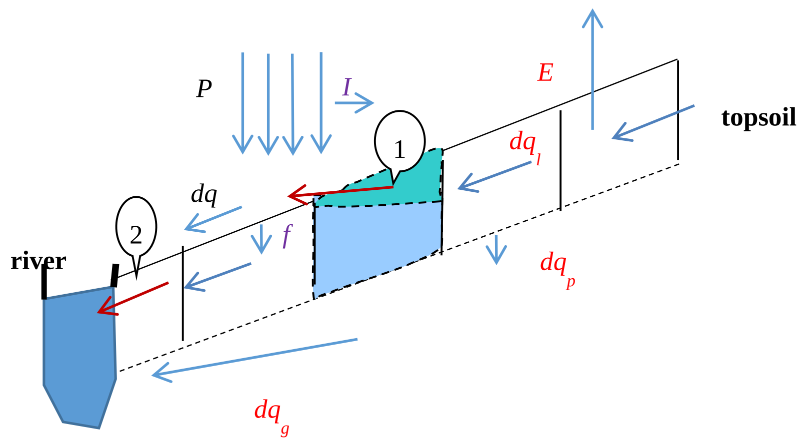

Figure 3-3. Two kinds of return flow are considered in the model.

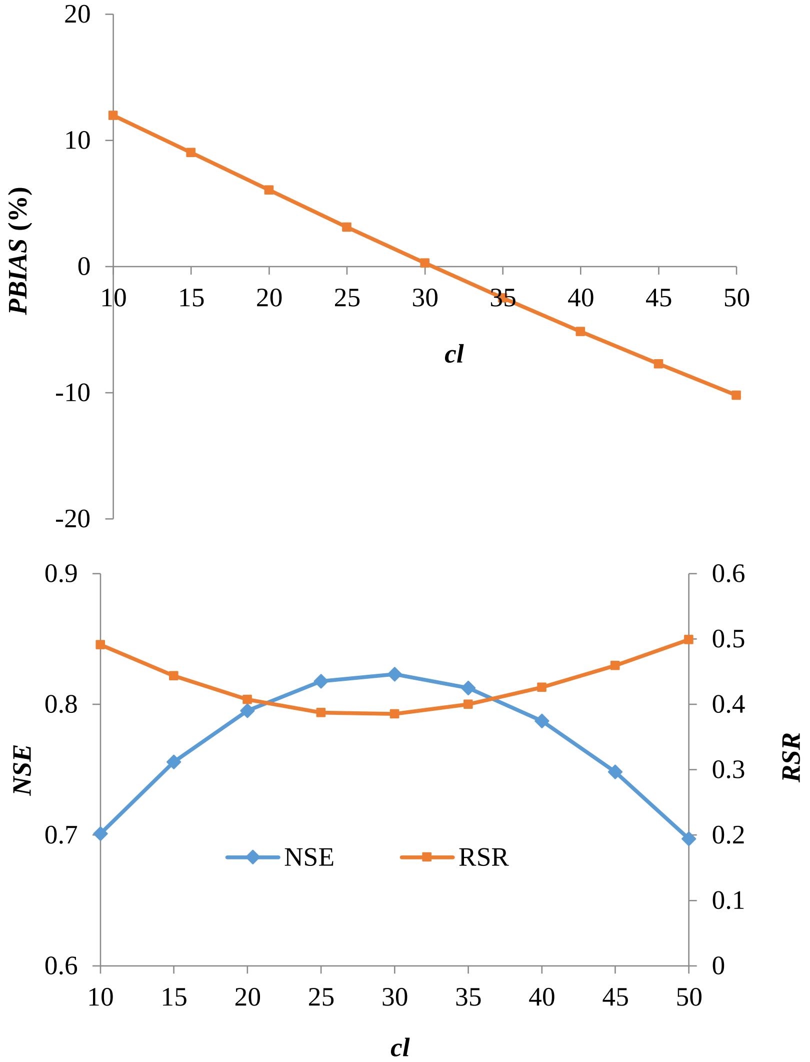

Figure 3-4. Averaged evaluation criteria values for the selected 10 cases.

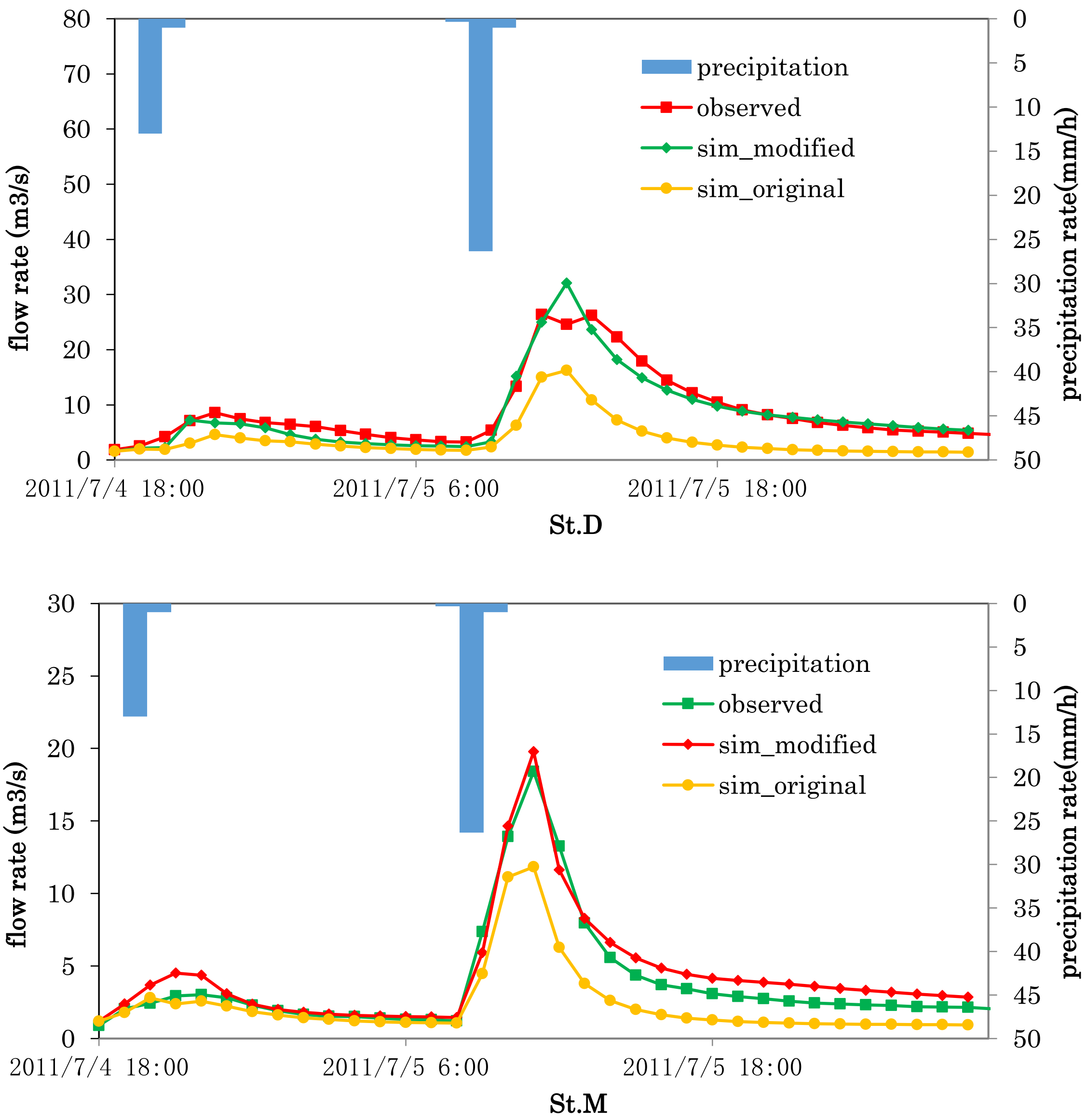

Figure 3-5. Simulated flow rates of event 20110704 at the downstream site (St.D) and middle stream site (St.M). sim_modified and sim_original mean simulated flow rate based on the modified model and original model, respectively. Precipitation rate is the average value.

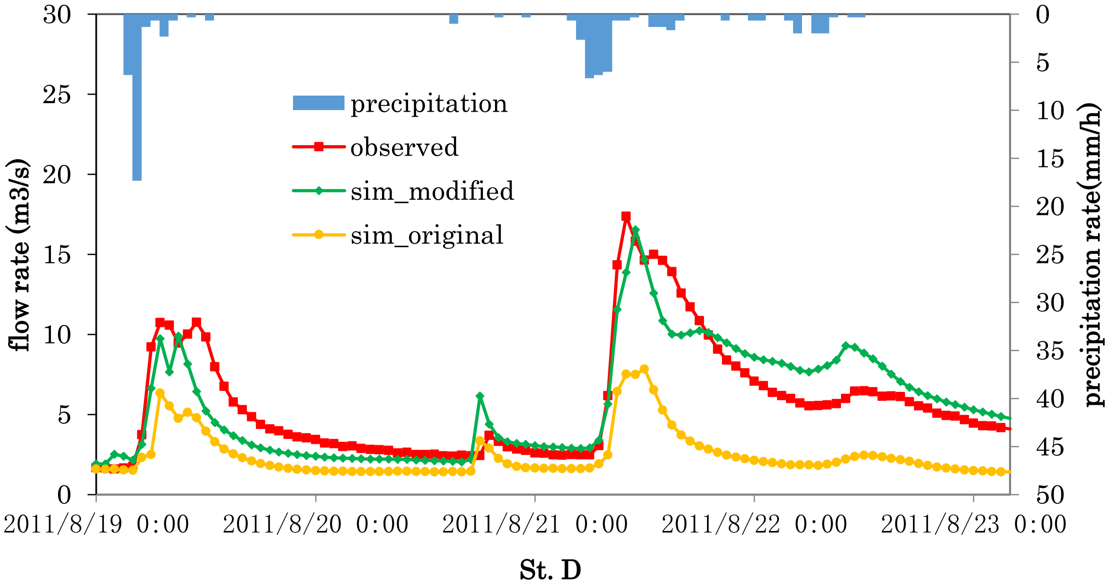

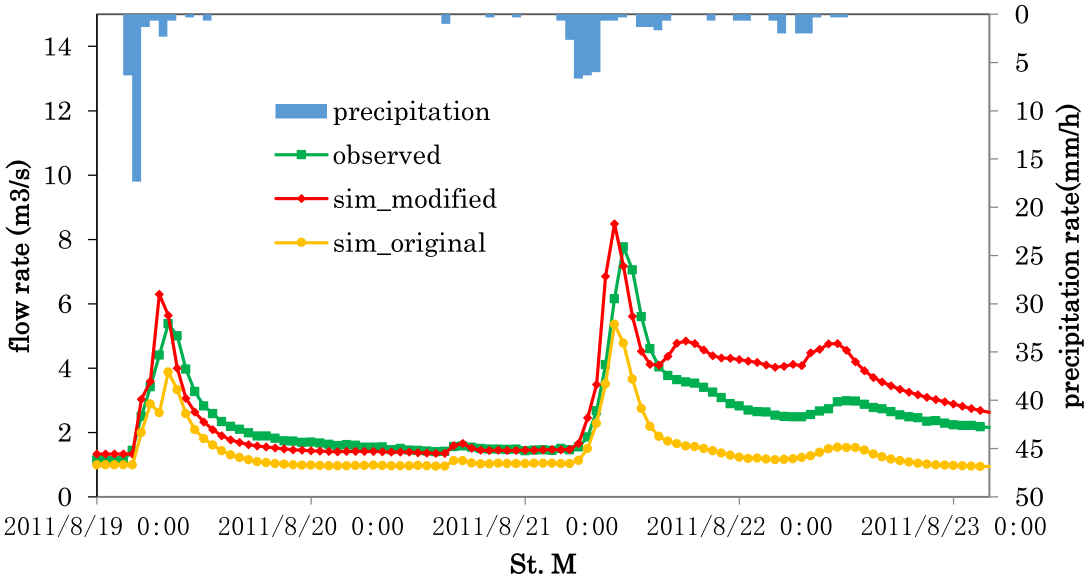

Figure 3-6. Simulated flow rates of event 20110819 at the downstream site (St. D) and middle stream site (St. M). (legends are same as Figure 3-4).

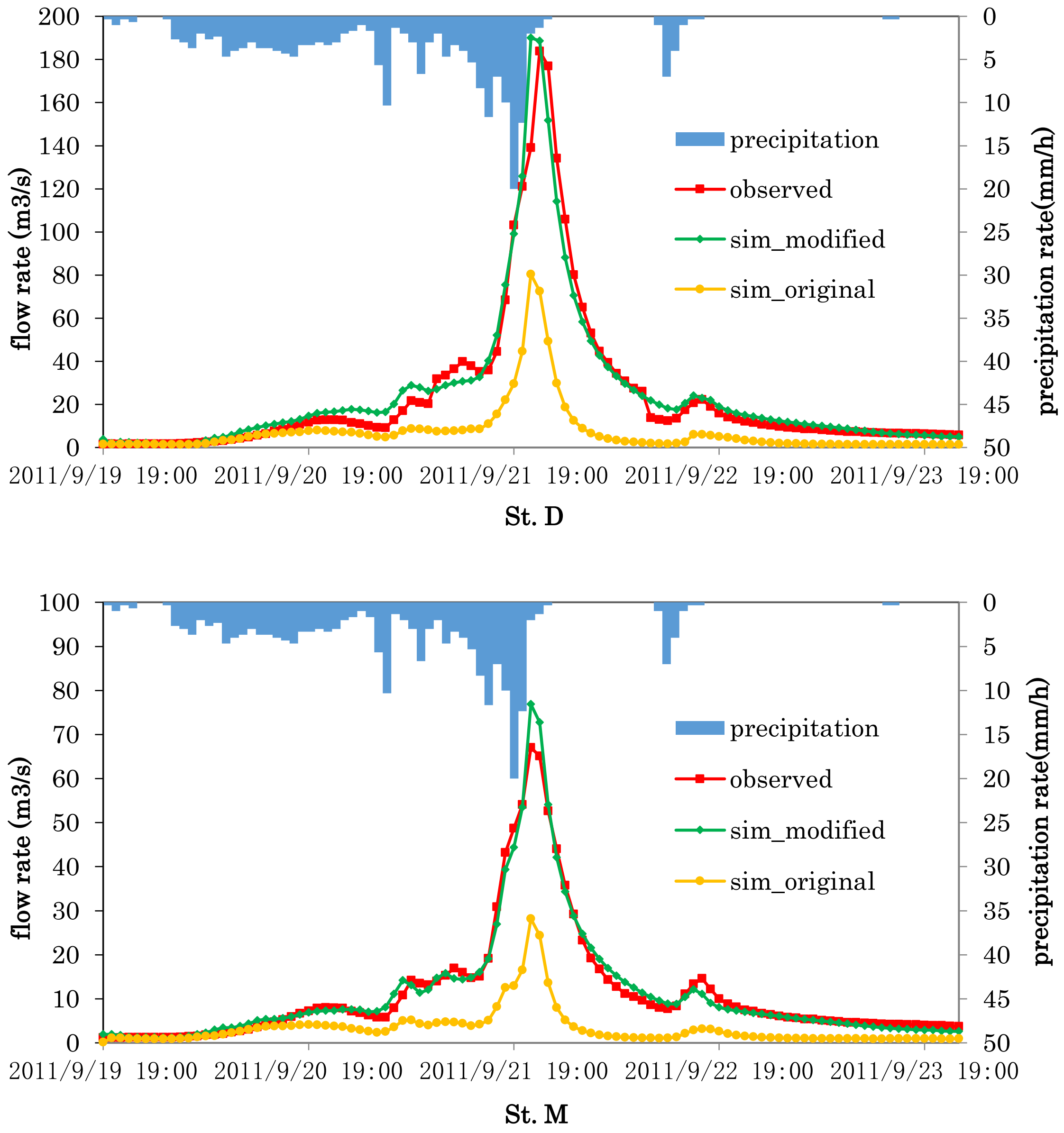

Figure 3-7. Simulated flow rates of event 20110919 at the downstream site (St. D) and middle stream site (St. M). (legends are same as Figure 3-4).

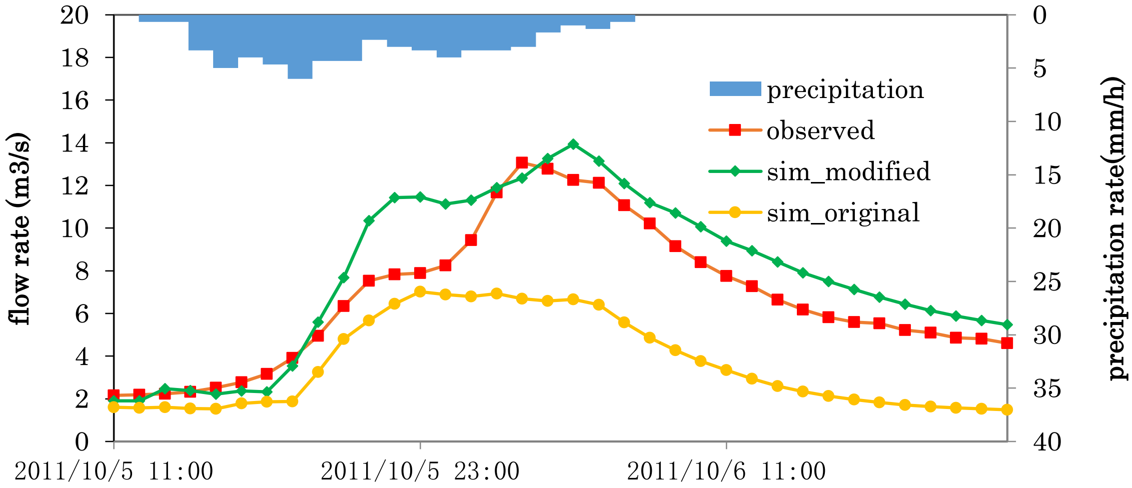

St. D

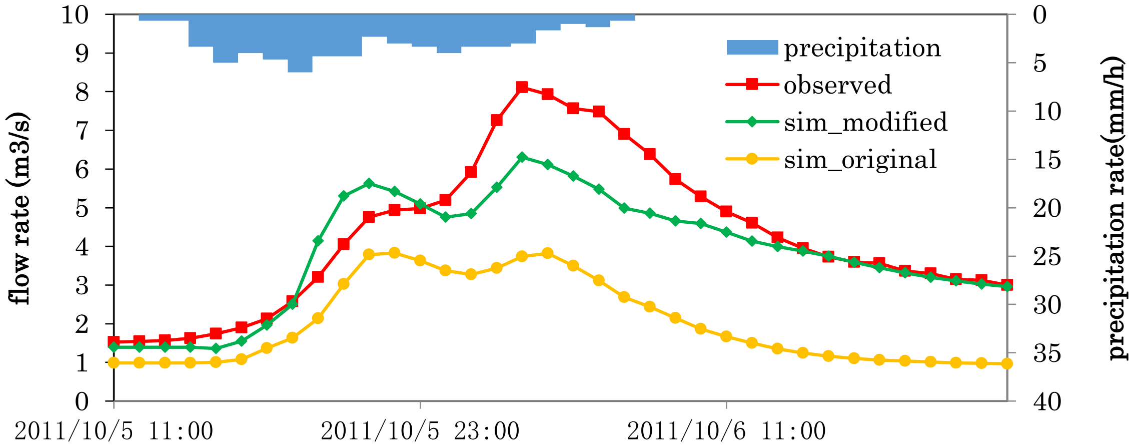

St. M

Figure 3-8. Simulated flow rates of event 20111005 at the downstream site (St. D) and middle stream site (St. M). (legends are same as Figure 3-4).

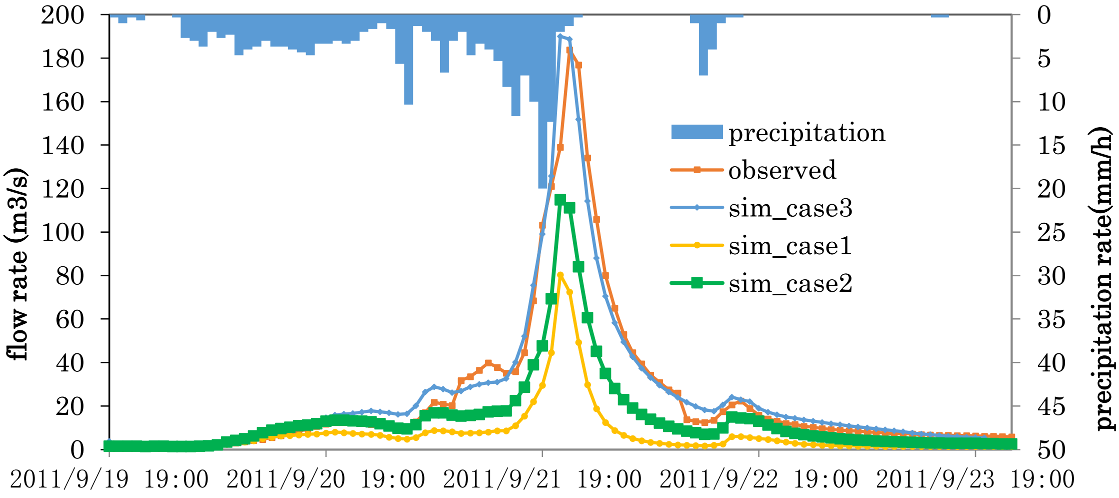

case 1: the original TREX model;

case 2: only change infiltration constraint condition.

case 3: add subsurface flow module and modify infiltration constraint condition.

Figure 3-9. Comparison of simulated results at the downstream site for the biggest typhoon event for different cases

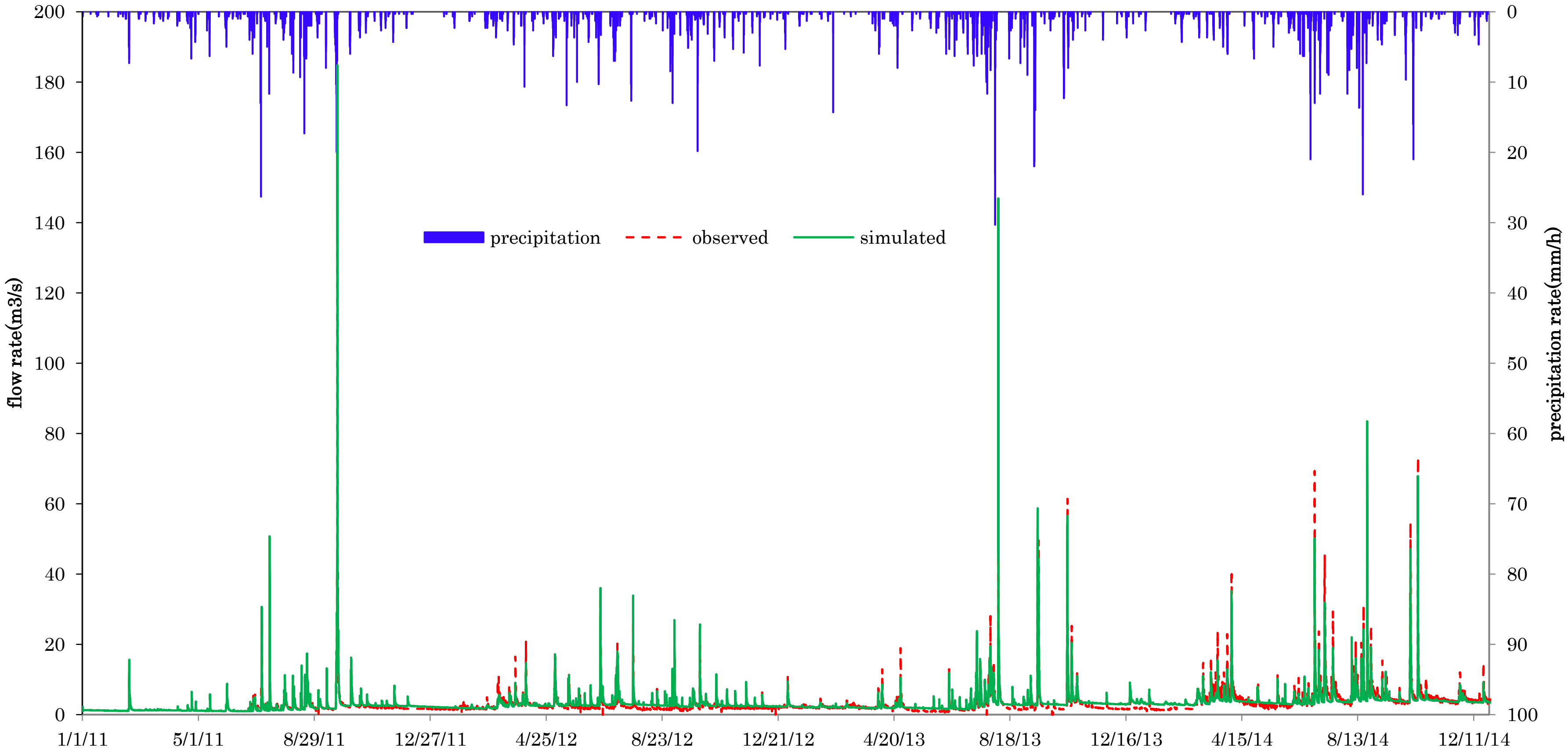

Figure 3-10. Simulated flow rates from 2011 to 2014 at the downstream site (St. D).

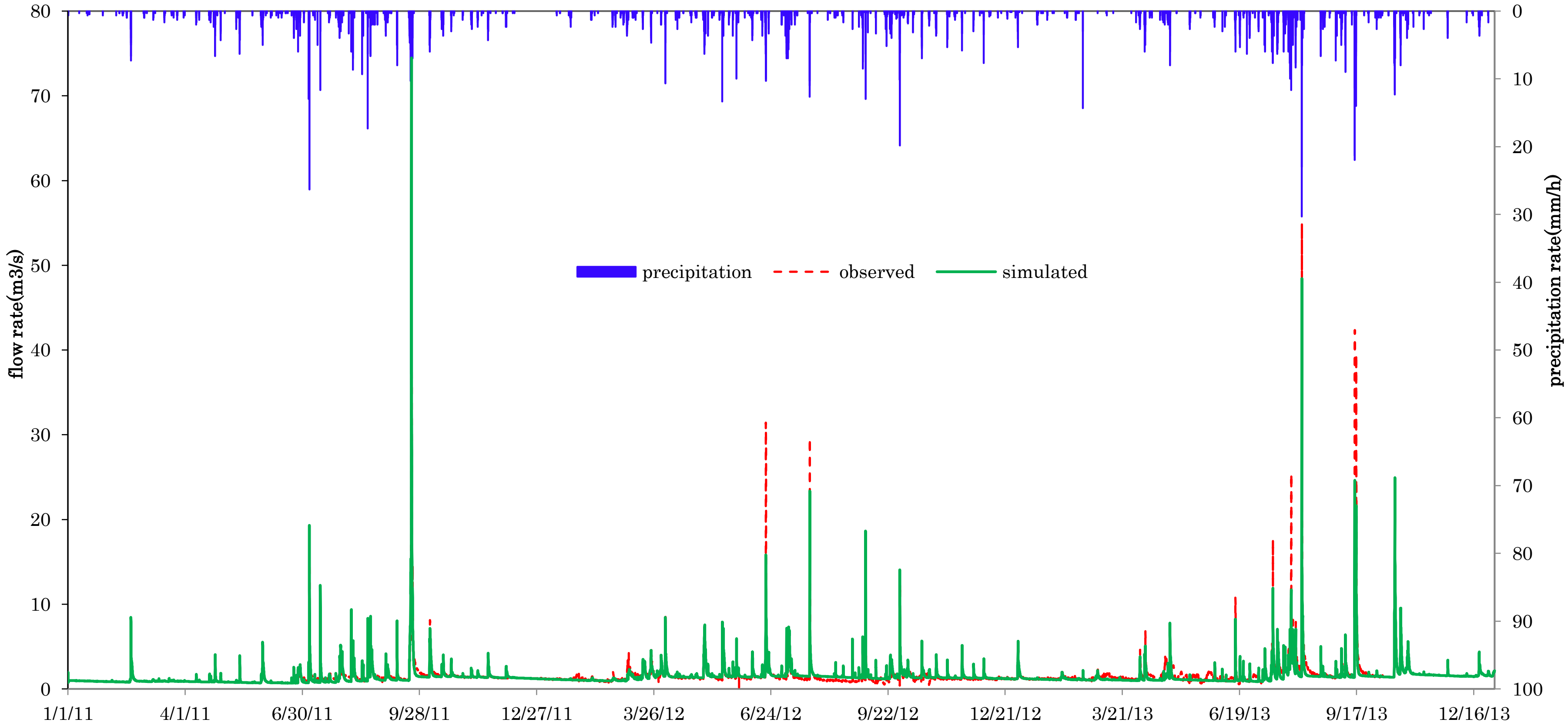

Figure 3-11. Simulated flow rates from 2011 to 2014 at middle stream site (St. M).

Reference

Allen, R. G., Pereira, L. S., Raes, D., Smith, M. (1998) Crop evapotranspiration - Guidelines for computing crop water requirements – FAO Irrigation and Drainage Paper 56, FAO, Rome, Italy. http://www.fao.org/docrep/X0490E/x0490e00.htm.

Allen, R.G., Pruitt, W.O., Wright, J.L., Howell, T.A., Ventura, F., Snyder, R., Itenfisu, D., Steduto, P., Berengena, J., Beselga, J., Smith, M., Pereira, L.S., Raes, D., Perrier, A., Alves, I., Walter, I., Elliott, R. (2006) A recommendation on standardized surface resistance for hourly calculation of reference ET0 by the FAO56 Penman–Monteith method. *Agric. Water Manage.*, 81, pp1–22.

Arnold, J. G., Srinivasan, R., Muttiah, R. S., and Williams, J. R. (1998) Large area hydrologic modeling and assessment: Part I. Model development. *J. American Water Resour. Assoc.* 34(1): 73-89.

Borah, D.K., Arnold, J.G., Bera, M., Krug, E.C., Liang, X.Z. (2007) Storm event and continuous hydrologic modeling for comprehensive and efficient watershed Simulations. *J Hydrol. Eng.* 12(6): 605-616,

Brooks, E. S., J. Boll, and McDaniel P. A. (2004) A hillslope-scale experiment to measure lateral saturated hydraulic conductivity. *Water Resour. Res.*,, doi:10.1029/2003WR002858.

Eagleson, P. S. (1970) Dynamic Hydrology. McGraw-Hill Book Company, New York, New York. 462 p.

England, J., Velleux, M.L., Julien, P.Y. (2007) Two-dimensional simulations of extreme floods on a large watershed. *Journal of Hydrology*, 347: 229–241.

Ishihara, T. and Takasao, T. (1962) a study on subsurface runoff and its effect on runoff process. *Trans. of JSCE*, No. 79: 15-23.

Julien PY, Saghafian B, Ogden FL. 1995. Raster-based hydrologic modeling of spatially-varied surface runoff. Water Resour. Bull. 31: 523–536.

Julien, P.Y., Rojas, R. (2002) Upland erosion modeling with CASC2DSED. *Int. J. Sed. Res.* 17 (4): 265–274.

Kinouchi, T., and Musiake, K. (2008) Simulating hydrological impact of environmental change in the Abukuma Watershed, Japan. 4th APHW Conference.

Kozak, J., Ahuja, L., Green, T., Ma, L. (2007) Modelling crop canopy and residue rainfall interception effects on soil hydrological components for semi-arid agriculture. *Hydrological Processes*, 21: 229–241.

Linsley, R. K., Kohler, M. A., and Paulhus, J. L. H. (1982) Hydrology for Engineers (Third Edition). McGraw-Hill Book Company, New York, New York. 508 p.

Moriasi, D. N., Arnold, J. G., Van, Liew, M. W., Bingner, R. L., Harmel, R. D., Veith, T. L. (2007) Model Evaluation Guidelines for Systematic Quantification of Accuracy in Watershed Simulations. *Transactions of the ASABE,* 50(3): 885–900.

Velleux, M. (2005) Spatially distributed model to assess watershed contaminant transport and fate. Ph.D. dissertation, Department of Civil Engineering, Colorado State University, Fort Collins, Colorado.

Velleux, M., Julien, P.Y., Rojas-Sanchez R., Clements, W.H., England. J.F. (2006) Simulation of metals transport and toxicity at a mine impacted watershed: California Gulch, Colorado. *Environ. Sci. Technol.,* 40(22): 6996–7004.

Velleux, M., England, J., Julien, P. (2008) TREX: Spatially Distributed Model to Assess Watershed Contaminant Transport and Fate. *Science of the Total Environment*, 404(1): 113-128.

Von Hoyningen-Huene J. (1981) Die Interzeption Des Niederschlags in landwirtschaftlichen Pflanzenbestanden. Arbeitsbericht Deutscher Verband fur Wasserwirtschaft und Kulturbau, DVWK, Braunschwig, Germany.

Sloan, P. G., Moore, I. D., Coltharp, G. B., Eigel, J. D. (1983) Modeling surface and subsurface storm flow on steeply-sloping forested watersheds. Water Resources Institute Rep. No. 142, Univ. of Kentucky, Lexington, Ky.

Zhao, R. J. (1977) Flood forecasting method for humid regions of China, East China College of Hydraulic Engineering, Nanjing, China.

Chapter 4

Simulation of soil erosion and transport with consideration of multiple solid classes

4.1 Introduction

Soil/sediment particles to which radionuclides have sorbed are the transmission media of primary concern. Soil particles are transported at different rates as a function of particle size as they move from terrestrial to aquatic systems and from headwater streams to downstream areas, particularly during rainfall and flood events when soil erosion tends to be at its highest levels. Therefore, soil erosion and transport must be studied to better understand the behavior and fate of radiocesium at watershed scale. Although prior studies of the Kuchibuto River catchment and the larger Abukuma River watershed focused on modeling radiocesium and soil transport (Tanaka *et al.*, 2013; Yamashiki *et al.*, 2013; Kinouchi *et al.*, 2015), the models they used either did not consider multiple solid classes (e.g. Yoshimura *et al.*, 2015; Kinouchi *et al.*, 2015), or utilized very limited observed data to validate model results (e.g. Tanaka *et al.*, 2013; Yamashiki *et al.*, 2014). Moreover, those studies did not describe the potential impact that spatial and temporal variations in soil erosion have on radiocesium. Analysis of the spatial patterns of erosion allows critical erosion areas to be identified and can inform decision-making to prioritize soil decontamination efforts and predict future radiocesium transport. Given the limitations of prior studies, this study uses an enhanced version of the TREX to simulate radiocesium-contaminated soil erosion and transport at finer spatial and temporal scales than was possible in prior studies. The advantage of this model is its consideration of multiple grain sizes to account for preferential sorption of radiocesium to finer particles and its fine time step (less than one hour) so that it can trace soil/sediment dynamics for every flood event. The specific objectives of this chapter were to: (1) simulate soil erosion and transport processes with considering multiple particle size classes; (2) calibrate and validate the model using nearly 4-years of measurements in the Kuchibuto River catchment; and (3) identify critical erosion areas within the catchment based on simulated spatial and temporal distributions of soil erosion.

4.2 Model description

The hydrological module of the TREX watershed model has been introduced in chapter 3, so, in this chapter, soil erosion and transport module will be described in the following sections.

4.2.1 Soil erosion and transport on the upland

Our study also did some minor modifications to simulate soil erosion on the upland. In the model, the governing equation of upland soil erosion and transport is expressed as:

$$\frac{\partial AC_s}{\partial t}+\frac{\partial C_s q_x}{\partial x}+\frac{\partial C_s q_y}{\partial y}=e_s+e_h \qquad (4.1)$$

where, C_s is suspended sediment concentration in water (kg/m^3); e_s is erosion by rainfall splash(kg/s/m);e_h is net erosion by water flow(kg/s/m).

The splash erosion rate can be approximated as a function of the square of the rainfall rate, which is proposed in KINEROS model (Woolhiser *et al.*, 1990):

$$e_s=(1-kv)w\rho_s C_f e^{-hC_h} i_n{}^2 \qquad if\,(q>0) \qquad (4.2a)$$

$$e_s=0 \qquad if\,(q=0) \qquad (4.2b)$$

where, kv is fraction of vegetation in each cell (-); w is cell size (m); ρ_s is solid density (kg/m^3); i_n is net rainfall intensity (m/s); q is water flow discharge (m^3/s); h is surface water depth (m); C_f, C_h are coefficients(s/m, 1/m).

Overland flow detaches soil particles by exerting a shear stress. Overland flow typically consists of a combination of shallow flow of large width (sheet flow) and concentrated flow in small eroding channels (rills) (Wicks and Bathurst, 1996). A way to describe soil erosion process involves detachment of soil particles by raindrop, transport of this material to rills by sheet flow, and further detachment and transport of soil particles by the rill flow (e.g. Foster *et al.*, 1977), and detachment by overland flow is largely concentrated in the rills. The other way is not separate rill and sheet flows, and use averaged water depth and velocity of each computational cell to predict overland flow detachment (e.g. KINEROS model (Woolhiser *et al.*, 1990), SHESED model (Wicks and

Bathurst, 1996), EUROSED model (Morgan *et al.*, 1998)). In this study we used the later one. Water flow erosion is the function of water transport capacity:

$$e_h = \alpha_{soil} w v_s (C_m - C_s) \tag{4.3}$$

where, α_{soil} is coefficient, when it is net deposition ($C_m < C_s$), α_{soil} equals to 1, otherwise, it is determined according to soil cohesion (Morgan *et al.*, 1998); v_s is solid setting velocity (m/s); C_m is total sediment transport capacity (kg/m^3).

The transport capacity is important in determining hydraulic erosion. Many experiments have been conducted to determine C_m. In this model, the Engelund and Hansen (1967) equation is used to calculate C_m:

$$C_m = \beta_{soil} \frac{0.05\rho_s}{d_p(G-1)} \sqrt{\frac{hS_f}{g}} (\Omega - \Omega_0) \tag{4.4}$$

$$\Omega = \mu S_f \tag{4.5}$$

where, S_f is friction slope (-); μ is flow velocity(m/s); Ω, Ω_0 are unit stream power and the threshold unit stream power (m/s) respectively; d_p is solid diameter (m); G is particle specific gravity (-); β_{soil} is coefficient (-); g is acceleration of gravity.

Because C_m was developed for experimental flow conditions (e.g. streams, flumes) that differ from the shallow surface runoff, the coefficient β_{soil} was used as a calibration factor to adjust total sediment transport capacity.

4.2.2 Sediment resuspension and transport in the river channel

The governing equation of sediment erosion and transport in river channel is expressed as:

$$\frac{\partial AC_s}{dt} + \frac{\partial C_s q_{tx}}{dx} = J_e - J_d \tag{4.6}$$

where,

$$J_e = V_r C_{sb} \tag{4.7}$$

$$V_r = \frac{J_c - v_a C_s}{\rho_b} \qquad if\,(J_c > v_a C_s) \tag{4.8a}$$

$$V_r = 0 \qquad if\,(J_c \le v_a C_s) \tag{4.8b}$$

where, V_r is resuspension velocity (m/s), C_{sb} is concentration of sediment at the bottom boundary (in the bed) (kg/m^3), which is updated timely in each time step according to mass balance of sediments; v_a is flow velocity (m/s), ρ_b is bulk density of bed sediments (kg/m^3), J_c is sediment transport capacity areal flux (kg/m^2/s).

$$J_c = \frac{v_a C_t}{A} \tag{4.9}$$

where, C_t is concentration of entrained sediment particles at the transport capacity (kg/m^3), it is calculated by:

$$C_t = 10^6 \frac{G C_w}{G + (1 - G) C_w} \tag{4.10}$$

where, C_w is concentration of entrained sediment particles by weight at the transport capacity (-), C_w is expressed by:

$$C_w = 0.05 \left(\frac{G}{G-1}\right) \frac{(v_a - v_c) S_f}{[(G-1) g d_p]^{0.5}} \left[\frac{R_h S_f}{(G-1) g d_p}\right]^{0.5} \tag{4.11}$$

where, v_c is critical velocity for erosion in channel (m/s); R_h is hydraulic radius of flow (m).

The deposition flux in river channel can be expressed as a mass rate of particle removal from the water column over time and the concentration of sediment particles that are entrained in the flow:

$$J_d = w v_s P_{dep} C_s \tag{4.12}$$

where, P_{dep} is probability of solid setting (-).

The probability can be approximated as (Abramowitz and Stegun, 1972):

$$P_{dep} = 1 - F(Y)(0.4362X - 0.1202X^2 + 0.9373X^3) \qquad if\,(Y > 0) \qquad (4.13a)$$

$$P_{dep} = 1 - P_{dep}(|Y|) \qquad if\,(Y \leq 0) \qquad (4.13b)$$

where

$$X = \frac{1}{1 + 0.3327Y} \qquad (4.14)$$

$$F(Y) = \frac{1}{\sqrt{2\pi}} e^{-0.5Y^2} \qquad (4.15)$$

The model gives two options to calculate Y:

for non-cohesive particles (Gessler,1965; 1967; 1971):

$$Y = \frac{1}{\sigma}\left(\frac{\tau_{cd,n}}{\tau_0} - 1\right) \qquad (4.16a)$$

where, σ is experimentally determined constant (= 0.57); τ_0 is bottom shear stress (N/m^2) $\tau_{cd,n}$ is critical shear stress for deposition of non-cohesive particles, defined as the shear stress at which 50% of particles deposit (N/m^2).

for cohesive particles (Partheniades, 1992):

$$Y = \frac{1}{\sigma}\ln\left(0.25\left(\frac{\tau_0}{\tau_{cd,c}} - 1\right)e^{1.27\tau_{cd,c}}\right) \qquad (4.16b)$$

where, σ is experimentally determined constant (= 0.49); τ_0 is bottom shear stress (N/m^2); $\tau_{cd,c}$ is critical shear stress for deposition of cohesive particles, defined as the shear stress at which 100% of particles deposit (N/m^2).

4.3 Results and discussion

4.3.1 Comparison of SS concentration, flux and mass

The hydrological variables in the Kuchibuto River catchment calculated in the chapter 3 were used for soil erosion and transport simulation. Sensitivity analyses for soil erosion model were performed and we found that C_f in eq. 4.2a and β_{soil} in eq. 4.4 needed to be calibrated to optimize the model performance. Flood events on Sep. 22 2011 (the biggest typhoon event) and Oct. 16 2013 were used to parameterize C_f and β_{soil} for clay, silt and sand separately, and the results are shown in Table 4-1.

Instantaneous particle size distributions (PSD) were typically measured on an hourly basis at the downstream site, although data were not obtained for all flood events due to equipment problems. Figure 4-1(a) and 4-1(b) are comparisons of simulated and observed SSCs for calibration periods, and Figure 4-2 shows the SSC of clay, silt and sand during Jul. 2013 when PSD were obtained. SSCs of water grab samples were used for comparison. Taking account of temporal-spatial variation, water grab samples from multiple sites dispersed over the catchment during two flood events in Oct. 2013 were collected for model validation (Figure 2-1). SSCs of the water samples were measured in lab., and the results were used to compare with our simulated results as shown in Figure 4-3. Simulated SSCs were agree well against measurement. SSCs for the flood Oct. 14, 2014 were overestimated in general, while at some sites such as St. 3 and St.5 SSCs were underestimated. The possible reason may be the peaks of SSC at the sites were not reproduced well, it were earlier or later than real time and the sediment graphs shifted, so the simulated SSCs didn't match well with measured data. Long term field measurements were done at the downstream site (St. D) and the middle site (St. M). For 2011~2014, |*PBIAS*| value of TSS flux at the stations were not more than 33% (Table 4-2). As for 2012, *NSE* and *RSR* were not satisfied, however, the bias was much closed to 0. Figure 4-4(a) and 4-4(b) show the comparison of simulated and measured SS fluxes for the calibration events, and Figure 4-5 show the comparison for other big flood events in 2012~2014 at the downstream for model validation. As Figure 4-6 shown, during the monitoring period (i.e. Jun. 21, 2011 to Dec. 31, 2014), simulated TSS transported from the downstream site was 78273 tonnes (t) and is in very close agreement with measured transport (about 81646 t). Thus, simulation results were judged to be acceptable from above comparisons of SSCs, fluxes and mass. Our simulation results also show from Mar. 12, 2011, when the accident began, to Dec. 31, 2014, an estimated about 5530 t of clay, 51879 t of silt, 22339 t of sand were eroded from the Kuchibuto River watershed and transport to the Abukuma River. Overland flows have a smaller transport capacity (C_m)

for sand relative to silt. Thus, the amount of sand was smaller than silt. Although the transport capacity of clay is larger, the fraction of clay available for transport is very small (i.e., supply is limited), so the amount of clay was smallest.

4.3.2 Sediment budget

Soil erosion and transport processes from Jan. 1, 2011 to Dec. 31, 2014 were simulated. Figure 4-7 shows mass balance of SS transport in the catchment for simulation period. According to our simulated sediment budget, over these four years, 84631 t of SS was delivered from upland areas to river channels and 80313 t was transported out of the catchment at its outlet. A relatively small mass of solids remained within the channel at the end of the simulations, with 3017 t deposited to the channel bed and 3 t remaining in suspension. The amount of suspended sediment still remaining in river channels at the end of the simulation period was very small. An appreciable amount of sediment deposited onto river bed and was largely comprised of sand, representing roughly 12% of total sand inflow. Because their setting velocity is low, the deposition flux of finer sediments is generally small and relatively little of material eroded from the watershed deposits. In contrast, sands have much higher settling velocities and readily deposit in river channels. Consequently, the "erosion–deposition–resuspension" process for sand transport is different than the "transport directly" process for clay (Figure 4-7). The same phenomenon also occurs in upland areas, where eroded sand mainly deposited on hillsides near the source of erosion. In contrast, clay can be transported for long distances before settling out of suspension, so that limited clay deposition occurs is mainly distributed in the floodplain near the river (Figure 4-8).

4.3.3 Critical erosion area identification

The area-specific sediment yield was about 155 $t/km^2/y$. This is within the range of values estimated other studies. Based on simulations for 2004 and 2005, Itoshiro *et al.* (2014) estimated that the annual sediment yield was about 100~200 $t/km^2/y$ from tributaries of the Abukuma River watershed. Although weathered granitic material covers most of the Kuchibuto River catchment and other tributary catchments in the western Abukuma River watershed, other factors (land use, and etc.) may contribute to soil erosion and transport variations in those catchments. Even within the Kuchibuto River catchment, the sediment supplies from different areas are various. According to our simulated results in Table 4-3, the Middle main stream area supplied more sediment to river channel for unit area (about 178 t/km^2/y), while the sediment supply ratio (SSR) for the Upper main stream area was smaller than the middle portion of the catchment (i.e. the Tributary and the Middle main stream areas). It indicates the middle portion of the catchment which suffers more serious soil erosion, can be identified as critical erosion areas. The SSR for subbasin in the critical erosion areas, such as subbasin No. 16, No. 19, No. 17, No. 8, No. 13, No. 20, No. 21, No. 4, No. 5, and No. 11 (Figure 4-9), were more than average sediment yield for the whole catchment (i.e. 155 t/km^2/y). Spatial distributions of net erosion and deposition of clay, silt and sand as shown in Figure 4-8 also have the same spatial trend.

Multi-site measurements confirm this finding. Based on the empirical mass budget for measurements in 2011, approximately 56% of sediment and 64% of water was generated in the entire catchment passed the middle stream station (St. M) and was transported downstream. This indicates that the upper portion of the catchment produced and delivered less sediment than areas further downstream, which generated roughly 44% but only 36% of the flow.

The topographic and land use characteristics are major controlling factors for the sediment yield of most small mountainous rivers (Milliman and Syvitski, 1992; Shi *et al.*, 2014). Agricultural land with steep slope always produced more sediment (Table 4-3). In Figure 4-10 we can see, in the middle portion of the catchment, slopes are also very steep. Areas with slopes greater than 15° are rare in upper portions of the watershed but occur much more frequently in the middle part. According to our simulation, SSR in the areas with slopes greater than 15° was 412 t/km^2/y, while the rest areas was 116 t/km^2/y. Steeper slopes lead to larger friction slopes (S_f) and consequentially big transport capacities (C_m). Thus, areas with steep slope are more prone to suffer serious erosion. Our results show that SSR in agricultural land was about 343 t /km^2/y, which is much larger than for other land use types (e.g. about 64 t /km^2/y in forest). In forested land, fraction of vegetation (kv) is usually larger than agricultural land. Another factor is water flow generation. In forested areas subsurface flow rather than overland flow is expected to be predominant. This combination of factors act to limit rainfall splash and water flow hydraulic erosion in forested areas, whereas farmland and paddy field land uses supply and deliver more sediment. From upstream to downstream areas, the increasing portion of agricultural land intensified soil erosion (Figure 2-2 and Figure 4-8).

4.3.4 Implication for ^{137}Cs migration

Sediment transport processes determine sediment-bound ^{137}Cs migration. ^{137}Cs inventory in Figure 2-1 shows the northern part of the Kuchibuto River catchment was more seriously contaminated, especially the Upper main river catchment, where decontamination work is urgent. However, our finding suggests that soil decontamination actions in mid-watershed critical erosion areas are also of great priority to reduce soil erosion induced ^{137}Cs transport downstream to the Abukuma River. Although ^{137}Cs is less enriched in coarse solids (silt and sand), their deposited areas can accumulate ^{137}Cs gradually and become ^{137}Cs hotspot areas, therefore, the larger deposition areas as shown in Figure 4-8 may be targeted areas for further ^{137}Cs field survey. Information about sediment transport helps to understand ^{137}Cs transport and fate in Fukushima.

4.4 Conclusions

In this chapter, soil erosion and transport processes in the Kuchibuto River watershed were simulated for the four-year period Jan. 1, 2011 to Dec. 31, 2014, using a TREX watershed model. Simulated flow rates were found to be acceptable in comparison to measurements for 2011 ~ 2014 over the catchment. The correspondence between simulated and measured SS concentrations of water grab samples for multiple sites for flood events and SS concentrations, fluxes and mass at the stations during 2011 ~ 2014 demonstrates that the simulated results are acceptable. Simulation results also indicate that between Mar. 12, 2011, when the accident began, and Dec. 31, 2014, about 5500 t of clay, 52000 t of silt, 22000 t of sand were eroded and transported to the Abukuma River. Model results also indicate that critical erosion areas are located in the middle portion of the catchment, where slopes are steep and the primary land use is agricultural. Our study suggests that soil decontamination actions of critical erosion areas in the middle portion of the Kuchibuto River watershed are also of the great priority to avoid soil erosion induced ^{137}Cs transport to the Abukuma River. The results of this study are useful for understanding radiocesium transport at the watershed scale and ultimately for assessing environmental risks.

Table 4-1. Properties of sand, silt and clay

Solid types	d_p(μm)	G(-)	V_s(cm/s)	C_f (-)	β_{soil} (-)
sand(> 63μm)	100	2.65	0.8	850	0.001
silt (3 - 63μm)	20	2.65	0.0385	1500	0.0035
clay (< 3μm)	2	2.65	0.0004	70	0.000003

Table 4-2. Evaluation criteria of simulated TSS flux

location	coefficient	2011	2012	2013	2014
down stream (St. D)	*NSE*	0.91	0.22	0.85	0.57
	RSR	0.30	0.89	0.39	0.65
	PBIAS	-4%	-5 %	-5%	33%
middle stream (St. M)	*NSE*	0.90	-	-	-
	RSR	0.32	-	-	-
	PBIAS	-5%	-	-	-

Table 4-3. Prioritized SSR and characteristic of landuse and slope in subwatershes

location	sub. no.	area (km^2)	average slope(°)	fraction of agricultural land	sediment supply (t)	SSR ($t/km^2/y$)
	7	2.8	8.30	0.40	721	64
Middle main stream	16	3.8	10.89	0.48	5162	337
(178 $t/km^2/y$)	19	12.4	10.53	0.25	10990	222
	17	3.8	13.28	0.25	3064	203
	8	3.9	9.56	0.34	2958	188
	13	8.7	11.24	0.24	6224	179
	20	6.0	5.68	0.51	4250	178
	21	8.4	8.66	0.37	5392	160
	18	5.7	5.21	0.61	3098	136
	14	6.7	7.72	0.40	3384	127
	15	4.2	6.08	0.48	846	50
Upper main stream	3	10.9	8.61	0.24	6190	142
(160 $t/km^2/y$)	1	5.5	9.75	0.20	2719	123
	2	5.3	8.24	0.26	2006	95
	9	4.7	7.96	0.40	1757	94
	6	7.8	10.08	0.15	2595	83
Tributary	4	3.1	12.88	0.04	2592	206
(112 $t/km^2/y$)	5	4.1	10.84	0.20	3025	183
	11	11.7	9.61	0.37	8488	181
	12	10.5	10.85	0.34	5997	142
	10	6.8	7.08	0.41	3174	116
all	-	137	9.21	0.32	84631	155

* SSR = Inflow sediment / 4 years / Area

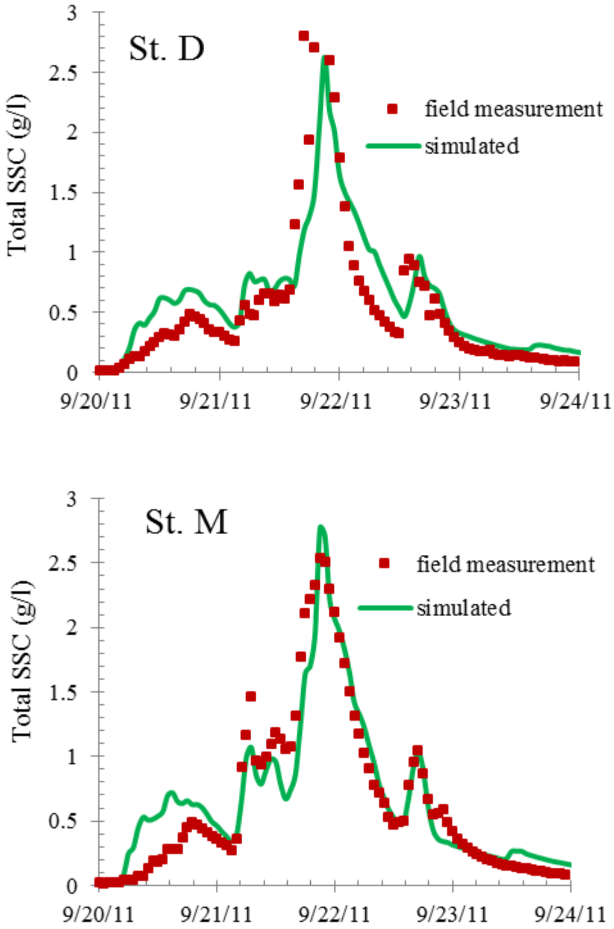

Figure 4-1 (a). Total SSC at the downstream site (St. D) and the middle stream site (St. M) for the event on Sep. 22 2011.

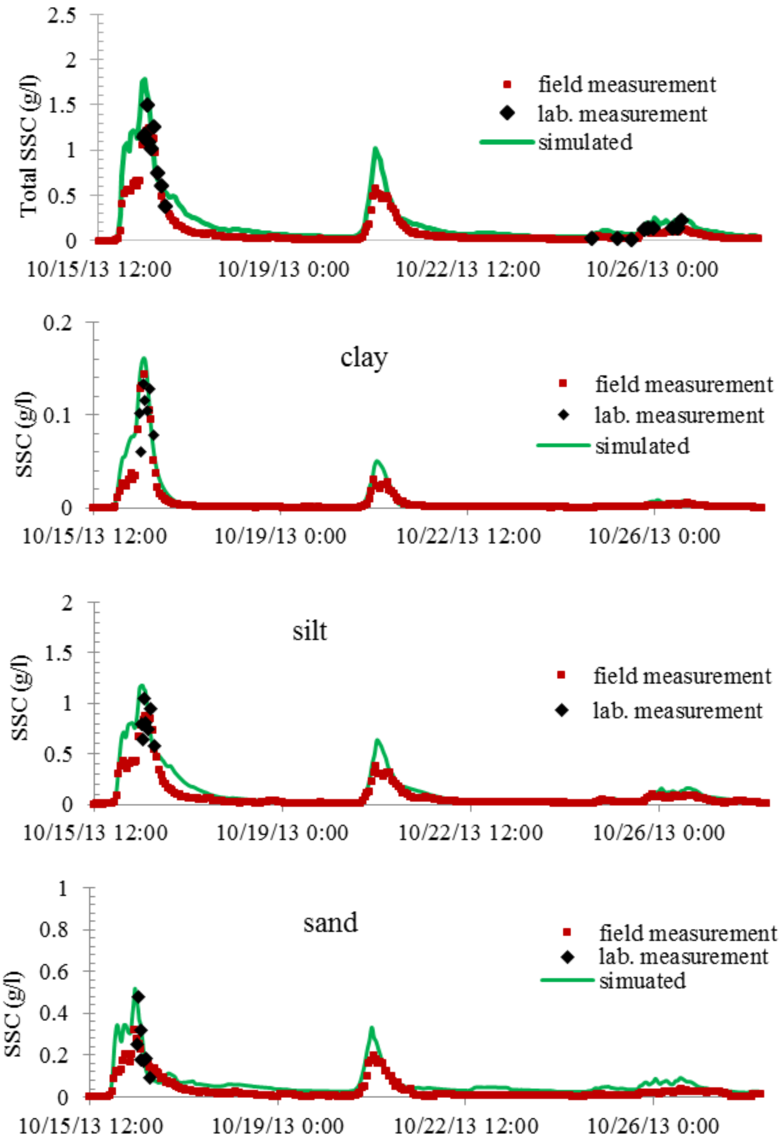

Figure 4-1 (b). SSC at the downstream site (St. D) for the event on Oct. 16 2013. (Field measured data was concentration converted from measured turbidity, lab. measured data was concentration of water samples)

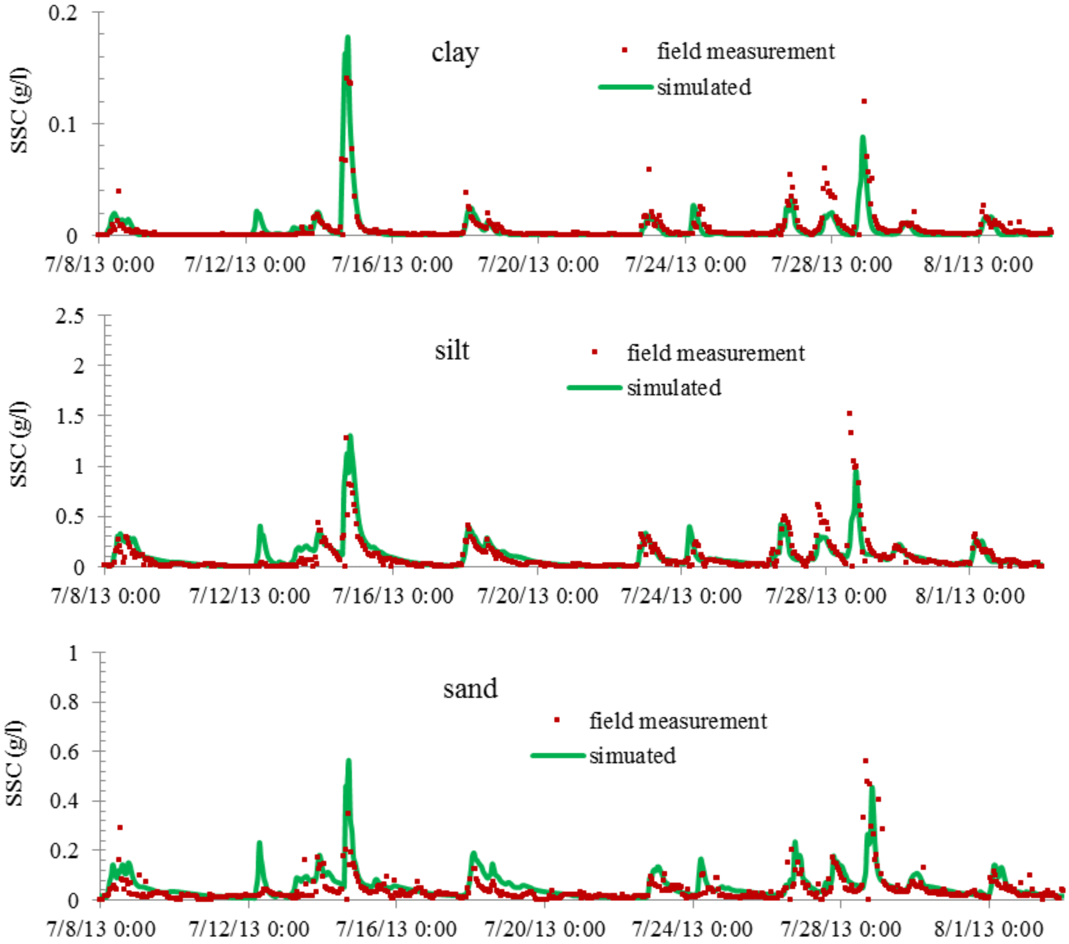

Figure 4-2. SSC of clay, silt and sand respectively, at the downstream site (St. D) for model validation.

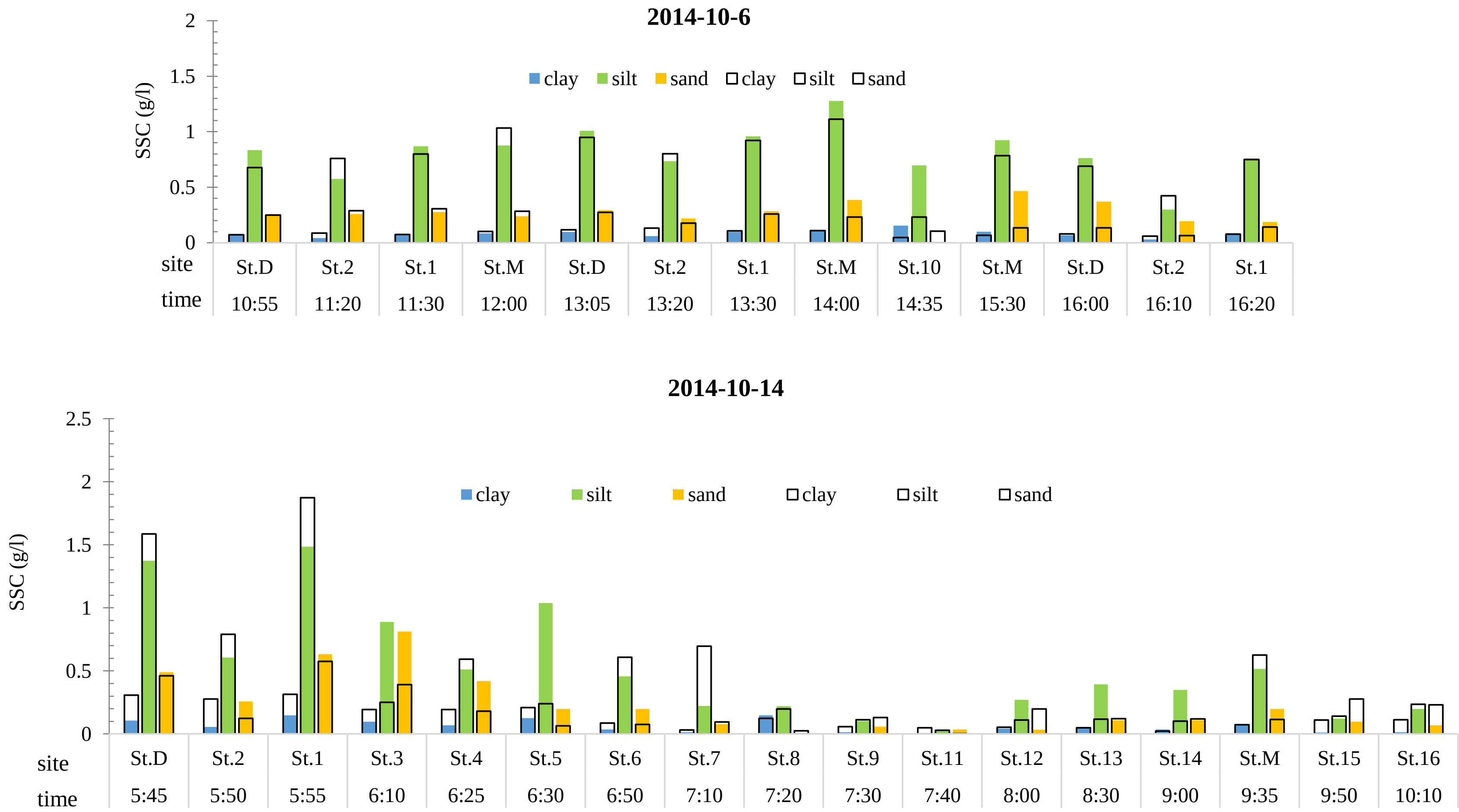

Figure 4-3. Comparison of measured of suspended solid concentration of multi-site water samples and simulated results for different sites in the river during flood events. (Color bar represents measured data and box means simulated results)

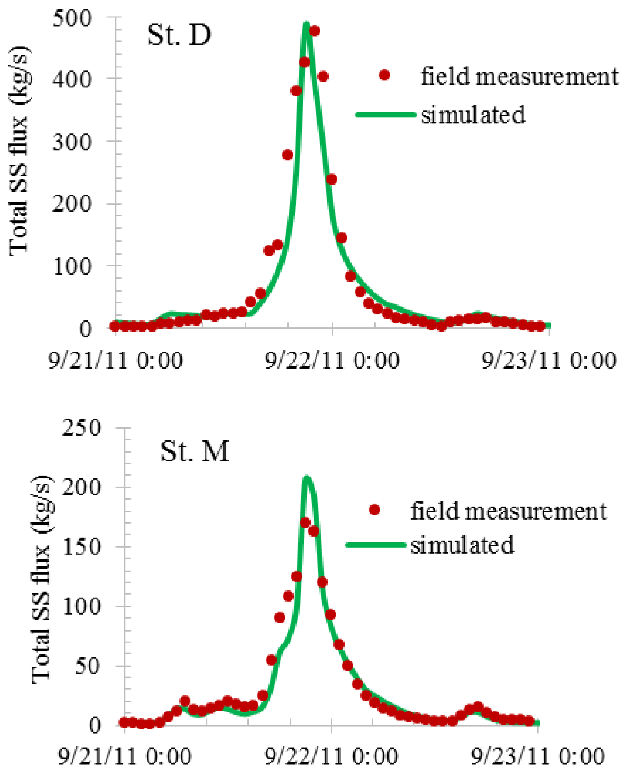

Figure 4-4 (a). Total suspended solid flux at the downstream site (St. D) and the middle stream site (St. M) for the typhoon event on Sep. 22 2011.

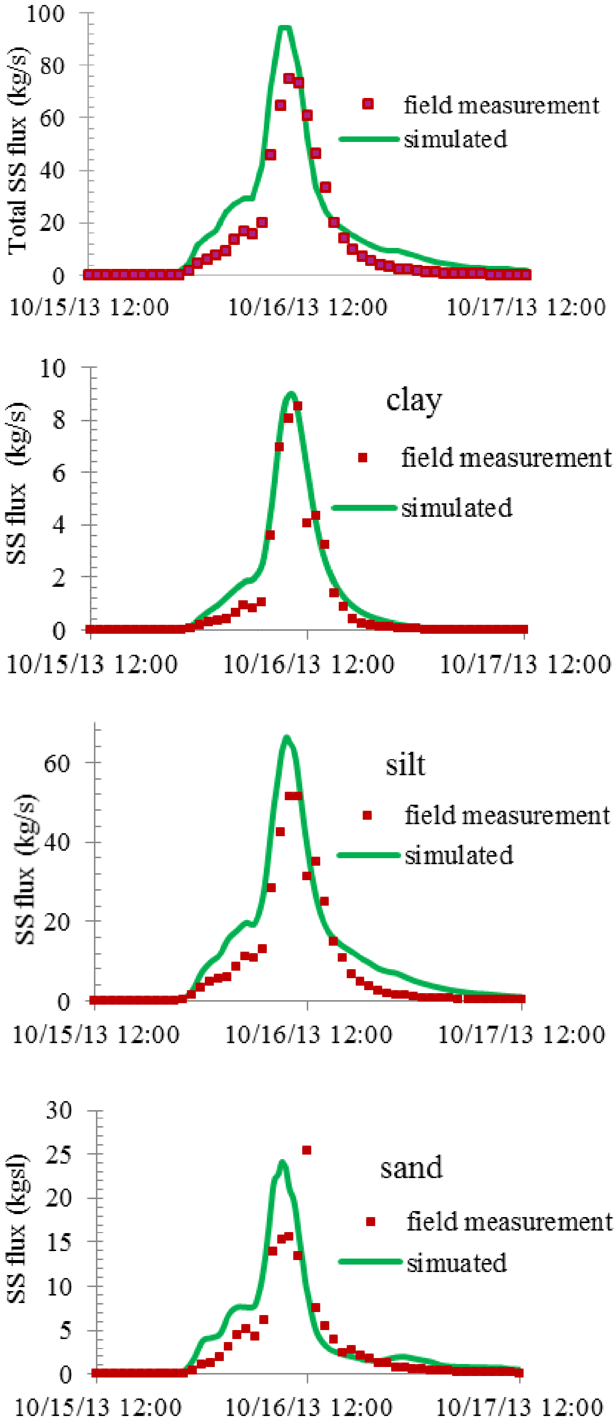

Figure 4-4 (b). Suspended solid flux at the downstream site (St. D) for the event on Oct. 16 2013.

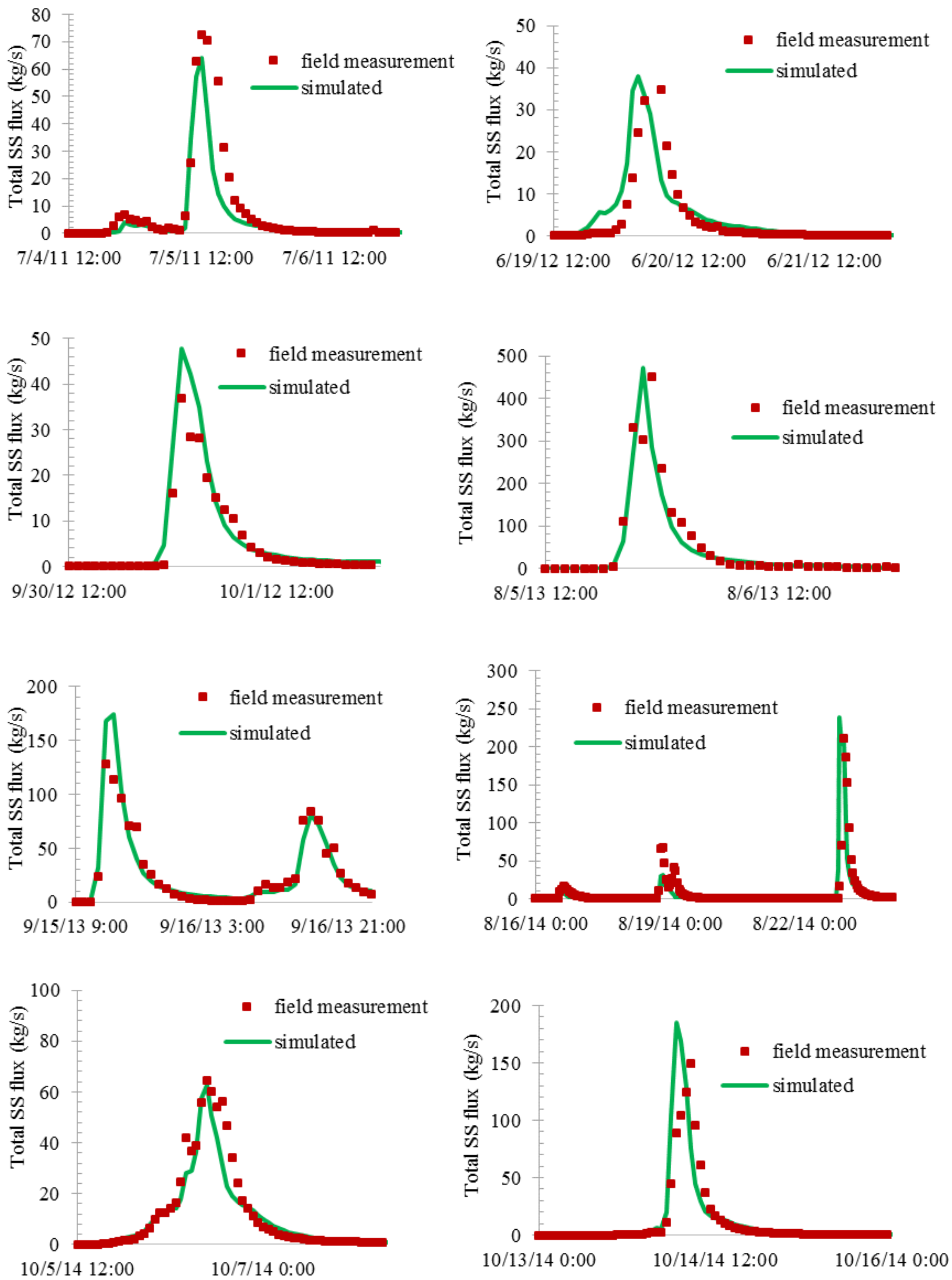

Figure 4-5. Total suspended solid flux at the downstream site (St. D) for flood events for model validation.

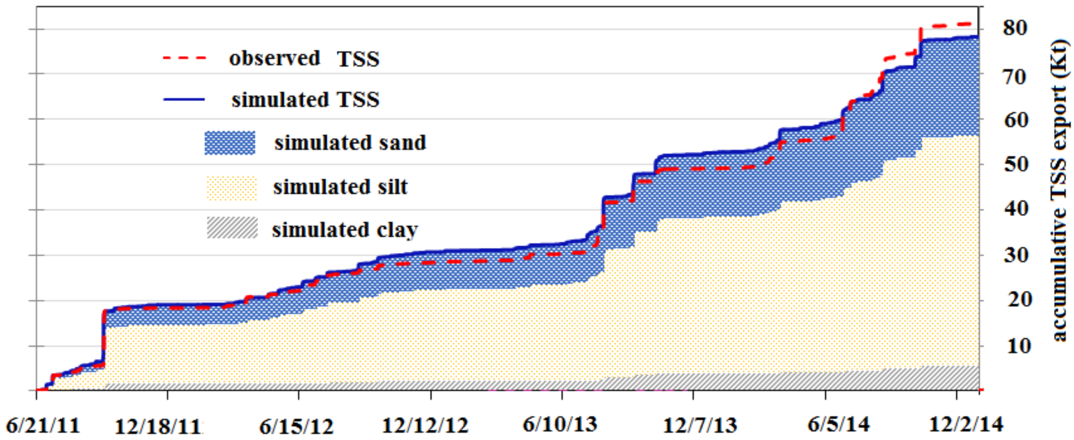

Figure 4-6. Comparison between simulation and observed accumulated TSS export from Jun. 21, 2011 to Dec. 31, 2014.

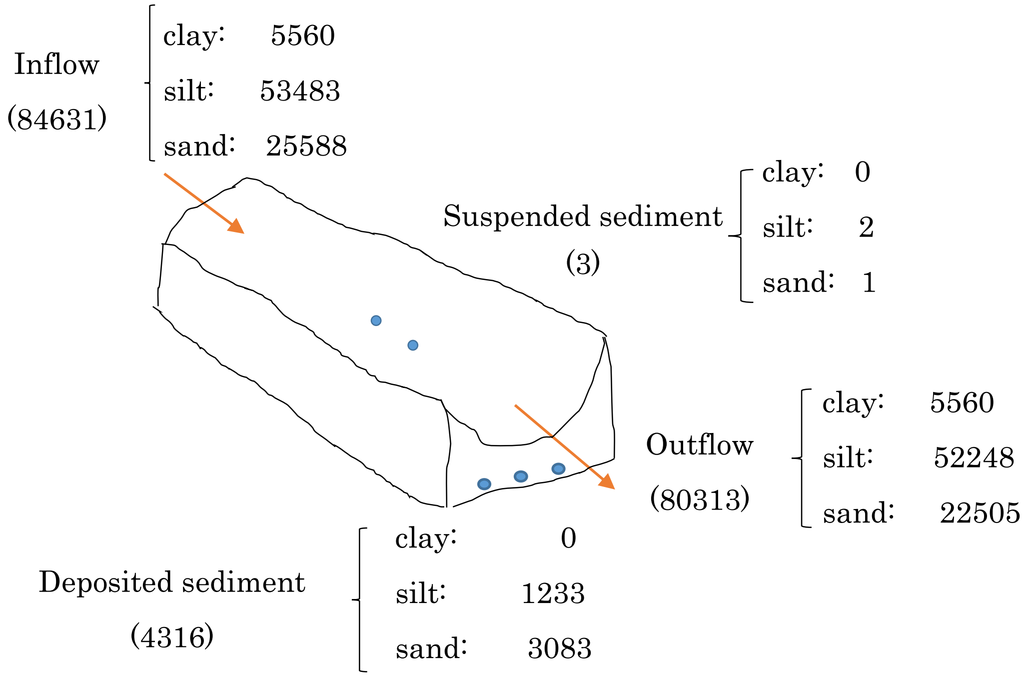

* Inflow = Outflow + Suspended sediment + Deposited sediment

Figure 4-7. Mass balance of SS transport in the catchment (unit: t)

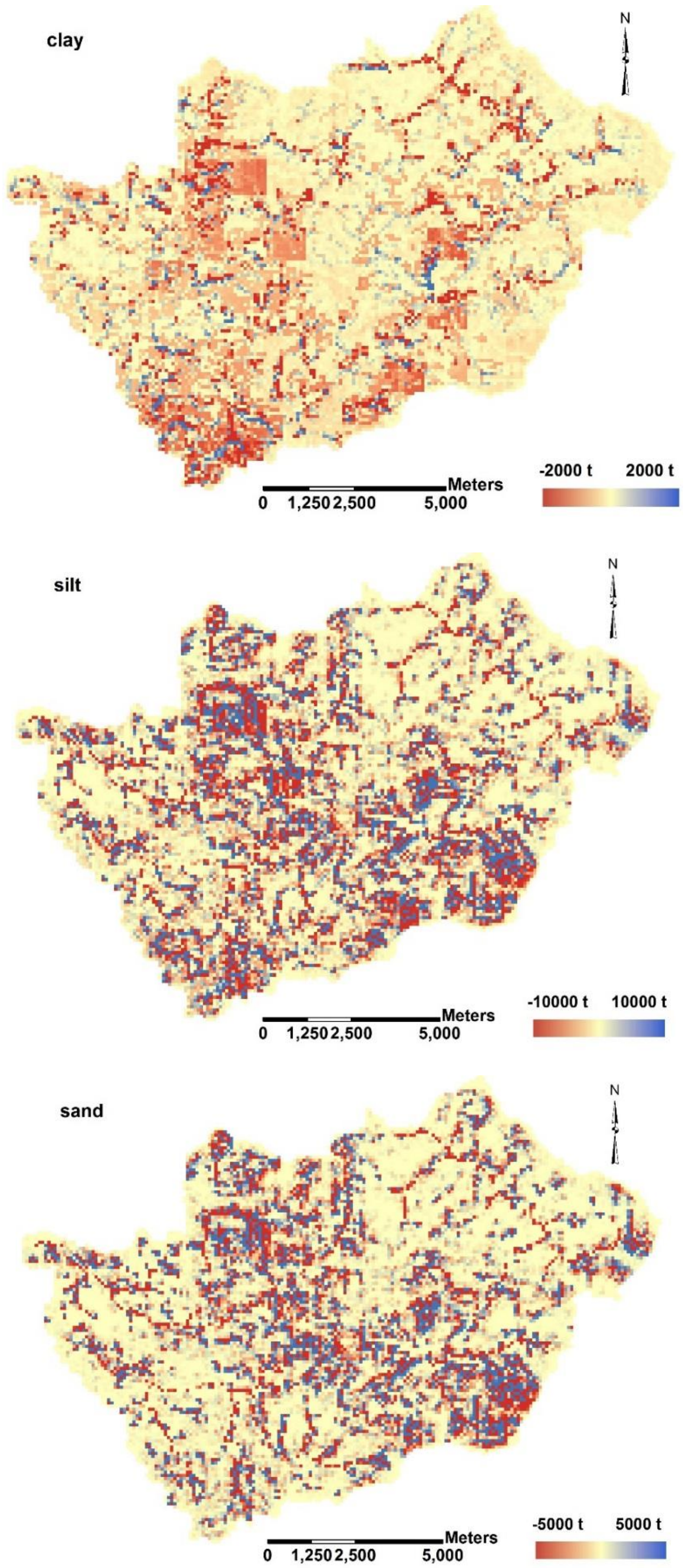

Figure 4-8. Simulated net erosion and deposition of clay, silt and sand respectively, for the period Jan. 1, 2011 to Dec. 31, 2014 (negative value means erosion)

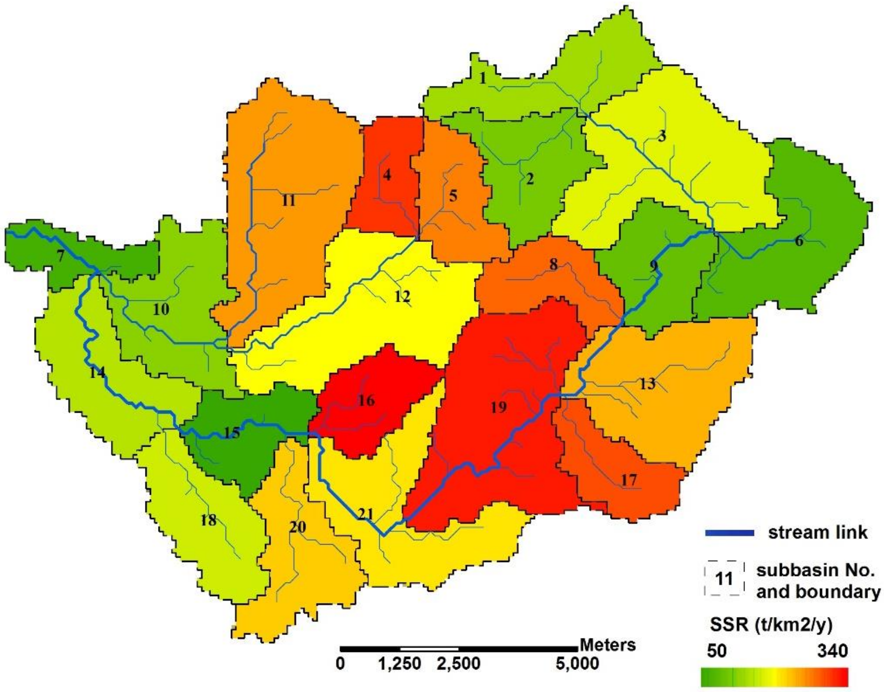

Figure 4-9. Simulated sediment supply ratio from upland to river for 21 subbasin

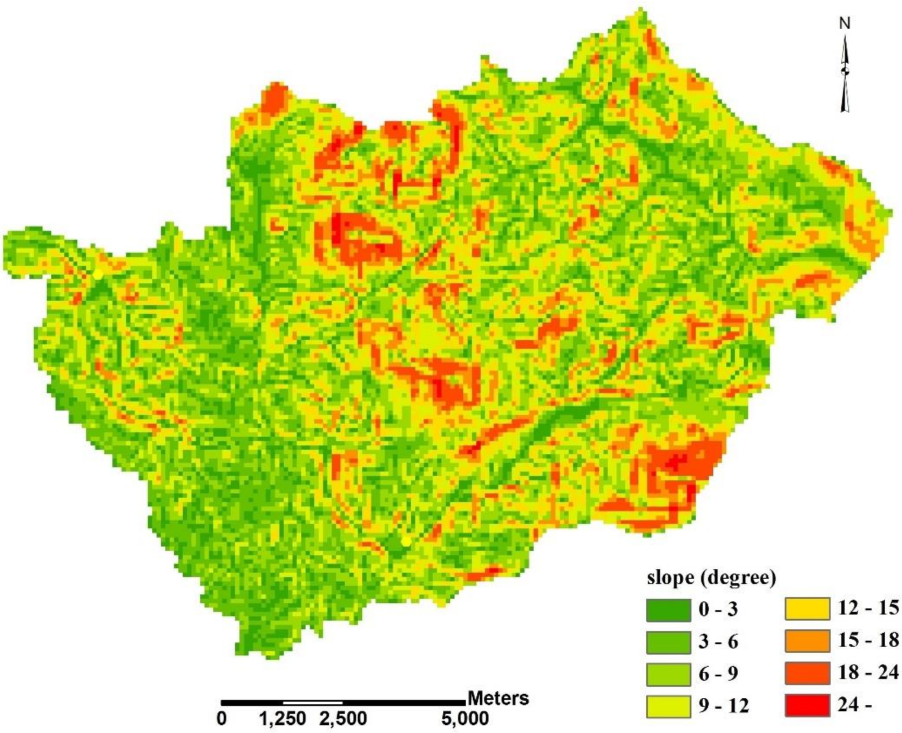

Figure 4-10. Slope distribution of the Kuchibuto River catchment

Reference

Abramowitz, M. and Stegun, I. A. (1972) Handbook of Mathematical Functions. Applied Mathematics Series 55. National Bureauof Standards, Washington, D.C.

Engelund, F. and Hansen, E. (1967) A Monograph on Sediment Transport in Alluvial Streams, Teknisk Forlag, Copenhagen, 62 p.

Foster, G.R., Meyer, L.D. and Onstad, C.A., 1977. An erosion equation derived from basic erosion principles. Trans. ASAE, 20(4): 678-682.

Gessler, J. 1965. The beginning of bed load movement of mixtures investigated as natural armouring in Channels. Technical report No. 69, the laboratory of hydraulic research and soil mechanics, Swiss Federal Institute of Technology, Zurich.

Gessler, J. (1967) The beginning of bed load movement of mixtures investigated as natural armoring in channels. California Institute of Technology, Pasadena, California. 89pp.

Gessler, J. (1971) Beginning and ceasing of sediment motion. In: River Mechanics, Shen, H.W., ed. H.W. Shen, Fort Collins, Colorado. pp. 7:1–7:22.

Itoshiro, S., Takemura, K., Kashiwagi, S., Goto, K., Tatsuta, J., Nagasawa, N., Hoshino, T., Mori, Y., Yamanaka, K. (2014) Study on water and substance cycle structure. *Report of Japan River Front Research Center*, No.25.

Kinouchi, T., Yoshimura, K., Omata, T. (2015) Modeling radiocesium transport from a river catchment based on a physically-based distributed hydrological and sediment erosion model. *Journal of Environmental Radioactivity,* 139: 407–415.

Morgan, R. P. C., Quinton, J. N., Smith, R. E., Govers, G., Poesen, J. W. A., Auerswald, K., Chisci, G., Torri, D., Styczen, M.E. (1998) The European soil erosion model (EUROSEM): a process-based approach for predicting sediment transport from fields and small catchments. *Earth Surface Processes and Landforms*, 23: 527–544.

Moriasi, D. N., Arnold, J. G., Van, Liew, M. W., Bingner, R. L., Harmel, R. D., Veith, T. L. (2007) Model Evaluation Guidelines for Systematic Quantification of Accuracy in Watershed Simulations. *Transactions of the ASABE,* 50(3): 885–900.

Partheniades, E. (1992) Estuarine sediment dynamics and shoaling processes. In: Handbook of Coastal and Ocean Engineering, Volume3: Harbours, Navigation Channels, Estuaries, and Environmental Effects, pp. 985-1071. Herbich, J. B.,Ed. Gulf Publishing Company, Houston, Texas.

Tanaka, T., Tachikawa, Y., Shiiba, M., Yorozu, K., Kim, S. (2013) Numerical modeling and estimation of radioactive cesium movement at the Kuchibuto river basin, Fukushima. *Journal of Japan Society of Civil Engineers, Ser. B1 (Hydraulic Engineering)* 69: 1_487-1_492.

Wicks, J. M., and Bathurst, J. C. (1996). ‘‘SHESED: A physically based, distributed erosion and sediment yield component for the SHE hydrological modelling system.’’ J. Hydro., Amsterdam, 175, 213–238.

Woolhiser, D. A., Smith, R. E., Goodrich, D. C. (1990) KINEROS, A Kinematic Runoff and Erosion Model: Documentation and User Manual. U S. Department of Agriculture, Agricultural Research Service, ARS-77, 130 p.

Yoshimura, K., Onda, Y., and Kato, H. (2015) Evaluation of radiocaesium wash-off by soil erosion from various land uses using USLE plots. *Journal of Environmental Radioactivity*, 139: 362-369. DOI: 10.1016/j.jenvrad.2014.07.019.

Yamashiki, Y., Onda, Y., Smith, H. G., Blake, W. H., Wakahara, T., Igarashi, Y., Matsuura, Y., Yoshimura, K. (2014) Initial flux of sediment-associated radiocesium to the ocean from the largest river impacted by Fukushima Daiichi Nuclear Power Plant. *Scientific Reports* 4, 3714. doi:10.1038/srep03714.

Chapter 5

Modeling ^{137}Cs migration based on a hydrological and sediment erosion model in a forested catchment

5.1 Introduction

The released ^{137}Cs from the Fukushima Daiichi Nuclear Power Plant in 2011 in Japan has induced serious regional environmental problems and drawn much attention not only on a local level but also worldwide. Modeling watershed-scale ^{137}Cs migration is a profitable method for understanding contaminant transport mechanism, identifying contaminant sources and sinks, predicting future ^{137}Cs distribution in the watershed, and evaluating possible decontamination countermeasures. Although, some prior models were applied in Fukushima (Yamaguchi *et al*., 2014; Kitamura *et al*., 2014; Kinouchi *et al*., 2015; Tanaka *et al*., 2013), ^{137}Cs transport along with hydrological processes is still not well studied. In forest areas, a portion of ^{137}Cs was initially intercepted by the canopy and litter layer (Kato, *et al.*, 2012; FAJ, 2012). The interception and retention of this layer are important processes that affect ^{137}Cs transport and fate. However, the previous studies on ^{137}Cs migration simulation in Fukushima did not consider the interception, retention and wash-out processes of ^{137}Cs in the vegetation canopy/litter layer. Vertical migration inhibits ^{137}Cs horizontal transport across landscapes because such migration associated with hydrological processes such as rainfall-runoff and soil erosion from upland to rivers occurs mainly on the ground surface. The unknown factors of ^{137}Cs downward movement in previous studies affect the simulation accuracy, particularly in long-term prediction. Dissolved radiocesium occupies a smaller fraction than particulate radiocesium, particularly during flooding periods (Sakaguchi *et al.*, 2015; Ueda *et al.*, 2013), which results in a limited contribution of the dissolved phase to the total amount of radiocesium delivery. Therefore, prior studies in Fukushima focus mainly on sediment-bound radiocesium, and ignore the dissolved phase. However, dissolved ^{137}Cs should be of critical importance regarding its uptake to aquatic organisms (Sakaguchi *et al.*, 2015). Therefore, simulation on both sediment-sorbed and dissolved ^{137}Cs can help to better understand the transport of ^{137}Cs and its ecological influence in fluvial environments. The objectives of this chapter are to: (1) develop a watershed ^{137}Cs transport model based on the improved TREX framework and (2) analyze ^{137}Cs transport characteristics associated with the hydrological processes by using a case study of the Kuchibuto River catchment.

5.2 Methodology

The hydrology and soil erosion and transport modules of TREX model have been introduced in chapter 3 and chapter 4. The ^{137}Cs transport module is described in this section.

As Figure 5-1 shown, the released ^{137}Cs is deposited onto covered forest areas (*kv*) or bare soil (1-*kv*). Once the radiocesium reaches to soil surface, it tends to be adsorbed by finer solid particles. During flood storms, ^{137}Cs trapped by forests will be washed off gradually (D_c), and become part of the overland flow. ^{137}Cs can be transported in the interface of the overland water column and top soil (D_s), and downslope along with the water flow (D_a). Because of its physical and biochemical processes, radiocesium also can move in the soil profile (*J*). In this study, the physical transport processes of radiocesium will be described by the model.

5.2.1 Initial ^{137}Cs distribution

^{137}Cs is deposited onto vegetation-covered areas and non-vegetation-covered areas. ^{137}Cs intercepted by the vegetation canopy/litter layer is calculated by

$$I_{0c} = kv f_c I_0 \tag{5.1}$$

The remaining portion reaches to the soil matrix, which can be expressed as

$$I_{0s} = I_0 - I_{0c} = (1 - kv f_c) I_0 \tag{5.2}$$

or

$$I_{0s} = kv(1 - f_c) I_0 + (1 - kv) I_0 = (1 - kv f_c) I_0 \tag{5.3}$$

where, I_{0c} is the initial inventory of ^{137}Cs trapped by the vegetation canopy/litter layer (Bq/m^2); I_0 is the initial total ^{137}Cs inventory measured by airborne survey (Bq/m^2); I_{0s} is the initial inventory of ^{137}Cs reaching the soil layers (Bq/m^2); *kv* is the fraction of vegetation (-); and f_c is the fraction of deposited ^{137}Cs trapped by the vegetation canopy/litter in vegetation-covered areas (-).

^{137}Cs concentration in soil is an exponential function of soil depth z and can be estimated by (Kinouchi *et al.*, 2015)

$$C_{cb}(z) = C_{cb}(0)e^{-kz} \tag{5.4}$$

$$C_{cb}(0) = \frac{kI_{0s}}{\rho_s[1-e^{-kz_0}]} \tag{5.5}$$

where, $C_{cb}(z)$ is the ^{137}Cs concentration at depth z (Bq/g); k is a relaxation constant (1/m); ρ_s is soil density (= 2.65×10^3 kg/m^3); and z_0 is the soil depth (= 0.05 m).

Thus, the concentration in each soil layer can be averaged by

$$C_{cb,ilayer} = \rho_s \frac{1}{z_2 - z_1}\int_{z_1}^{z_2} C_{cb}(z)dz \tag{5.6}$$

where, $C_{cb,ilayer}$ is the ^{137}Cs concentration in the soil layer *ilayer* (Bq/m^3); and z_1, z_2 are the upper and lower boundary depths of layer i (= 1, 2… n), respectively.

5.2.2 ^{137}Cs phases in water

^{137}Cs transport and interactions depend on the chemical phase. The partition coefficient of ^{137}Cs is defined as the ratio of the ^{137}Cs concentration in particulate form to the dissolved phase concentration. The substance transport time from upland to river mouth in watershed is usually longer than the time for local equilibrium. Therefore, the local equilibrium was assumed.

$$K_{d,n} = \frac{\dfrac{C_{c,p,n}}{m_n}}{C_{c,dis}} \tag{5.7}$$

where, $K_{d,n}$ is the partition coefficient of ^{137}Cs to solid particle n (e.g. clay, silt and sand) (m^3/kg); $C_{c,p,n}$ is the concentration of ^{137}Cs bounds to solid particle n (Bq/ m^3); m_n is the concentration of solid particle *n* (kg/m^3); and $C_{c,dis}$ is the concentration of dissolved ^{137}Cs (Bq/ m^3).

$$f_{p,n} = \frac{C_{c,p,n}}{C_{c,total}} \tag{5.8}$$

where, $f_{p,n}$ is the fraction of ^{137}Cs in the particulate phase associated with solid particle *n* (-); and $C_{c,\,total}$ is the total concentration of ^{137}Cs (particulate and dissolved) (Bq/ m^3).

$$C_{c,total} = \sum_{n=1}^{N} C_{c,p,n} + C_{c,dis} \tag{5.9}$$

Combined eq. (5.7), eq. (5.8) and eq. (5.9):

$$f_{p,n} = \frac{C_{c,p,n}}{\sum_{n=1}^{N} C_{c,p,n} + C_{dis}} = \frac{K_{d,n} m_n C_{c,dis}}{\sum_{n=1}^{N} K_{d,n} m_n C_{c,dis} + C_{dis}} = \frac{K_{d,n} m_n}{\sum_{n=1}^{N} K_{d,n} m_n + 1} \tag{5.10a}$$

and

$$f_d = \frac{C_{c,dis}}{\sum_{n=1}^{N} C_{c,p,n} + C_{dis}} = \frac{C_{c,dis}}{\sum_{n=1}^{N} K_{d,n} m_n C_{c,dis} + C_{c,dis}} = \frac{1}{\sum_{n=1}^{N} K_{d,n} m_n + 1} \tag{5.10b}$$

5.2.3 ^{137}Cs loss from the vegetation canopy/litter layer

The trapped radiocesium by vegetation canopy can reduce by radioactive decay and by the environmental processes such as translocation and weathering by rainfall, wind, dew and other factors. This decrease after decay correction, generally known as field loss (Milbourn and Taylor, 1965; Chadwick and Chamberlain, 1970; Madoz-Escande *et al.*, 2005), is time-dependent reduction with a feature of rapid initial loss followed by a slower loss (Fraley, *et al.*, 1993). Loffredo *at al.* (2014) reported that the field loss of ^{137}Cs in Fukushima was strongly influenced by rainfall. The same as canopy, radioactive substances in litter layer also can be lost by litter decomposition and weathering. Therefore, in the present study, we assumed that ^{137}Cs in the vegetation canopy/litter layer reduced by fast and slow methods and can be modeled by a double exponential model

(Ertel, *et al.*, 1989; Loffredo *at al.*, 2014; Loffredo *at al.*, 2015). The field loss of ^{137}Cs from the vegetation canopy/litter layer was estimated as

$$D_c = A i_n C_p \tag{5.11}$$

where, D_c is ^{137}Cs loss in the vegetation canopy/litter layer (Bq/s); A is area of computational cell (m^2); i_n is net rainfall intensity (mm/s); and C_p is the concentration of ^{137}Cs from the canopy/litter layer (Bq/m^2/mm), which can be calculated by

$$C_p = C_v \frac{I_{o,c}}{1+\frac{1}{r12}} \left(\frac{1}{r12}\lambda_f e^{-\lambda_f (t-t_0)} + \lambda_s e^{-\lambda_s (t-t_0)}\right) \qquad if\ (I_c > 0) \tag{5.12a}$$

$$C_p = 0 \qquad if\ (I_c \le 0) \tag{5.12b}$$

C_v is a coefficient (1/mm); *r12* is the ratio between slow and fast loss (=0.22 (Loffredo *at al.*, 2015)); λ_f and λ_s are constants for fast and slow loss respectively (1/s); t is simulation time(s); t_0 is start time (s); and I_c is ^{137}Cs storage in the vegetation canopy/litter layer (Bq/m^2), which can be updated according to mass balance:

$$I_{c,t2} = I_{c,t1} - \frac{Dc \times \Delta t}{A} \tag{5.13}$$

where, subscripts *t1* and *t2* refer to the beginning and end of the time period, respectively; and Δt is the time interval (s).

5.2.4 ^{137}Cs in the water column of the overland plane

^{137}Cs in the overland water column in each computational cell is supplied from field loss of the vegetation layer and eroded sediments from the bottom soil matrix. Conversely, deposited sediments carry ^{137}Cs to the soil matrix, resulting in a decrease in ^{137}Cs concentration in the water column. Dissolved ^{137}Cs is infiltrated into the soil matrix. If no overland flow occurs, the washed ^{137}Cs cannot be transported and instead accumulates in the top soil. As a result of the lateral water flow, ^{137}Cs can be transported in the lateral direction. The mass balance of ^{137}Cs in the water column of the overland plane is calculated by

$$\frac{\partial C_{c,ov}}{\partial t} = \frac{D_c + D_s - D_a + D_l}{Vol_w} \quad (5.14)$$

$$D_s = A_s(\sum_{n=1}^{N} v_r C_{cb,1} f_{pb,n} - \sum_{n=1}^{N} v_{se} C_{c,ov} f_{p,n} - v_i C_{c,ov} f_d) \quad (5.15)$$

$$D_a = A_c(v_x + v_y + v_f) C_{c,ov} \quad (5.16)$$

where, $C_{c,ov}$ is the total ^{137}Cs concentration in the water column (Bq/m^3); D_s is the ^{137}Cs vertical transport associated with soil erosion, deposition and dissolved ^{137}Cs to the top soil layer along with water infiltration, which also includes ^{137}Cs accumulation when on overland flow generations (Bq/s); D_a is the lateral ^{137}Cs advection (Bq/s); D_l is the lateral dissolved ^{137}Cs transport along with subsurface flow from adjacent soil layers (Bq/s); A_c and A_s are the cross-sectional area in the flow direction and surface area, respectively (m^2); $f_{p,n}$ is the particulate ^{137}Cs fraction in the water column (-); $f_{pb,n}$ is the particulate ^{137}Cs fraction in the first soil layer (-); v_r, v_{se} and v_i are soil erosion, deposition, and infiltration velocities respectively(m/s); v_x, v_y and v_f are flow velocity in the x- or y-direction and between the overland plane and channel (floodplain), respectively (m/s); and Vol_w is the volume of water (m^3).

5.2.5 ^{137}Cs in the soil profile on the upland

The interaction of ^{137}Cs between the first soil layer and overland water involves particulate ^{137}Cs transport associated with soil erosion and deposition and dissolved ^{137}Cs migration in the water along with water infiltration and subsurface flow. The ^{137}Cs vertical dynamics in soil layers are attributed to advection and diffusion resulting from physical and biochemical processes. Thus, the mass balances in the soil layers are calculated by

$$\frac{\partial C_{cb,ilayer}}{\partial t} = \frac{-D_s + \Delta J_{ilayer} - D_l}{Vol_s} \qquad if\,(ilayer = 1) \quad (5.17a)$$

$$\frac{\partial C_{cb,ilayer}}{\partial t} = \frac{\Delta J_{ilayer} - D_l}{Vol_s} \qquad if\,(ilayer > 1) \quad (5.17b)$$

where, *ilayer* is the layer index of the soil/sediment bed (-); Vol_s is the volume of the soil layer (m^3); D_l is the dissolved ^{137}Cs lateral transport along with subsurface flow in soil layer (Bq/s); and ΔJ_{ilayer} is the net ^{137}Cs vertical advection and diffusion in each soil layer (Bq/s).

$$J_{ilayer} = A(v_{adv} C_{cb,ilayer} - v_{dif} \frac{\Delta C_{cb,ilayer}}{\Delta z}) \tag{5.18}$$

where, J_{ilayer} is ^{137}Cs advection and diffusion in soil layer *ilayer* (Bq/s); v_{adv} is ^{137}Cs vertical advection velocity (m/s); v_{dif} is ^{137}Cs diffusion velocity (m^2/s); $\Delta C_{cb,ilayer}$ is the difference of ^{137}Cs concentration in the soil layers *ilayer and ilayer* +1; and Δz is thickness of the soil layer *ilayer* +1.

$$D_l = A_c v_l C_{cb,ilayer} f_{db} \tag{5.19}$$

where, v_l is the lateral flow velocity from soil (m/s); and f_{db} is the dissolved ^{137}Cs fraction in the soil layer (-).

5.2.6 ^{137}Cs transport in river channel

^{137}Cs transport processes in the river channel are almost same as those in overland areas:

$$\frac{\partial C_{c,ch}}{\partial t} = [\sum_{n=1}^{N} v_r C_{cb,ch} f_{pb,n} - \sum_{n=1}^{N} v_{se} C_{c,ch} f_{p,n}] \frac{A_s}{Vol_w} - (v_f - v_x) C_{c,ch} \frac{A_c}{Vol_w} \tag{5.20}$$

$$\frac{\partial C_{cb,ch}}{\partial t} = [\sum_{n=1}^{N} v_{se} C_{c,ch} f_{p,n} - \sum_{n=1}^{N} v_r C_{cb,ch} f_{pb,n}] \frac{A_s}{Vol_s}) \tag{5.21}$$

where, $C_{c,ch}$ is the total ^{137}Cs concentration in the water column in river (Bq/m^3); $C_{cb,ch}$ is the total ^{137}Cs concentration in the bottom sediment layer (Bq/m^3); and v_x and v_f are flow velocity in the x-direction and between the overland plane and channel, respectively (m/s).

5.2.7 Mass transfer and transformation processes (chemical reactions).

The fate of chemicals is potentially influenced by a number of other processes such as biodegradation and oxidation. For our ^{137}Cs migration study, all transformation processes were neglected except radioactive decay.

$$C_{t2} = C_{t1} e^{-\lambda_d \Delta t} \tag{5.22}$$

where, λ_d is the decay constant coefficient (1/s); and C_{t1}, C_{t2} are the amounts of ^{137}Cs at time *t1* and *t2*, respectively;

5.3 Case study in the Kuchibuto River catchment

The Kuchibuto River catchment was heavily contaminated by radiocesium. The 3rd airborne survey by MEXT reported ^{137}Cs inventory in this catchment of about 10^5–10^6 Bq/m^2 (see chapter 2 for detailed introduction). Our simulation began on Jun 21, 2011 when the field observation began, which was near the time of 3rd airborne survey by MEXT on July, 2, 2011. Thus, the surveyed result (Figure 2-5) served as the initial ^{137}Cs distribution for our simulations. Several parameters in the model were determined according prior field studies in this catchment. ^{137}Cs distribution coefficients ($K_{d,n}$) were set in Table 5-1 by referring to measurements in the Kuchibuto River (Fan *et al.*, 2015). Land use patterns have a large influence on some soil properties and ^{137}Cs downward migration, resulting in different distributions of ^{137}Cs in the soil profile. Thus, the relaxation constant (*k*) and vertical advection and diffusion velocities (v_{adv}, v_{dif}) varied according to land use type (Table 5-2) (Takahashi *et al.*, 2015; JAEA, 2015). Since there was no data for paddy field, the vertical advection and diffusion velocities in paddy field were set as that in cropland. The areal fractions of the other land use types such as built-up area and water body are very small, thus, no contribution of these types was assumed for ^{137}Cs transport. A survey conducted by Forestry and Forest Products Research Institute (FFPRI) and Forestry Agency of Japan (FAJ) reported that about 18%-34% of radiocesium was already in the soil matrix in the vegetation area by early August and September 2011 (FAJ, 2012). Thus, the fraction of deposited ^{137}Cs trapped by vegetation canopy/litter in vegetation-covered areas (f_c) was set as 0.8 in our study. C_v and λ_f were calibrated to match the observation during the calibration period of June and September 2011, when the ^{137}Cs fast loss from vegetation is significant at the downstream site as shown in Table 5-3; the decay constant (λ_d) of ^{137}Cs was 0.023 year^{-1}.

5.3.1 Initial ^{137}Cs distribution over the catchment

According to our calculation, the initial total amount of ^{137}Cs over the Kuchibuto River catchment was about 37.12 TBq[1]. An estimated 7.63 TBq of ^{137}Cs was trapped in the canopy/litter layer, most of which was located in the upper stream areas (Figure 5-2). This means the total deposited ^{137}Cs in the vegetation-covered area was 9.54 TBq, of which about 1.91 TBq of ^{137}Cs (i.e. 20%) have penetrated or washed out from the canopy/litter layer and reached to the underlying soil matrix three months after the accident. 10 layers with the thickness of 5 mm for each layer were divided to characterize ^{137}Cs distribution in the soil profile. The simulated ^{137}Cs distributions in the soil profile followed exponential function (Figure 5-3).

5.3.2 Comparison of observed and simulated ^{137}Cs concentration

A time-integrated suspended sediment sampler (Phillips *et al.*, 2000) was installed at the downstream site to collect sediment samples for a certain period. The ^{137}Cs concentrations of collected samples were measured in lab (this time integrated concentration is an average concentration for a period). The measured results were plotted in Figure 5-4 for comparison with our simulated results. Three cases with the same parameters but different scenarios were calculated as shown in Figure 5-4. The observation data and our simulation (case 1) agree well except during November and March 2011. During that period our simulation underestimated the ^{137}Cs concentration of Suspended Sediment (SS). One possible reason is the effect of dry ^{137}Cs deposition from the atmosphere. That period coincided with winter and early spring, in which the wind was stronger than that in other seasons as shown in Figure 5-5. Strong wind could have resuspended and deposited ^{137}Cs into the river. Although the total amount of ^{137}Cs deposition may be small, the total amount of sediment was also quite small during this period. Therefore, the particulate ^{137}Cs concentrations of SS were sensitive to the total and consequently become larger. This is one explanation for our underestimated results. Moreover, other factors such as wind direction, surface wetness, and natural decreases in ^{137}Cs can affect ^{137}Cs dry deposition. Because the period was not rainy, the total amount of ^{137}Cs loads during that period was smaller than the total during the flood period, which

[1] 1 TBq = 10^3 GBq = 10^6 MBq = 10^9 KBq = 10^{12} Bq

is our main focus. As shown in Figure 5-6, during November 2011 to April 2012, less than about 3% of annual ^{137}Cs was transported out of the catchment. Thus, the effect of our underestimation was negligible in the annual ^{137}Cs load estimation.

Figure 5-7 shows the comparisons of simulated and observed ^{137}Cs concentrations of SS at the upper stream, middle stream site and downstream sites for three periods, respectively. The sediment samples were collected and measured by researchers from the University of Tsukuba and the results can be found in the JAEA annual report (2014).

Figure 5-8 shows the comparisons between calculated and measured instantaneous particulate ^{137}Cs concentrations at the downstream and middle stream site in normal flows and flood storms on Oct. 16 and 25, 2013, respectively. The ^{137}Cs concentrations of SS with different grain sizes were measured during the storms on Oct. 16 2013, Oct. 6 2014 and Oct. 14 2014, and were plotted and compared with simulated data in Figure 5-9. ^{137}Cs concentrations in 2014 were smaller than simulation. A possible reason is decontamination work decreased ^{137}Cs inventory in the upper stream area (JME, 2016). Both the observed and simulated data showed that finer solid particles had higher absorption capacities to ^{137}Cs. During the simulation period, the ratio of particulate ^{137}Cs flowing from the catchment carried by clay, silt, and sand was 17:70:13, respectively, whereas, the ratio of flux for clay, silt and sand was 7:65:28, respectively.

Sakaguchi *et al.* (2015) collected water samples from the Kuchibuto River within one year after the accident and measured size distributions of ^{137}Cs in river water. Comparing with the measured water samples data, our simulation underestimated ^{137}Cs of SS (Figure 5-10). It was non-rainy and normal flow period, thus, the flow rate and sediment concentration were very small (Table 5-4). ^{137}Cs concentrations were easily affected by other factors, e.g. dry deposition from atmosphere as explained above. However, the dissolved ^{137}Cs concentrations were well calculated. Our time-integrated dissolved ^{137}Cs concentrations also well agree with measurements by JAEA (2014) for the two periods at the three sites in the river (Figure 5-11). Our simulation indicates the dissolved ^{137}Cs concentrations were generally less than 30 mBq/L in the Kuchibuto River.

By comparing with the observed time-integrated and instantaneous ^{137}Cs concentration, we concluded the simulated results were generally acceptable.

To analyze the effects of vegetation and ^{137}Cs downward movement in the soil, two cases were assumed as shown in Figure 5-4. The simulated result indicates that the vegetation canopy/litter layer played an important role in ^{137}Cs transport, especially at the early stage of the simulation. If the vegetation effect is not considered, the ^{137}Cs concentration of SS in the river will be underestimated at the early simulation stage (case 3). The ^{137}Cs concentration in the soil profile changes because of its downward movement in the soil; otherwise, all ^{137}Cs is accumulated in the surface above the soil. As shown in Figure 5-4, the error between case 1 and case 2, which considers and does not consider ^{137}Cs downward movement in the soil, respectively, increased as the simulation period progressed.

The ^{137}Cs concentration of SS in the Kuchibuto River decreased rapidly from June to September 2011, and then became relatively stable. By 2014, the level was about 1-10 Bq/g. According to field measurement at two sites in Fukushima (Matsunaka et al., 2016), the pre-accident levels of ^{137}Cs in the soil were about 0.558×10^{-3} ~ 48.4×10^{-3} Bq/g. Therefore, more than three years later, the ^{137}Cs concentration of SS in the Kuchibuto River was still 100 times larger than that before that accident.

5.3.3 ^{137}Cs transport from different components

Figure 5-12 shows ^{137}Cs transport in the vegetation canopy/litter layer-ground surface-river components. During the simulation period (i.e. Jun. 21th, 2011-Dec. 31, 2014) ^{137}Cs field loss was about 2.36 TBq (②), and 4.85 TBq of ^{137}Cs remained in the vegetation canopy/litter layer at the end of our simulation. Kato (2012) reported that in a coniferous forest in Tochigi Prefecture, Japan, an estimated 60% of the total deposited ^{137}Cs remained in the forest canopy five months after the accident. In our simulation, the retention ratio of the vegetation layer was similar during the same period in mid-August, 2011, at 59%. Hence, as a stock, this layer still can be decontamination target. A portion of the field loss was considered as a supplement to the top soil layer, and the remaining portion was transported to rivers along with water flow and eroded sediments. About 0.59 TBq ^{137}Cs was transported from the upland regions to river systems (④), most of which was transported from the catchment through the river outlet as the particulate phase. During the 3.5-year study, the ^{137}Cs reduction rate by rainfall–runoff wash-off was 1.24 GBq/km^2/y, and the reduction ratio was 1.6% (Table 5-5). JAEA (2013) estimated the

^{137}Cs load was 542 MBq/d based on on-site observation at the downstream site from Jun. 21th, 2011 to Jan. 22, 2013. Our simulation shows about 3500 GBq of ^{137}Cs was transported out of the catchment (i.e. 608 MBq/d) during the same period, so, they agree well. The amount of ^{137}Cs that bound to deposited sediments in river channels was very small, about 4% of the total inflowing ^{137}Cs from the upland areas. The natural radioactive decay was about 2.82 TBq (①+③+⑤). Thus, the ^{137}Cs reduction mainly depended on radioactive decay. If we consider ^{137}Cs reduction by natural radioactive decay, the total loss of ^{137}Cs was 3.39 TBq (①+③+⑤+⑥), which indicates that about 90% ^{137}Cs remained in the catchment. This estimation confirms the necessity of artificial decontamination in the following years.

5.3.4 Spatial distribution of ^{137}Cs transport

Like chapter 4, the catchment was divided into 21 subwatersheds. The ^{137}Cs reduction rate and reduction ratio by rainfall-runoff for these subwatershes were calculated and summarized in Table 5-5, and appear in Figure 5-13 and Figure 5-14, respectively. The ^{137}Cs reduction rate demonstrates the ^{137}Cs inventory in the upper part of the catchment decreased faster than that in the other areas, which corresponds to the initial ^{137}Cs distribution (Figure 2-5). In contrast, the ^{137}Cs reduction ratio of the subwatersheds in the middle portion of the catchment was higher, which have similar spatial trends with sediment supply ratio (Figure 4-9).

Because only several months after the accident, we can consider the temporal change of ^{137}Cs during the period of 3rd and 4th airborne surveys by MEXT mainly resulted from natural decontamination. As we expected, the spatial distribution of the ^{137}Cs change (Figure 5-15) partially corresponds to our simulated result (Figure 5-14). However, the total reduction of ^{137}Cs calculated from the data of airborne surveys (about 2200 GBq) is much larger than the calculated amount of ^{137}Cs transported out of the catchment (about 245 GBq) in this period. This large gap may attribute to the uncertainties included in the results of airborne survey.

The ^{137}Cs contamination level and spatial variation of soil erosion affected the distribution of the ^{137}Cs reduction rate and ratio. Sediment-bound ^{137}Cs from detached soil particles is a main source of ^{137}Cs in the water flow; thus, severe soil erosion resulted in rapid ^{137}Cs reduction (Table 5-5). Although the soil erosion was gentle in the upper catchment, the ^{137}Cs concentration of soil particles was higher. Higher concentration indicates a larger amount of ^{137}Cs per unit of eroded sediment. Consequently, the total amount of ^{137}Cs reduction in those heavily contaminated subwatersheds was higher. This contrast supplies more information on ^{137}Cs transport behavior beyond the field station observations. Undoubtedly, the ^{137}Cs reduction rate was higher in the upper stream areas. Nevertheless, decontamination works in the critical ^{137}Cs-adsorbed sediment erosion zone including subwatersheds 16, 20, 11, and 8 in the middle portion of the catchment are also urgently needed, particularly for the assessment of long-term radiocesium environmental risk.

Figure 5-16 shows the spatial distribution of ^{137}Cs transport in each 90-m computational cell. The source of transported ^{137}Cs originated from the hillside and areas near the river bank (Figure 5-17). As a result of sediment deposition, ^{137}Cs accumulated near the source of eroded areas, which may be considered ^{137}Cs "hotspots" and can be targeted as areas for future decontamination. The spatial identification of ^{137}Cs transport shown in the figures should be helpful for developing various decontamination strategies in this catchment.

5.4 Conclusions

In this chapter, a watershed ^{137}Cs model was developed based on the improved TREX framework and was applied in a forested catchment. The conditions of ^{137}Cs field loss from the vegetation canopy/litter layer and downward movement in soil in additional to two ^{137}Cs distribution phases in water were considered in the model. The ^{137}Cs distributions in the computational cells were defined in vegetation canopy/litter and soil layers. Comparisons between observed and simulated time-integrated and instantaneous ^{137}Cs concentration at stations revealed that the model reproduced ^{137}Cs transport well. Our simulations showed the total ^{137}Cs reduction was 3.39 TBq by the end of 2014, which means about 90% ^{137}Cs remained in the catchment. This estimation confirms the necessity of artificial decontamination in the following years. An estimated 4.85 TBq of ^{137}Cs remained in the canopy/litter layer, which indicates this layer stored a considerable amount of radiocesium and can be targeted for decontamination. During the 3.5-year-study, 0.57 TBq of ^{137}Cs was transported from the catchment. It mainly carried by eroded suspended sediment. During the period, the average ^{137}Cs reduction rate and reduction ratio by rainfall-runoff wash-off were 1.24 GBq/km^2/y and 1.6%, respectively. Both of values show spatial distributions related to the spatial variation of the ^{137}Cs contamination level and soil erosion. The spatial variation implies: the ^{137}Cs reduction rate was higher in the upper stream areas, nevertheless, decontamination works in the critical erosion zone in middle portion of the catchment are also urgently needed, particularly for the assessment of long-term radiocesium environmental risk. The sinks of ^{137}Cs, which accumulated an appreciable amount of ^{137}Cs owing to sediment deposition, can be targeted areas for future decontamination. The results of this study helped us to understand the ^{137}Cs transport behavior and fate better and should be useful for decision-making.

Table 5-1. K_d value for different solids (ml/g)

Clay (<3μm)	Silt (3-63μm)	Sand(>63μm)
$10^{6.2}$	$10^{6.0}$	$10^{5.8}$

Table 5-2. Parameters related to land use type

Land use	k(1/cm)	V_{adv} (cm/y)	V_{dif} (cm^2/y)
Paddy field	0.7	0.04	0.006
Cropland	1.2	0.04	0.006
Forest	0.6	0.09	0.016

* k, V_{adv} and V_{dif} were determined by referring prior field measurements (Takahashi *et al.*, 2015; JAEA, 2014).

Table 5-3. Calculated parameters related to field loss

C_v	λ_f	λ_s
0.05	3.5×10-2	0.5×10-3

*λ_s was set by referring Loffredo *et al.*' results (2015).

Table 5-4. Field measured flow rates and SSC for Sakaguchi's sampling data

Sampling time	Flow rate(m^3/s)	Sediment concentration(g/l)
31-Jul-11,10:00-12:00	2.8	0.04~0.06
12-Dec-11,09:00-11:30	1.7	0.02
03-May-12,09:30-11:00	2.6~2.8	0.018~0.032
02-Aug-12,09:30-11:00	1.5	0.018
02-Dec-12,10:30-12:00	1.9	0.014

Table 5-5. ^{137}Cs reduction by wash-off in subwatershes

sub.No.	deposited ^{137}Cs (GBq)	^{137}Cs reduction (GBq)	reduction rate ($GBq/km^2/y$)	reduction ratio (%)
1	2370.5	39.95	2.06	1.70
2	1950.8	28.07	1.52	1.45
3	5274.0	92.27	2.42	1.76
4	861.7	11.08	1.01	1.28
5	1152.7	15.85	1.09	1.38
6	5784.0	54.91	2.00	0.98
7	817.8	9.50	0.96	1.17
8	891.7	19.75	1.44	2.18
9	1166.8	19.23	1.18	1.67
10	1614.3	29.51	1.24	1.80
11	2474.1	58.90	1.43	2.38
12	2135.1	38.44	1.04	1.79
13	1690.3	24.79	0.81	1.50
14	1838.9	25.90	1.11	1.38
15	798.9	6.72	0.46	0.83
16	707.7	20.01	1.49	2.82
17	648.3	11.74	0.89	1.83
18	1013.2	21.47	1.08	2.08
19	1904.5	14.65	0.34	0.75
20	794.4	23.54	1.13	2.91
21	1228.2	26.65	0.90	2.15
whole catchment	37117.9	592.93	1.24	1.60

* subwatersheds are shown in Figure 5-13.

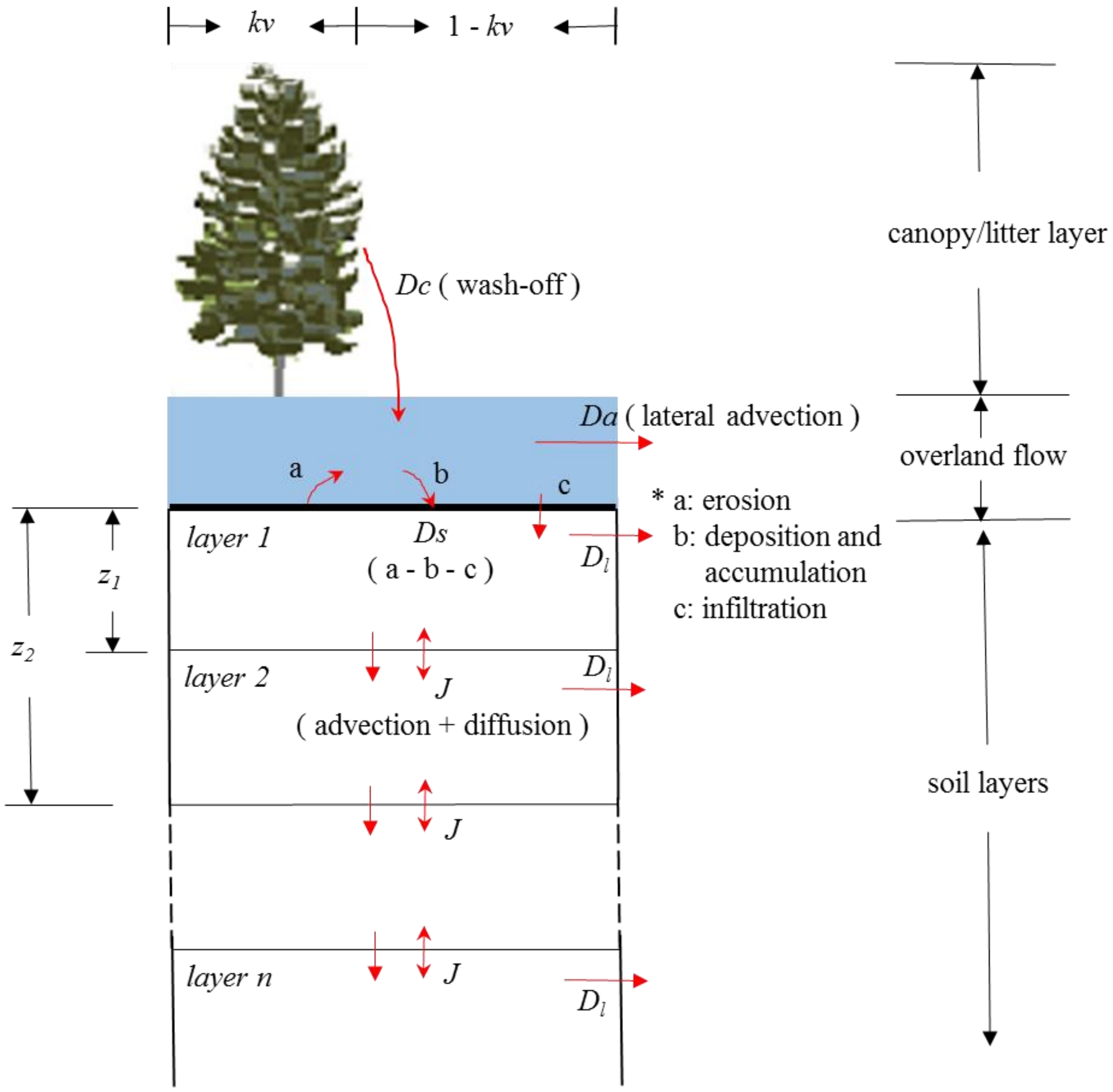

kv: the fraction of vegetation when the accident occurred;

z_1, z_2: the upper and lower boundary depths of layer *i* (*i*=1,2,…,n).

D_c: the ^{137}Cs loss from the vegetation canopy/litter layer.

D_s: the ^{137}Cs transport associated with soil erosion (a) and deposition (b) (including ^{137}Cs accumulation to top soil layer), and dissolved ^{137}Cs to soil along with water infiltration (c);

D_a: the lateral ^{137}Cs advection;

D_l: the dissolved ^{137}Cs transport along with subsurface flow;

J: the ^{137}Cs advection and diffusion in soil layers.

Figure 5-1. Schematic diagram of ^{137}Cs migration in each computational cell.

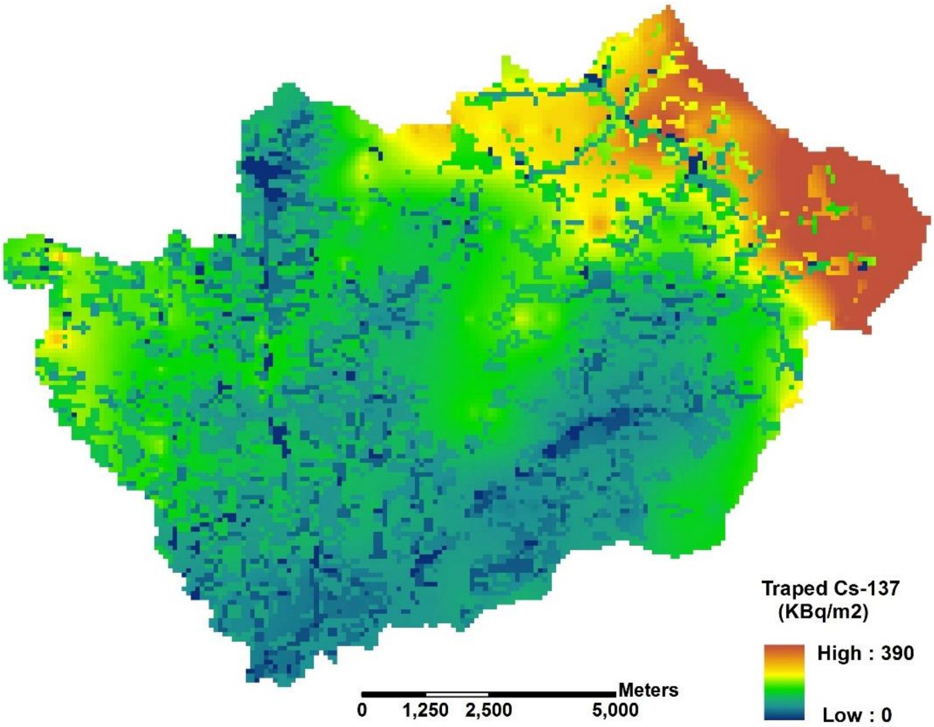

Figure 5-2. Calculated distribution of trapped ^{137}Cs by the vegetation canopy/litter layer (I_{0c}).

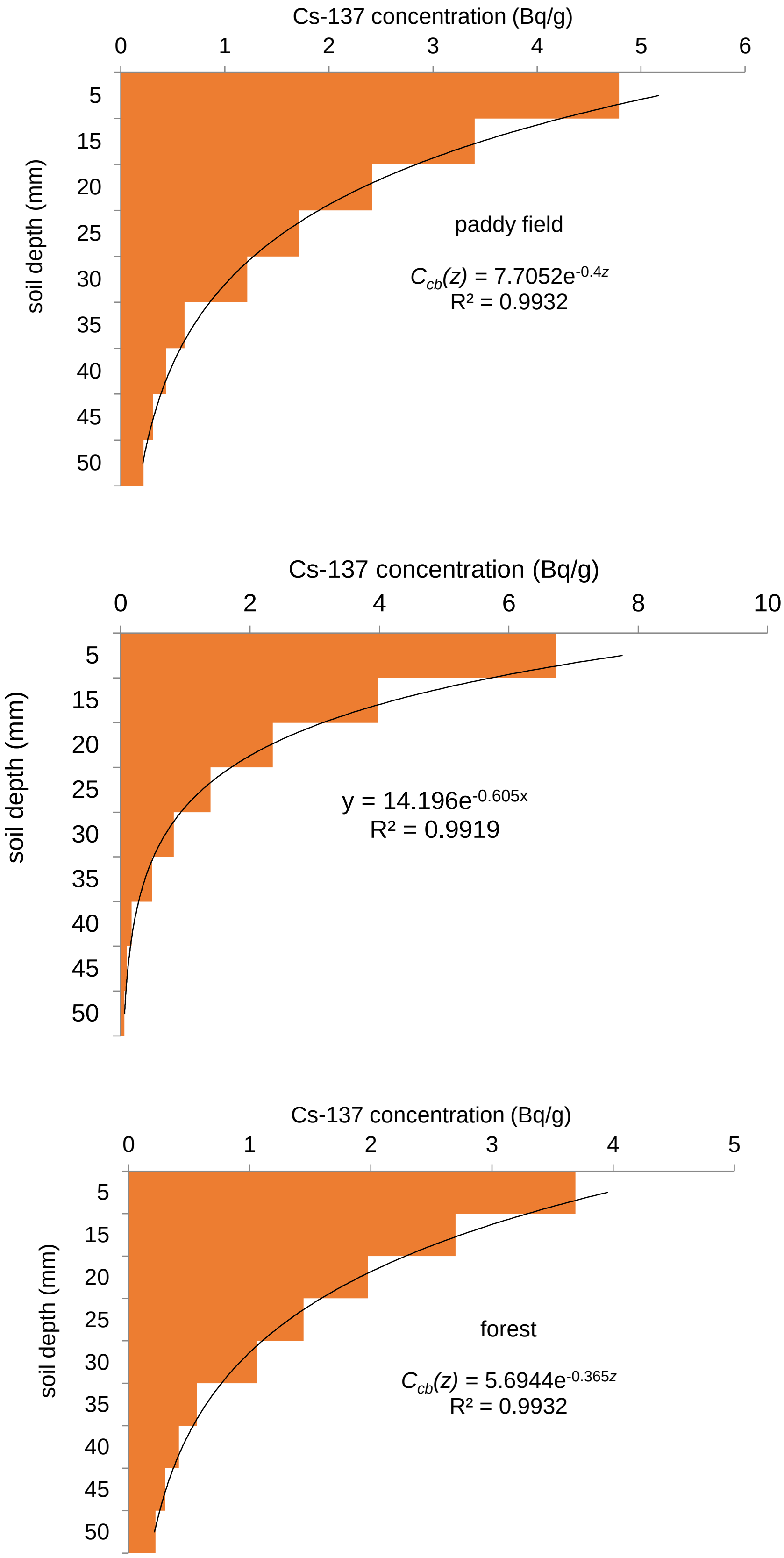

Figure 5-3. Calculated average initial ^{137}Cs concentration in the three main types of land use in the catchment.

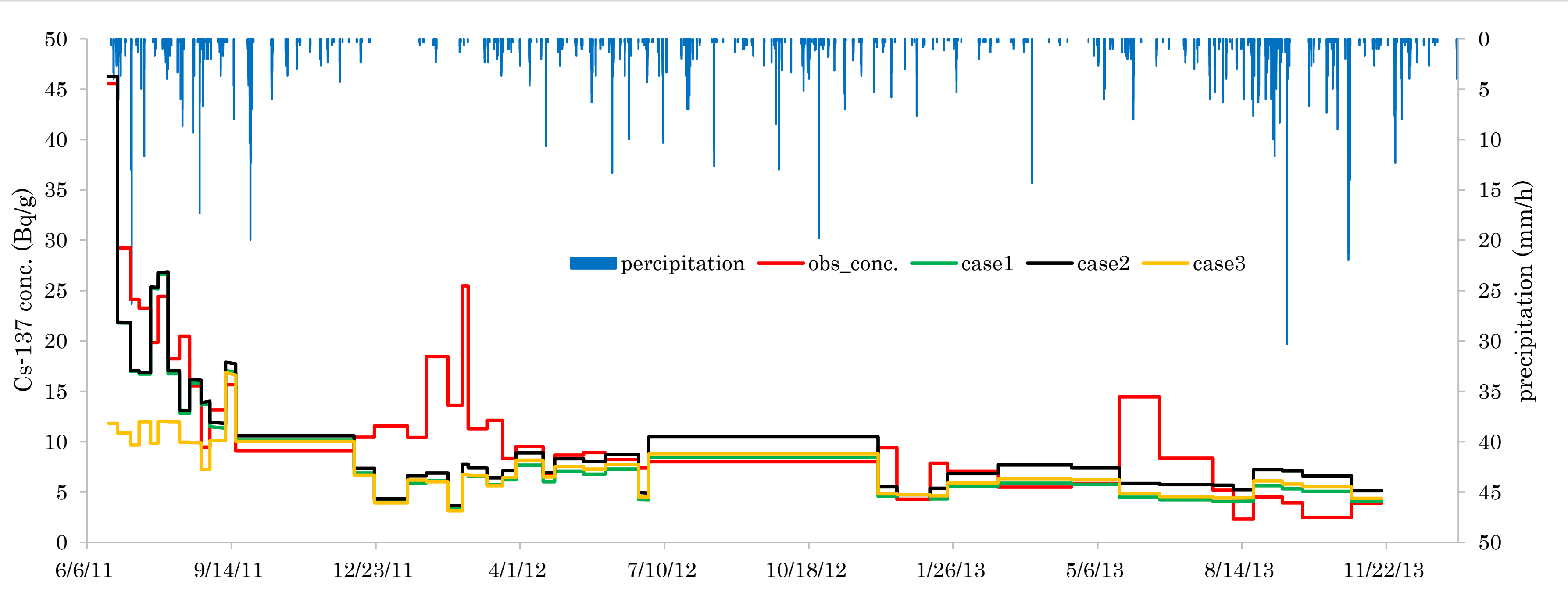

case 1: considered both ^{137}Cs wash-off processes from vegetation canopy/litter layer and ^{137}Cs downward movement.

case 2: considered ^{137}Cs wash-off processes from vegetation canopy/litter layer but no ^{137}Cs downward movement.

case 3: did not consider vegetation canopy/litter layer, and all deposited ^{137}Cs reached to ground surface and was absorbed by soil particles (^{137}Cs downward movement was considered).

Figure 5-4. Comparison of simulated and observed ^{137}Cs concentration of Suspended Sediment (SS) at the downstream site (^{137}Cs concentration is averaged value for a certain period)

* The measurements were done by research group from the University of Tsukuba.

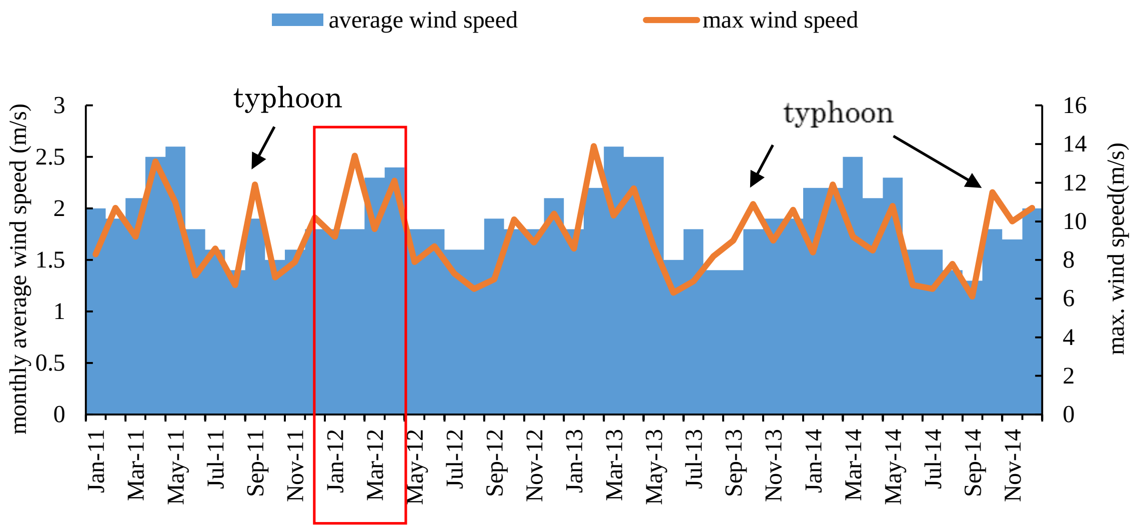

Figure 5-5. Monthly wind speed in meteorological observation site (Fukushima city)

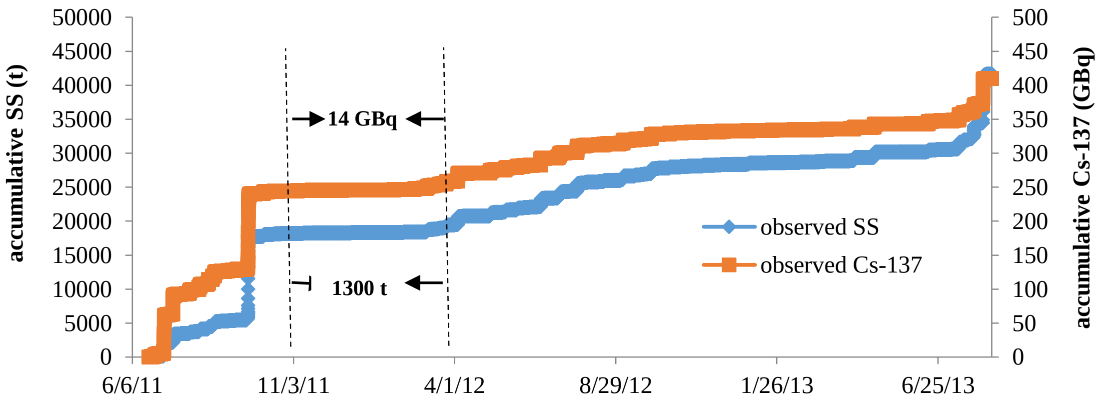

The total amount of SS and ^{137}Cs transport from the downstream site were about 1300 t and 14 GBq respectively during the period Nov. 1 2011 to Apr. 1 2012 (dash line).

Figure 5-6. Observed accumulative SS and ^{137}Cs transport from the downstream site (St. D)

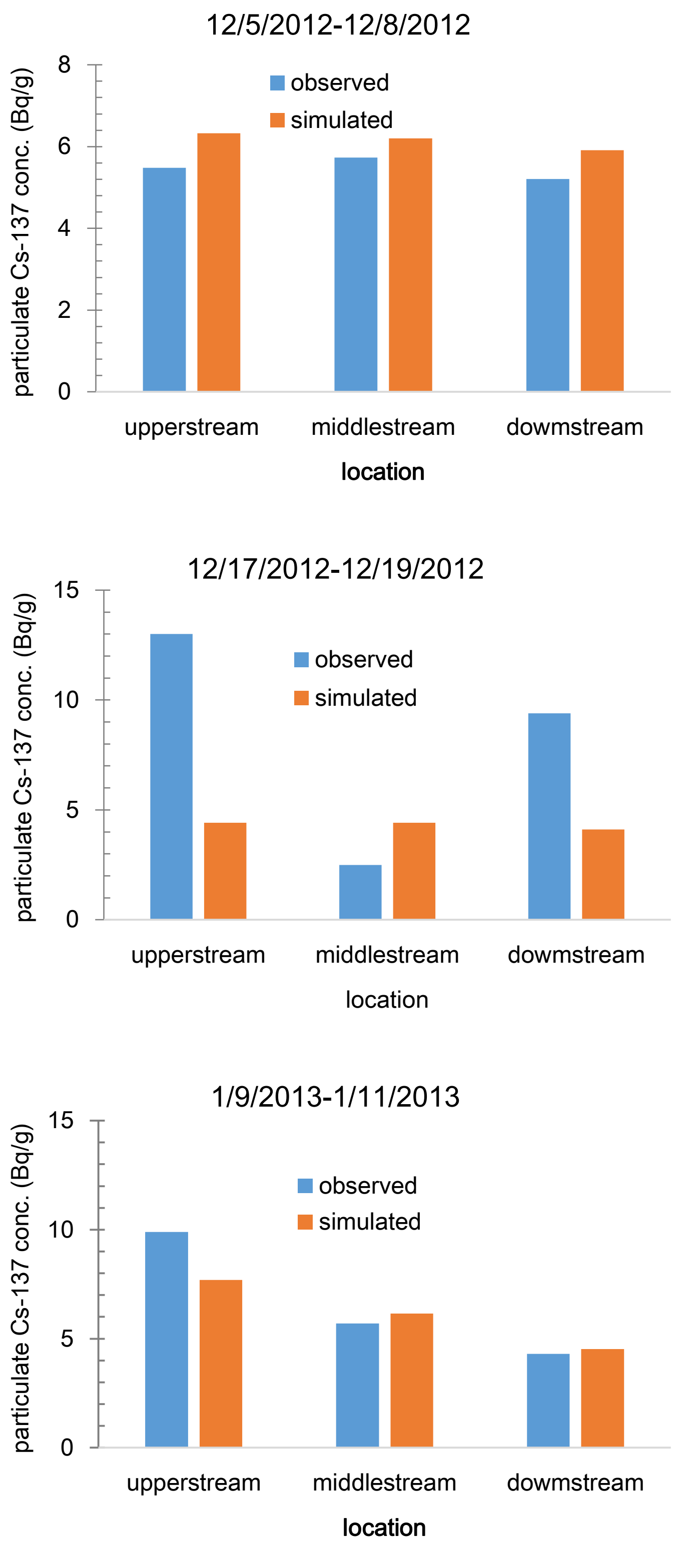

Figure 5-7. Comparison of simulated and observed ^{137}Cs concentration of SS for the three periods (the observed data was from JAEA annual report (2013))

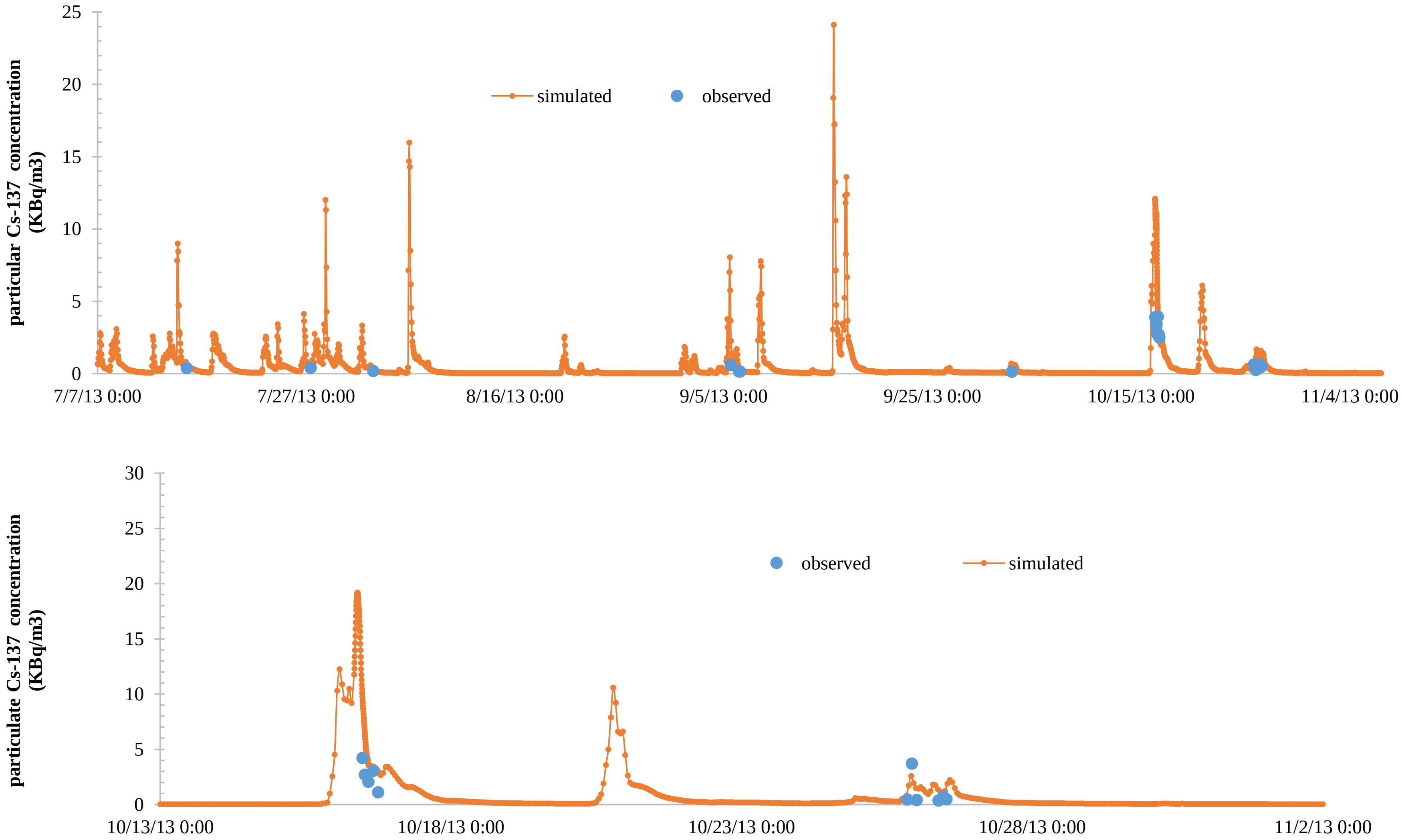

Figure 5-8. Instantaneous particulate ^{137}Cs concentration in river water at the middle stream site (top) and downstream site (bottom)

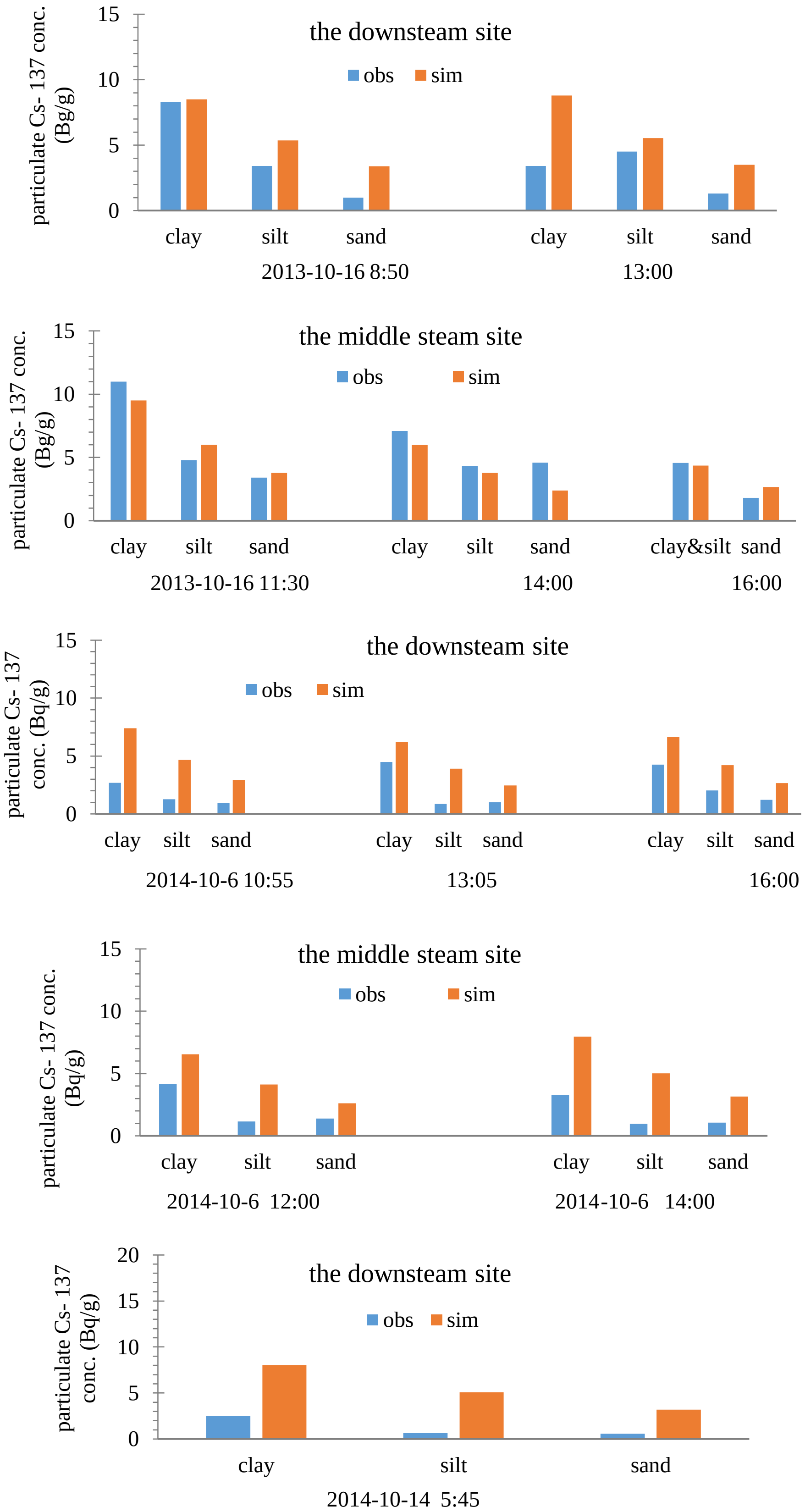

Figure 5-9. Comparison of simulated and observed instantaneous ^{137}Cs concentration of SS during flood events at the downstream site and middle stream site (For the measurement: clay (≤ 2.7μm), silt (2.7-63μm) and sand (63-132μm))

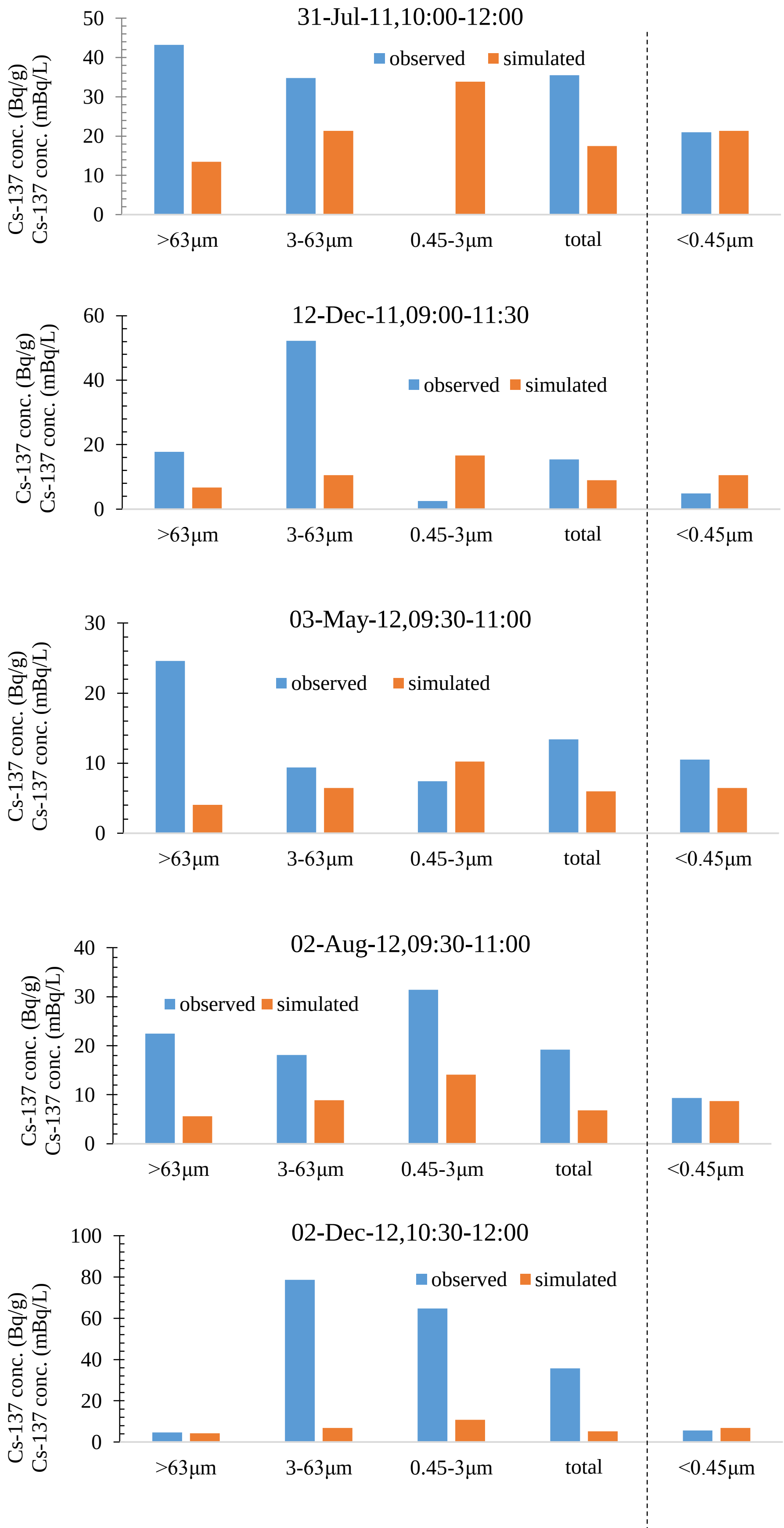

Figure 5-10. Comparison of simulated and observed instantaneous particulate (≥ 0.45μm) and dissolved (< 0.45μm) ^{137}Cs concentration.

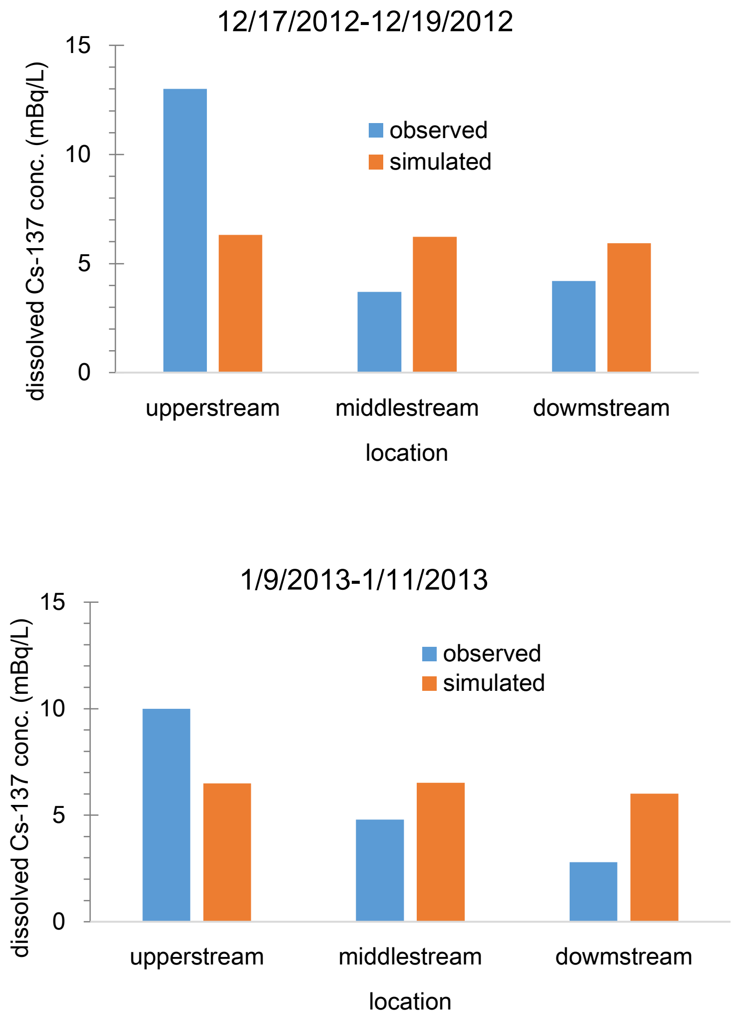

Figure 5-11. Comparison of simulated and observed dissolved ^{137}Cs concentration at the upper stream, middle stream and downstream sites from the two periods (observed data was from JAEA annual report (2013)).

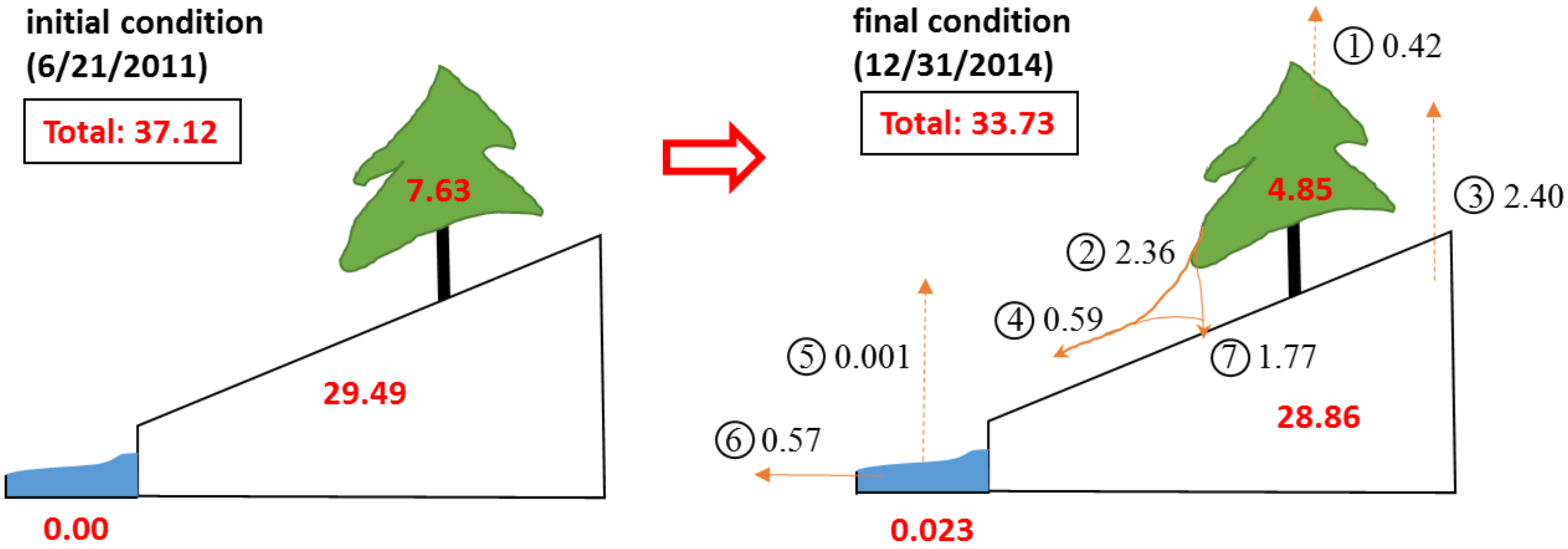

ΔMc = - ① - ② = - 0.42 – 2.36 = -2.78 (TBq)

ΔMs = - ③ + ⑦ = - ③ + ② - ④ = - 2.4 + 2.36 – 0.59 = -0.63 (TBq)

ΔMw = - ⑤ - ⑥ + ④ = - 0.001 - 0.57 + 0.59 = 0.02 (TBq)

ΔM = - ① - ③ - ⑤ - ⑥ = - 0.42 – 2.4 - 0.001 - 0.57 = -3.39 (TBq)

①: ^{137}Cs radioactive decay in canopy/litter layer;
②: ^{137}Cs loss from canopy/litter layer;
③: ^{137}Cs radioactive decay from ground surface;
④: ^{137}Cs transport from upland to river systems;
⑤: ^{137}Cs radioactive decay in river;
⑥: ^{137}Cs transport out of the catchment from outlet;
⑦: net incoming of ^{137}Cs in soil layer because of rainfall-runoff;
ΔMc: ^{137}Cs change in vegetation canopy/litter layer;
ΔMw: ^{137}Cs change in river;
ΔMs: ^{137}Cs change in soil;
ΔM: ^{137}Cs change in the catchment;

Figure 5-12. Mass balance of ^{137}Cs transport during the simulation period (units: TBq)

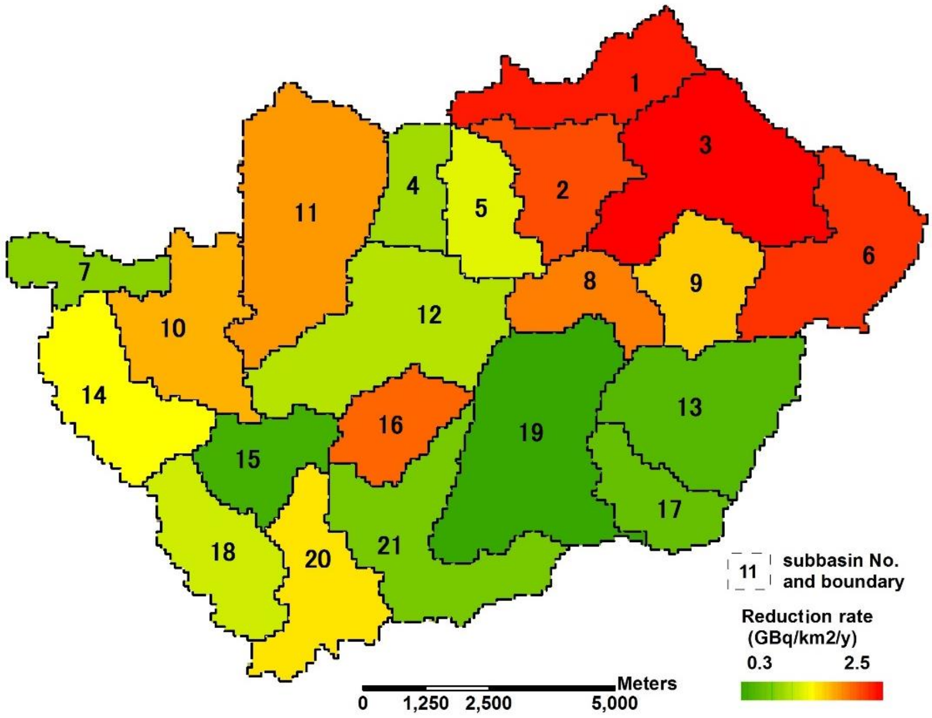

Figure 5-13. Spatial distribution of ^{137}Cs reduction rate by rainfall-runoff wash-off

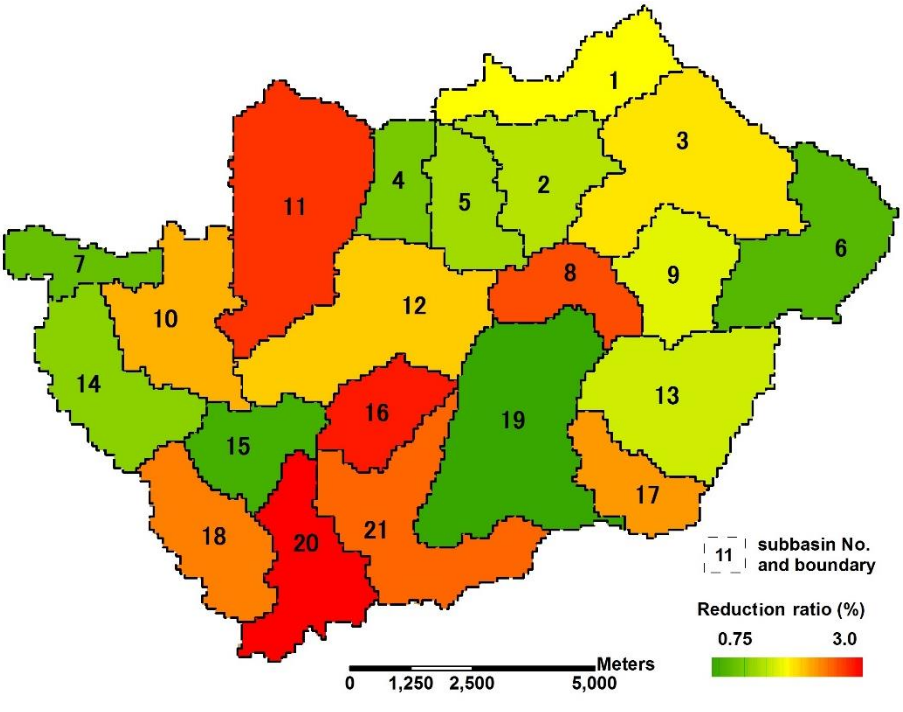

Figure 5-14. Spatial distribution of ^{137}Cs reduction ratio by rainfall-runoff by the end of 2014

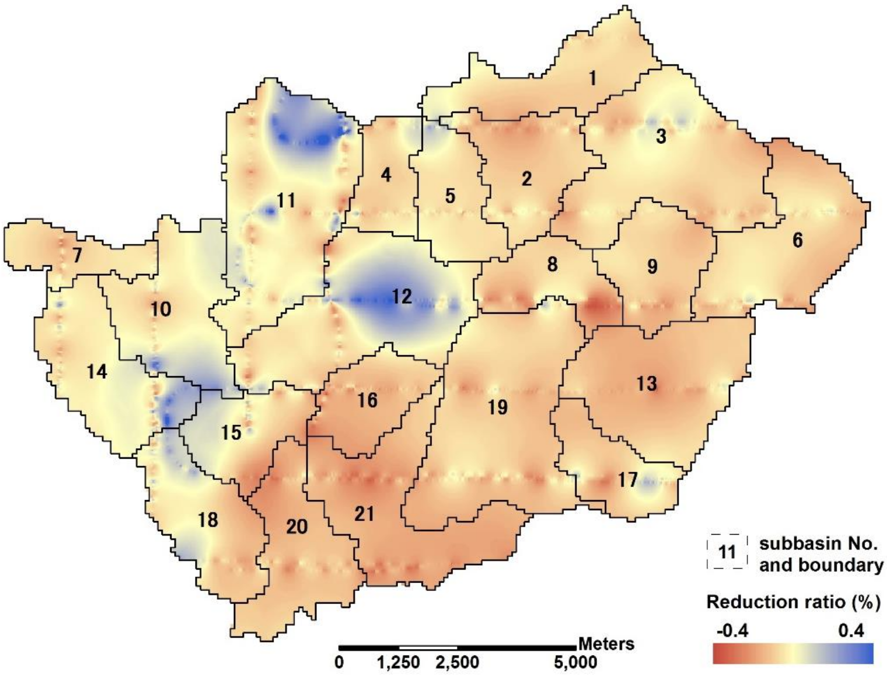

Figure 5-15. Percentage change of ^{137}Cs inventory from Jul. 2 to Nov. 5 in 2011, monitored by 3rd and 4th airborne survey, respectively (not includes radioactive decay). (Negative value means ^{137}Cs inventory decreasing.)

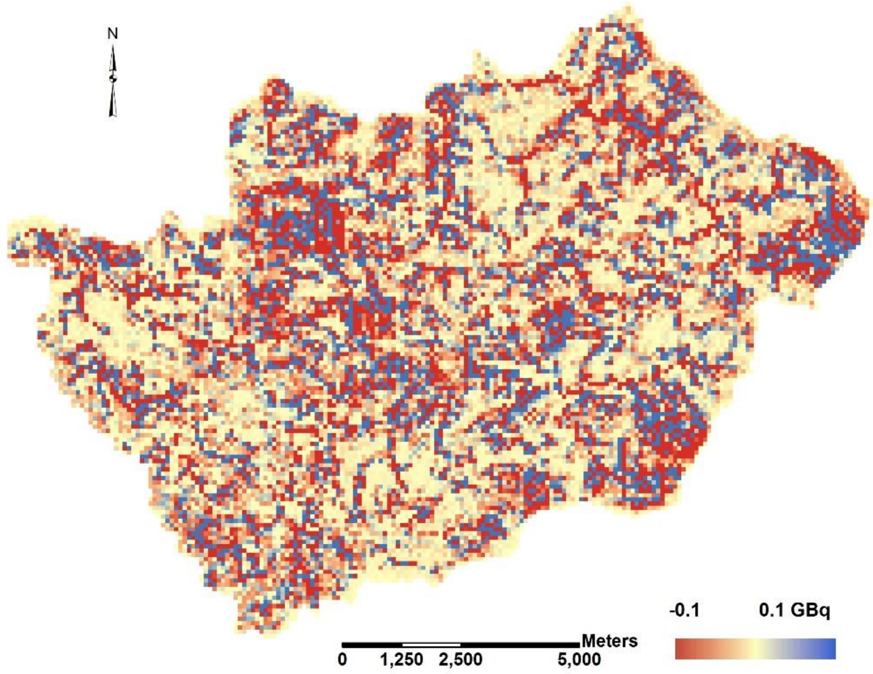

Figure 5-16. Spatial distribution of ^{137}Cs dynamics on the upland regions (negative values indicates decrease in ^{137}Cs).

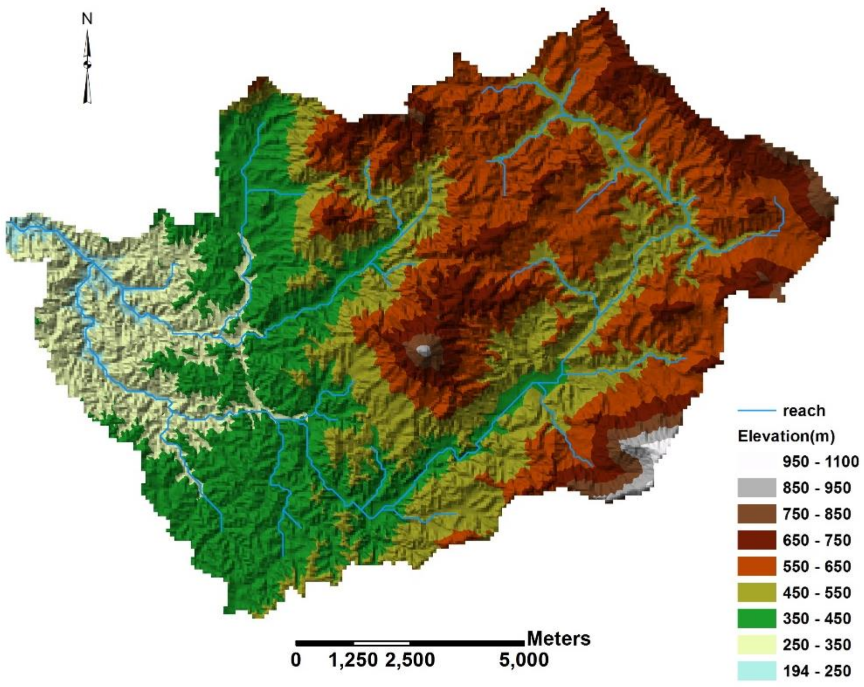

Figure 5-17. Geomorphological characteristics of the Kuchibuto River catchment

Reference

Chadwick, R. C. and Chamberlain A.C. (1970) Field loss of radionuclides from grass. Atmos. Environ., 4: 51–56.

Ertel J., Voigt G., Paretzke H.G. (1989) Weathering of $^{134/137}$Cs following leaf contamination of grass cultures in an outdoor experiment. *Radiat. Environ. Biophys.*, 28:319–326.

Fan, Q.H., Tanaka, M., Tanaka, K., Sakaguchi, A., Kondo, H., Takahashi, Y. (2014) Factors controlling radiocesium distribution in river sediments: field and laboratory studies after the Fukushima Dai-Ichi nuclear power plants accident. *Applied Geochemistry*, 48: 93–103.

FAJ (Forestry Agency of Japan). (2012) Preliminary results of surveys of distributions of radioactive elements in forest ecosystems.
http://www.rinya.maff.go.jp/j/press/hozen/111227_2.html

Fraley Jr. G Chavez, L. and Markham O.D. (1993) Seasonal variations in deposition and retention of cerium-141 and cesium-134 in cool desert vegetation. *J. Environ. Radioact.*, 21 (3):203–212.

Kitamura, A., Yamaguchi, M., Kurikami, H., Yui, M. and Onishi, Y. (2014) Predicting sediment and cesium-137 discharge from catchments in eastern Fukushima. *Anthropocene*, 5: 22–31.

Kato, H., Onda, Y., Gomi, T., (2012) Interception of the Fukushima reactor accident derived ^{137}Cs, ^{134}Cs and ^{131}I by coniferous forest canopies. *Geophys. Res. Lett.* 39, L20403. http://dx.doi.org/10.1029/2012GL052928.

Kinouchi, T., Yoshimura, K., Omata, T. (2015) Modeling radiocesium transport from a river catchment based on a physically-based distributed hydrological and sediment erosion model. *Journal of Environmental Radioactivity*, 139: 407–415.

Loffredo, N., Onda, Y., Kawamori, A., and Kato, H. (2014) Modeling of leachable ^{137}Cs in throughfall and stemflow for Japanese forest canopies after Fukushima Daiichi Nuclear Power Plant accident. *Science of Total Environment*, 493: 701-707.

Loffredo, N., Onda, Y., Hurtevent, P., Coppin, F. (2015) Equation to predict the ^{137}Cs leaching dynamic from evergreen canopies after a radio-cesium deposit. *Journal of Environmental Radioactivity*, 147, 100–107. DOI: 10.1016/j.jenvrad.2015.05.018.

Madoz-Escande, C., Garcia-Sanchez, L., Bonhomme, T., Morello, M. (2005) Influence of rainfall characteristics on elimination of aerosols of cesium, strontium, barium and tellurium deposited on grassland. *J Environ Radioact*, 84: 1–20.

Milbourn G.M. and Taylor R.. (1965) The contamination of grassland with radioactive strontium I. Initial retention and loss. *Radiat. Bot.*, 5: 337–347.

JAEA (Japan Atomic Energy Agency). (2015) Annual report on "research on distribution of the radioactive materials from the Fukushima Daiichi Nuclear Power Plant Accident" (Chapter 2.6). http://133.188.30.97/initiatives/cat03/entry06.html.

JAEA (Japan Atomic Energy Agency). (2014) Annual report on "research on distribution of the radioactive materials from the Fukushima Daiichi Nuclear Power Plant Accident" (Chapter 3.2). http://133.188.30.97/initiatives/cat03/entry05.html.

JME (Japanese Ministry of Environment) (2016) Information on off-site decontamination work. http://josen.env.go.jp/material/pdf/josen_gareki_progress_201601.pdf.

Phillips, J.M., Russell, M.A., Walling, D.E., (2000) Time-integrating sampling of fluvial suspended sediment: a simple methodology for small catchments. *Hydrol. Process*. 14: 2589-2602.

Sakaguchi, A., Tanaka, K., Iwatani, H., Chiga, H., Fan, Q., Onda, Y., Takahashi, Y., (2014) Size distribution studies of ^{137}Cs in river water in the Abukuma riverine system following the Fukushima Dai-ichi Nuclear Power Plant accident. *J. Environ. Radioact*. 139: 379-389.

Takahashi, J., Tamura, K., Suda, T., Matsumura, R., and Onda, Y. (2015) Vertical distribution and temporal changes of ^{137}Cs in soil profiles under various land uses after Fukushima Dai-ichi Nuclear Power Plant Accident. *Journal of Environmental Radioactivity*, 139: 351-361.

Tanaka, T., Tachikawa, Y., Shiiba, M., Yorozu, K., Kim, S. (2013) Numerical modeling and estimation of radioactive cesium movement at the Kuchibuto river basin, Fukushima. *Journal of Japan Society of Civil Engineers, Ser. B1 (Hydraulic Engineering)* 69: 1_487-1_492.

Ueda, S., Hasegawa, H., Kakiuchi, H., Akata, N., Ohtsuka, Y., Hisamatsu, S., (2013) Fluvial discharges of radiocaesium from watersheds contaminated by the Fukushima Dai-ichi Nuclear Power Plant accident, Japan. *J. Environ. Radioact.* 118: 96-104.

Yamaguchi, M., Kitamura, A., Oda, Y., Onishi, Y. (2014). Predicting the long-term ^{137}Cs distribution in Fukushima after the Fukushima Dai-ichi nuclear power plant accident: a parameter sensitivity analysis. *Journal of Environmental Radioactivity*, 135: 135-146.

Chapter 6

Summary and conclusions

6.1 Summary

【chapter 3】 The two-dimensional runoff, erosion and export (TREX) model was improved to simulate Fukushima derived ^{137}Cs transport associated with hydrological processes in the Kuchibuto River catchment. For our continuous hydrological simulation in a typical Japanese forested catchment, the model was firstly improved by considering additional hydrologic processes such as evapotranspiration, subsurface and groundwater flows. Lateral and vertical subsurface flows were calculated by a simple kinematic storage model and a storage routing method, respectively. A linear reservoir method was employed to calculate groundwater flow. Evapotranspiration was estimated by FAO Penman-Monteith method. Infiltration and interception parts also were modified according to the characteristic of our study catchment. The improved model reproduced better simulated flow rates by comparing with the original model. Simulated flow rates were found to be acceptable in comparison to measurements for 2011 ~ 2014 at the downstream and middle stream sites.

【chapter 4】 Soil erosion and transport for multiple particle size classes were simulated by the model. Critical erosion areas were identified by the spatial distribution of net soil erosion. Comparisons between simulated and measured suspended solid (SS) concentration of water samples from multiple sites, and field measured SS concentration, flux and mass at station near the outlet for 2011 ~ 2014 demonstrate that simulated results are acceptable. Model results indicate that from Mar. 12, 2011, when the accident began, to Dec. 31, 2014, about 5500 tonnes of clay, 52000 tonnes of silt, 22000 tonnes of sand were transported out of the basin. Soil erosion is estimated to have been most prevalent in the middle portion of the watershed where slopes are steep and the main land use is agricultural.

【chapter 5】 Watershed ^{137}Cs migration model was developed based on the improved TREX model with consideration of the effect of vegetation canopy/litter layer and unequal adsorption capacities of different solid particles. Two ^{137}Cs distribution phases in water and ^{137}Cs downward movement in soil were also considered in the model. Comparisons between observed and simulated (time-integrated and instantaneous) ^{137}Cs concentration at the station sites demonstrated the model reproduced ^{137}Cs transport well. Our simulations show about 4.85 TBq of ^{137}Cs remained in the vegetation canopy/litter layer, and 3.39 TBq of ^{137}Cs was lost by rainfall-runoff wash-off and natural radioactive decay in the catchment by the end of 2014, which means about 90% ^{137}Cs still remained in the catchment. This estimation confirms the necessity of artificial decontamination in the following years. During the simulation period, the average ^{137}Cs reduction rate and reduction ratio by wash-out were 1.24 GBq/Km^2/y and 1.6%, respectively. Radiocesium transport shows spatial heterogeneity because of spatial variation of the ^{137}Cs contamination level and soil erosion.

6.2 Conclusions

Based on the results of this study, we can conclude:

(4) The model calculated acceptable flow discharges, SS and ^{137}Cs concentrations at the observation sites in the Kuchibuto River catchment during the simulation period (Jan. 1, 2011 – Dec. 31, 2014). This case study shows the model is a good tool for study of ^{137}Cs transport along with hydrological processes at the watershed scale in Fukushima, Japan.

(5) For the case of the Kuchibuto River catchment, about 5500 t of clay, 52000 t of silt, 22000 t of sand along with 4.1×10^8 m^3 water were transported to the Abukuma River from Mar. 12, 2011, when the accident began, and Dec. 31, 2014. The area-specific sediment yield was about 155 t/y/km^2 according to our simulated sediment budget. By the end of 2014, the total ^{137}Cs reduction was 3.39 TBq (including natural radioactive decay), which means about 90% ^{137}Cs remained in the catchment. This estimation confirms the necessity of artificial decontamination in the following years. An estimated 4.85 TBq of ^{137}Cs remained in the vegetation layer. Hence, as a stock, this layer still stored a considerable amount of radiocesium. During the 3.5-year study, 0.57 TBq of ^{137}Cs was transported from the catchment. It mainly carried by eroded suspended sediment. During this period, the average ^{137}Cs reduction rate and

reduction ratio by rainfall-runoff wash-off were 1.24 $GBq/km^2/y$ and 1.6%, respectively.

(6) The ^{137}Cs reduction rate and reduction ratio by rainfall-runoff wash-off show spatial distributions related to the spatial variation of the ^{137}Cs contamination level and soil erosion. The ^{137}Cs reduction rate was higher in the upper stream areas, which corresponds to the initial ^{137}Cs distribution. In contrast, the ^{137}Cs reduction ratio and sediment supply ratio of the subwaterhseds in the middle portion of the catchment were higher, which indicates that decontamination for critical erosion areas in the middle portion of catchment is also of the great priority. The sinks of ^{137}Cs, which accumulated a considerable amount of ^{137}Cs owing to sediment deposition, can be targeted areas for decontamination. The results of this study are useful for understanding transport behavior and fate of radiocesium and ultimately for assessing environmental risks at the watershed scale.

6.3 Future works

Radiocesium will persist in the environment for long time. Prediction of long-term transport and fate of ^{137}Cs is an urgent work for radiocesium management. In one respect, without artificial decontamination, how much ^{137}Cs will reduce under natural rainfall conditions in the next years? If artificial decontamination work will be conducted, what will happen when different decontamination strategies are made? Different scenarios can be assumed and simulated by models to evaluate the effects of countermeasures to reduce the radiocesium contamination levels. Therefore, prediction of ^{137}Cs transport and fate and assessment of efficiency of different countermeasures by the model are continuous works for our study.

Acknowledgement

I would like to express the deepest appreciation to my supervisor Prof. Kinouchi. He gave me the chance to do this very interested study, and always encouraged me and gave me lots of suggestions when I can’t continue this study. Without his guidance and persistent help, this dissertation would not have been possible.

I would like to acknowledge Prof. Onda (University of Tsukuba) and his research group for supplying some measurement data for this study. Ms. Araya, Mr. Omata, Mr. Takahashi and Prof. Toyoda (Tokyo Institute of Technology) helped to do some measurements. I greatly appreciate all the work.

I am grateful to all reviewers: Prof. Ishikawa, Prof. Nakamura, Prof. Yoshimura, and Prof. Toyoda. Dr. Mark (HDR Engineering, Inc) was very kind for me when I began to learn numerical model, and also gave many suggestions and helps for my work. I would like to thank him at this moment.

As a member of Ishikawa-Kinouchi-Nakamura Lab, I feel very lucky. I would like to extend my thanks to all members of this lab: all professors, all students who study in the lab during 2012-2016, and sectaries. Thank you very much!

In addition, I also would like to acknowledge Chinese government and Japanese MEXT for financially supporting me for Ph.D. degree in Japan.

Finally, I sincerely thank my family, who know me, stand by my side and unconditionally support me.

WEI Lezhang

Jan. 28, 2016